Continuous Gas Phase Methane Oxidation Using Nitrous Oxide Over Fe-Based Zeolite

Ying Kit Chow

2018

Thesis submitted in accordance with requirements of the University of Cardiff for the degree of Doctor of Philosophy

DECLARATION

This work has not been submitted in substance for any other degree or award at this or any other university or place of learning, nor is being submitted concurrently in candidature for any degree or other award.

Signed ……...…… (candidate) Date……..…

STATEMENT 1

This thesis is being submitted in partial fulfillment of the requirements for the degree of ……(insert MCh, MD, MPhil, PhD etc, as appropriate)

Signed ……...…… (candidate) Date……..…

STATEMENT 2

This thesis is the result of my own independent work/investigation, except where otherwise stated, and the thesis has not been edited by a third party beyond what is permitted by Cardiff University's Policy on the Use of Third Party Editors by Research Degree Students. Other sources are acknowledged by explicit references. The views expressed are my own.

Signed ……...…… (candidate) Date……..…

STATEMENT 3

I hereby give consent for my thesis, if accepted, to be available online in the University's Open Access repository and for inter-library loan, and for the title and summary to be made available to outside organisations.

Signed ……...…… (candidate) Date……..…

STATEMENT 4: PREVIOUSLY APPROVED BAR ON ACCESS

I hereby give consent for my thesis, if accepted, to be available online in the University's Open Access repository and for inter-library loans **after expiry of a bar on access previously approved by the Academic Standards & Quality Committee.**

Signed ……...…… (candidate) Date……..…

ACKNOWLEDGEMENTS

I wish to thank my supervisors Prof. Graham Hutchings and Prof. Stuart Taylor for giving me an opportunity to work towards a PhD. It is a privilege to have worked in one of the best research group in the country for catalysis.

This project was sponsored by ExxonMobil and I would therefore like to acknowledge for their financial support for making this work possible. Special thanks must be given to the individuals from ExxonMobil who are experts in the oil and gas research industry, I would like to thank my industrial sponsors and co-workers; Dr. Randall Meyer and Dr. Sara Yacob. The teleconferences we had over the past 3 years had provided many many invaluable comments and suggestions for the team and identified areas where works are required in order to gain more understanding for the methane challenge. A special thank you also goes to Prof. Madan Bhasin as a project advisor from Innovative Catalytic Solutions.

I would like to thank my post doc and team methane that I have worked with at Cardiff University in no particular order: Dr. Nick Dummer, Dr. Greg Shaw, Dr. James Carter and Dr. David Willock for their continuous support and guidance. My project teammate; Chris Williams and Nishtha Agarwal for their help. This is a tough project and I always feel like I have the full support from the team since day 1. A special thank you to Ouardia for reviewing this thesis and her kind words when I struggled at work.

Finally, I would like to thank my family, Qi YueXin and my housemates I met at 6 Lisvane Street in Cardiff for keeping me smiling throughout my PhD.

“Choose life”

SUMMARY

Methane is the major component of natural gas yet is currently underutilized as a chemical feedstock. This is due to a lack of sustainable strategies for the selective oxidation of methane to methanol. Although selective, the current industrial syngas production process that utilizes methane is highly energy intensive and is an indirect route to value added products. A process for direct partial oxidation of methane to methanol is highly desirable. Zeolite based catalysts have shown great potential for the partial oxidation of methane. In particular, it has been reported that iron containing zeolites are able to convert methane to methanol by oxidizing methane to form surface-bound methoxy species.

A one step continuous gas phase approach for methane oxidation to methanol using nitrous oxide over a range of different Fe containing zeolites was studied. Understanding the speciation of the active components required and the reaction paths taken for methane oxidation is crucial to design better catalysts for this reaction. The work in this thesis shows that the methanol desorption rate is crucial to obtain high methanol selectivity and mass balance. It is observed that the Brønsted acidity of the catalyst is vital to the hydrogen abstraction step for methane oxidation. The studies on varying the Fe loadings, adding water to the system, tuning the heat treatment temperatures of the Fe-containing zeolite catalyst, methanol control experiments were carried out to reveal how each parameter affects the performance of the catalysts. A kinetic study was also carried out to identify how water changes the reaction pathway and proposed the reaction rank of the observed gas phase products.

ABSTRACT

This study investigates the direct continuous gas phase methane partial oxidation using nitrous oxide (N_2O) over a range of Fe exchanged MFI framework catalysts. It has been shown that the required active species, namely α-oxygen can be generated over the biomimetic catalyst (Fe/ZSM-5) after heating treatment with N_2O. The hydrogen abstraction step is followed to cleave the C-H bond to form methoy and hydroxy groups on the Fe sites.

Investigating the influence of acid sites in continuous methane oxidation with N_2O over Fe/ MFI zeolites revealed that Bronsted acidity of the Fe-zeolite catalyst supports the α-oxygen active species for the hydrogen abstraction to activate methane. The calcination treatment could cause a significantly decrease for both the Brønsted and Lewis acidity of Fe/ZSM-5 via the migration of aluminium as the catalyst treatment temperature increases. A substantial decrease is observed in catalytic performance following such alteration. The desired methanol could undergo further transformation to ethene follow by coke which is observed to behave similar to the methanol to olefin (MTO) reaction over zeolite framework. This side reaction path led to poor carbon balance and limited selectivity to partial oxygenates.

The subsequent kinetic study on methane oxidation over 2 wt % Fe/ZSM-5 using N_2O for both water-free and water-assisted (20 %) system has shown that the addition of water significantly improves methanol selectivity. A delplot technique was applied after performing a series of reactions using different catalyst mass for both system to identify the product rank of reaction products. Control experiments carried out in the absence of methane shown that the N_2O decomposition rate also proceed similar to the full reaction mixture.

LIST OF ABBREVIATIONS

Å	Angstrom ($10x10^{-10}$ meters)
atm	Standard atmosphere
a.u.	Arbitrary unit
BET	Brauner, Emmet and Teller
cm	Centimetre
cm^{-1}	Reciprocal centimetre
^oC	Degree celcius
CVI	Chemical vapour impregnation
DRIFTS	Diffuse Reflectance Infrared Fourier Transform Spectroscopy
FID	Flame ionisation detector
g	Gram
GC	Gas chromatography
h	Hours
IW	Incipient Wetness impregnation
ICP-MS	Inductive Coupled Plasma Mass Spectroscopy
K	Kelvin
M	Molar
mol	Moles
min	Minutes
nm	Nanometre (10^{-9} meter)
NMR	Nuclear Magnetic Resonance
SiO_2/Al_2O_3	Molar ratio of SiO_2 to Al_2O_3 in zeolite
STEM	Scanning Transmission Electron Microscopy
SIL-1	Silicalite-1
TCD	Thermal conductivity detector
TEM	Transmission electron microscopy
Temp	Temperature
TGA	Thermalgravimetric Analysis
TOF	Turnover frequency
TS-1	Titanium silicalite-1
NH_3-TPD	Temperature programmed ammonia desorption
UV-Vis	Ultraviolet – Visible Spectroscopy
wt%	Weight percentage
XRD	X-ray diffraction
ZSM5	Zeolite ZSM-5
µmol	Micromoles (10^{-6} moles)

TABLE OF CONTENTS

1

Introduction

1.1 Introduction

Natural gas is a clean and effective energy source that produces fewer greenhouse gases upon its combustion than coal and crude oil.[1] It is estimated that the total world natural gas reserves in 2016 stood at 186.6 trillion cubic meters.[2] The location of the world supply of natural gas is shown in figure 1.1.[2] This shows that most of the natural gas deposits are located far away from the actual point of use. Natural gas is flammable with low boiling point, which makes it difficult for transportation. The major challenge of exploiting natural gas is the high cost for transportation and the compressor used for storage from remote sites. Liquefied natural gas (LNG) was invented to tackle this problem which intend to shrink its volume for safer and easier shipping and storage. This process is carried out by cooling natural gas to minus 162 °C to reduce its volume to approximately 600 fold.[3] Nonetheless, liquefy natural gas production consisted of a long value chain, i.e. exploration of natural gas, liquefaction and refrigeration, shipping, regasification, and storage. The combination of the cost associated with the steps stated supresses the growth rate of LNG trading and also it is a highly technically complex project which may not be a long term economical choice for energy sectors.[3]

Methane is the major component of natural gas (accounts for approximately 90 mol % depending on source) and the precursor to many valuable hydrocarbon products, including methanol, formaldehyde, formic acid and other short chain hydrocarbons.[3] These higher energy dense liquid derivatives can be transported around the world much more easily at lower cost. There are many different approaches to exploit methane such as oxidative coupling to form higher hydrocarbon chains and syngas production. In

particular, methane to methanol (MTM process) is the most attractive route. Methanol is a valuable precursor to many other valuable chemicals as well as gasoline. For instance, methanol is used in the methanol to gasoline (MTG) process that yields a mixture of aromatics developed by Mobil[4], the Lurgi methanol to propylene (MTP) process[5, 6] and the Syn Energy Technology Co.'s dimethylether methanol to olefin (DMTO) process that primarily produce ethene and propene.[7] In addition, methanol also offers efficient storage and possesses great volumetric energy density (6.09 kW h kg^{-1}), which is almost twice the value compare to the rocket fuel, liquid hydrogen (3.08 kW h kg^{-1}).[8]

However, the abundant methane is under-utilised as a direct chemical feedstock and is currently converted to synthesis gas (CO and H_2) using high temperatures and pressures prior to the production of more valuable platform chemicals. Although selective, the current industrial syngas production process is highly energy-intensive.[9] Therefore a process for the direct partial oxidation of methane to methanol is highly desirable.[10]

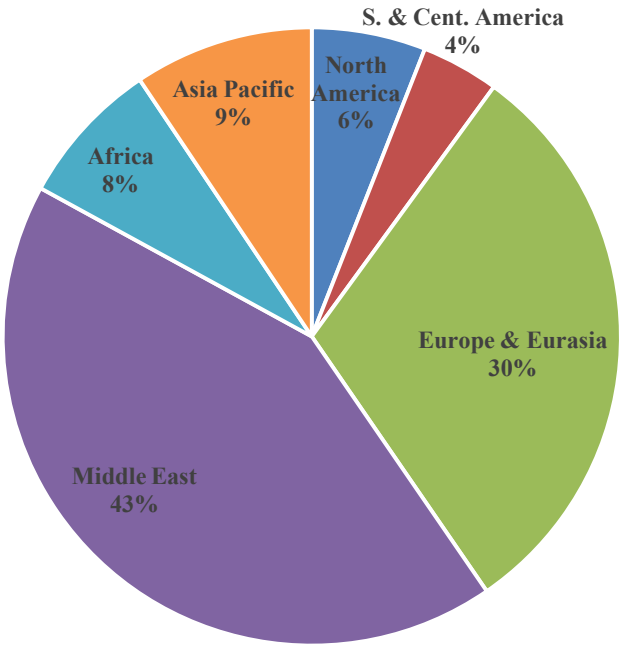

Figure 1.1 The world natural gas reserve in 2016 according to region. (The data is adapted from reference[2])

The direct selective oxidation of methane to methanol is considered one of the most challenging reactions for research scientists and there are no economically viable chemical process that has the efficiency to be commercialised to date.[11] The central issue concerns the strong C-H bonds in methane, which have a bond dissociation energy of 438.8 kJ mol^{-1}.[12] It requires an energy intensive condition and/or a highly active catalyst to activate this chemically inert molecule.[13] Furthermore, the partial oxidation products/unsaturated hydrocarbons typically have one or more C-H bonds weaker than the starting alkane.[14] The consequence is that the valuable partial oxidants such as MeOH is more reactive than methane. Therefore the over-oxidation product to CO_2 and water is always thermodynamically more favourable.[15, 16] The desired catalyst should be able to 1) activate methane 2) selectively oxidise methane to desired partial oxidants 3) does not carry out subsequent over oxidation process. The quest to design a system to crack the selective one step methane to methanol process requires a highly versatile catalyst, thus it continues to provide the chemical challenge and is often described as the "Holy Grail" of chemical catalysis.[17]

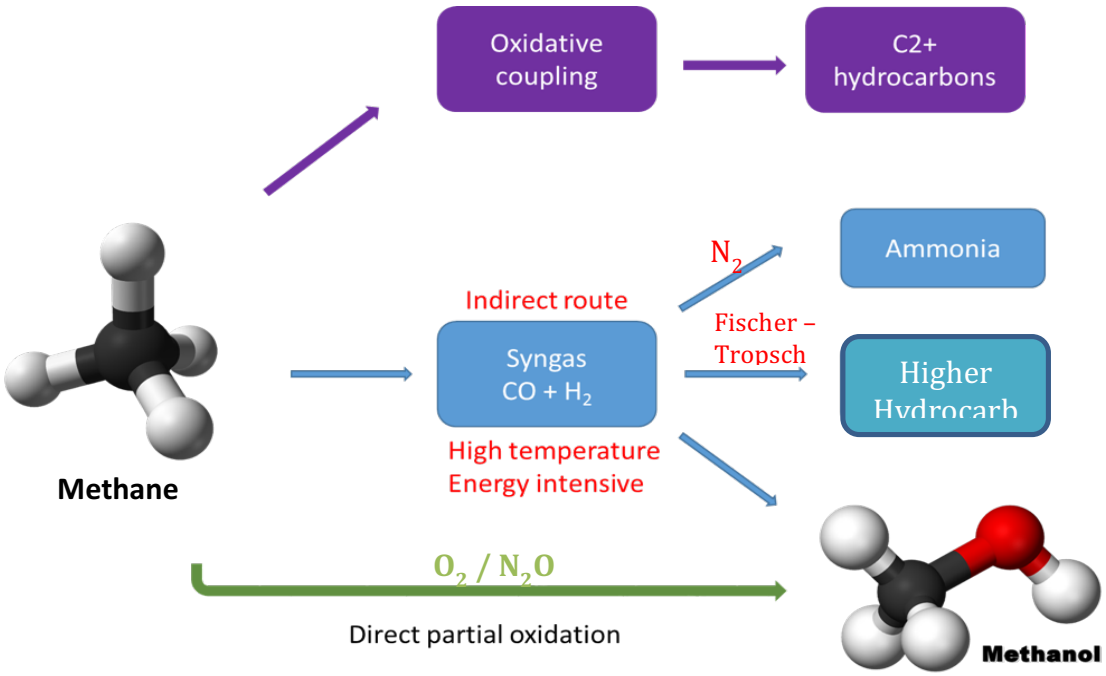

Figure 1.2. The conversion route from methane to other hydrocarbon fuels.[14]

1.2 Industrial proesses for methane utilisation

The currently used industrialised process to convert methane to useful chemicals and liquid fuels is viable through synthesis gas (syngas) production.[4, 18] The mixture of carbon monoxide and hydrogen are the intermediates, which can be further reacted to produce methanol and other hydrocarbons under multistep reactions. The steam methane reforming and oxygen reforming process are the two major processes used in the syngas production. Steam reforming operates typically between 775 to 975 °C at 20 to 30 atm pressure over a nickel based catalyst.[10, 19] Although Ni has been proven to be a good catalyst for the steam reforming process, it is well known that using nickel catalyst under these reaction conditions, coke can be generated via undesirable side reaction and result in catalyst deactivation. Coke is the unwanted carbonaceous deposit on the catalyst as the catalyst react with the hydrocarbon during thermal treatment.[20]

Rostrup-Nielsen reported that the coke resistance of the Ni catalyst can be improve by enhancing the adsorption of steam or CO_2 to improve the rate of surface reaction using rare earth oxide or alkaline metals promoters.[21] For instance, the Ni catalyst can be made more stale and supress coke formation when doping a Ni/SiO_2 catalyst with Ga_2O_3. The CO_2 adsorbed on the SiO_2 support and would be activated by Ga_2O_3 into carbonates species.[22]

The oxygen reforming is the partial oxidation of methane to form carbon monoxide and hydrogen. This is an exothermic reaction (ΔH_r^o = -36 kJ mol^{-1}) and the energy given as heat can be used to drive the reaction forward. It can be exploited to produce steam for reforming. Therefore the two processes can be combined together as known as the autothermal reforming process.

The chemical equations of the three types of reforming processes:

$$CH_4 + H_2O \rightleftharpoons CO + 3\ H_2 \quad \text{(Steam reforming) [eq. 1.1]}$$

$$CH_4 + 0.5\ O_2 \rightleftharpoons CO + 2\ H_2 \quad \text{(Oxygen reforming) [eq. 1.2]}$$

$$CH_4 + CO_2 \rightleftharpoons 2\ CO + 2\ H_2 \quad \text{(Dry reforming) [eq. 1.3]}$$

It is worth mentioning that the dry reforming process, which uses methane and carbon dioxide is another highly attractive process for the syngas production since it is using up two green house gases to generate useful fuel. However, this process is yet to be commercialised due to the absence of a stable and effective catalyst.[23]

$$CH_4 \xrightarrow{Ni/Al_2O_3} CO + H_2 \xrightarrow{Cu-ZnO/Al_2O_3} CH_3OH$$

[eq. 1.4]

Methanol can be synthesized from syngas produced from the methane reforming process and is described in equation 1.4.[24] Imperial Chemical Industries, Ltd. (ICI) discovered that a Cu-ZnO/Al_2O_3 catalyst is an effective catalyst in which it produces syngas with an adequate molar ratio of CO and H_2 that works at a temperature ranging between 240 to 260 °C under pressure of 50 to 100 bar.[25] It is reported that the addition of ZnO to copper enhances the activity due to a synergy effect. The benefits from Al_2O_3 provides protection for the active sites from agglomeration and improve the CO adsorption and activation on the surface.[26] The copper based system is also the most cost effective catalyst to date for the syngas to methanol step compare to Pd or other nobel metal based catalyst.[27, 28] Although the process can generate methanol at high yields and selectivity, this energy intensive, multistep processes is expensive and the large amount of steam required for reforming results in the corrosion of industrial plants thus it presents some serious drawbacks. The direct methane to methanol reaction pathway would avoid the high energy synthesis route and offers a more economical option for chemical industry.

1.3 Academic approach to methane oxidation

1.3.1 High temperature gas phase approach/ Homogeneous gas phase oxidation.

In the absence of a catalyst, methane oxidation to methanol occurs over the reactor wall and/or in the gas phase via free radical mechanism under high temperature and pressure using oxygen (typically operate between 500 to 700 °C and 30 to 60 bar pressure). The key reaction steps involved is listed in equation 1.5 to 1.7. After the initial step, the homolytic fission of the C-H bond to form methyl radical that is generated at the surface of the reactor and/or in the gas phase. The series of radical reactions are then initiated, which involves propagation and termination reactions. The subsequent chain reactions eventually lead to the formation of total oxidation product CO_2 and water.[29]

The elementary steps involved in the free radical reactions[30]:

$$CH_4 + O_2 \rightarrow {}^{\cdot}CH_3 + HO_2 \quad [\text{eq. 1.5}]$$

$$CH_4 + [\text{surface}] \rightarrow CH_3 + [\text{surface.H}] \quad [\text{eq. 1.6}]$$

$$CH_4 + [O] \rightarrow CH_3OH \rightarrow HCHO \rightarrow CO + H_2 \rightarrow CO_2 + H_2O \quad [\text{eq. 1.7}]$$

This partial oxidation to methanol consisted of more than 1000 elementary reactions with different reactive species scramble together. The reaction steps involved are highly exothermic and subsequent reactions are difficult to stop at any desired stages. The methanol selectivity towards higher conversions is poor, therefore the reaction parameters such as reactant pressure, temperature, concentration of feed oxygen and gas flow must be under strict control to find the optimum condition. It was shown that deep oxidation can be supressed using high methane pressure to drive for higher methanol selectivity.[30] Zhang *et al.* reported to have achieved 30 and 40% selectivity at conversions of 5 and 10%, respectively under methane pressure at 50 bar and heating to a temperature of 470 °C and concluded that the reactor wall must be made of quartz or Pyex glass to prevent any reaction from reactor wall and reactants/ products.[31, 32] However this type of catalyst-free high pressure homogeneous approach is still far too difficult to control and the reproducibility of such promising results are highly dependent on the type of reactors built which may be limited to laboratory scaled reactor.

1.3.2 Oxidative coupling of methane (OCM)

Another way of direct methane upgrading process is the oxidative coupling of methane (OCM) reported in 1982.[33, 34] This is to directly convert methane to ethene using oxygen which again involves numerous radical species and sequential partial oxidation of methane to ethane and then to ethene. The OCM reaction is exothermic (-177 kJ/mol) and occurs at temperature typically around 800 °C to active methane.

Chemical equations for the oxidative coupling reaction:

Main reactions

$$2\,CH_4 + 0.5\,O_2 \rightarrow CH_3CH_3 + H_2O \quad \Delta H_{298} = -177\ \text{kJ/mol} \quad [\text{eq. 1.8}]$$

$$CH_3CH_3 + 0.5\,O_2 \rightarrow C_2H_4 + H_2O \quad \Delta H_{298} = -105\ \text{kJ/mol} \quad [\text{eq. 1.9}]$$

Side reactions

$$CH_4 + 2\,O_2 \rightarrow CO_2 + 2\,H_2O \quad \Delta H_{298} = -802.2\ \text{kJ/mol} \text{ [eq. 1.10]}$$

$$CH_4 + 1.5\,O_2 \rightarrow CO + 2\,H_2O \quad \Delta H_{298} = -519.3\ \text{kJ/mol} \text{ [eq. 1.11]}$$

The chemical equations of the process are summarised in equations 1.8 to 1.11.[35] The catalytic process starts with a metal oxide catalyst surface forming an active oxygen species in the presence of oxygen to carry out a hydrogen abstraction, which cleaves the C-H bond of methane. This results in the formation of methyl radical species which go on to produce ethane and water. The ethane generated undergoes an in-situ dehydrogenation process to form ethene. The concentration of oxygen plays a big role in this reaction as an excess of oxygen shifts the exothermic process to deep oxidation with unwanted carbon oxides produced. The presence of CO_2 produced in the side reaction has been shown to lower the rate of production of ethane and ethene. Al-zahrani et al. reported a poisoning effect of CO_2 that using Li/MgO, CO_2 could undergo competitive adsorption with CH_4 and O_2 at the surface of the catalyst and changes the reaction pathway of the CO and H_2O.[36]

This result in the process would either have high selectivity at low conversion or high conversion at low selectivity.[37] The reported catalysts used that have shown activity for OCM are usually various form of transition metal oxide, for example, iron oxides in different oxidation state, Li/ZrO_2,[38] Mn/Mg,[39] CeO_2,[40] Na/CaO,[41] Na_2WO_4/La_2O_3,[42] MnO,[43] and combinations of these metal oxide catalysts.[15] Due to the higher operating temperature required, the methyl radicals generated over the catalyst surface would enter into the gas phase. The subsequent side reactions with oxygen and hydrogen are known to take place[44, 45] to form unwanted products such as carbon oxides, formaldehyde and methanol and led to the poor yield of the desired ethene.

Research into the OCM process seems to have made a major breakthrough in recent years and is getting closer to the commercialisation stage. Siluria Technologies has commissioned a demonstration plant in La Porte, Texas in 2015, for the OCM process using a metal oxide nanowire catalyst.[46] It is reported that the company uses a type of metal oxide nanowire catalyst that is synthesized via a Virus-enable synthesis approach published by Belcher and co-workers.[47] The method requires genetic modification of the virus enabling it to bind with the metal ions; thus acting as a template for growing

nanocrystals that are uniformly mineralised along the virus template.[48, 49] It is reported that this OCM nanowire catalyst could operate at a much lower temperature range of 200 to 300 °C.[49] However, the true nature of the catalyst employed in their OCM plant has not been made public.

1.3.3 Electrophilic activation

In the last 20 years, there has been remarkable progress made in methane activation at transitional metal centres operating under mild conditions with high selectivity to methanol protecting species. The electrophilic methane activation using a platinum catalyst was first reported by Shilov and co-workers[50] as shown in equation 1.12.

$$R - H + H_2O + PtCl_6^{2-} \xrightarrow{120^oC} R - OH(+R - Cl) + PtCl_4^{2-} + 2HCl$$

eq. 1.12

It is shown that when methane is reacted with the organometallic complex, a proton is first replaced by the Pt(II) centre and forming a methyl-Pt(II) complex. The methyl-Pt(II) complex is then oxidised to a methyl Pt(IV) complex by [Pt(IV)Cl_6^{2-}] via an electron transfer process and forming [Pt(IV)Cl_4^{2-}]. H_2O can carry out subsequent nucleophilic attack at the C-Pt bond and leads to the formation methanol and HCl, which also regenerates the Pt catalyst. This system operates in an aqueous medium at 120 °C and requires a stoichiometric amount of Pt(IV) which makes this impractical for industry due to the high cost of platinum source.[51] The other concern of this system is the stability of the catalytic Pt complex under the reaction condition that the Pt complex would also convert to metallic platinum due to the redox potential is similar to Pt(II) to Pt(IV).[52]

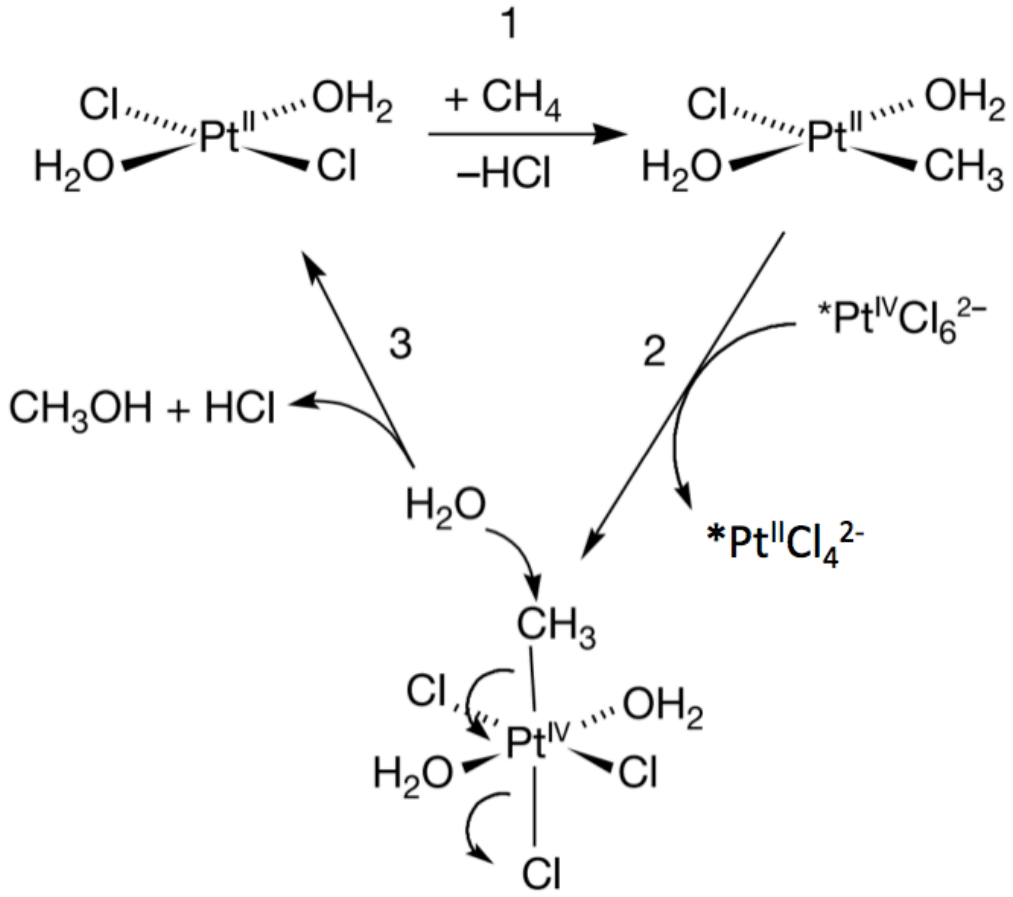

Figure 1.4. The reaction mechanism of the Shilov system adapted from [52].

Periana et al. reported an impressive electrophilic activation route based on the Shilov system using a bipyrimidyl Pt(II) complex for the methane oxidation to form methyl bisulphate with concentrated sulphuric acid.[53] The $[PtCl_6]^{2-}$ employed in the Shilov system is replaced by sulphuric acid as the oxidant. In this system, the Pt complex can overcome the stability issue associated with the Pt complex that eventually precipitated as Pt metal under reaction conditions. The use of hot sulphuric acid was able to dissolve any Pt metal formed. A proposed mechanism for the Periana's system for oxidation of methane by sulphuric acid over the Pt(II) catalyst is shown in figure 1.5.

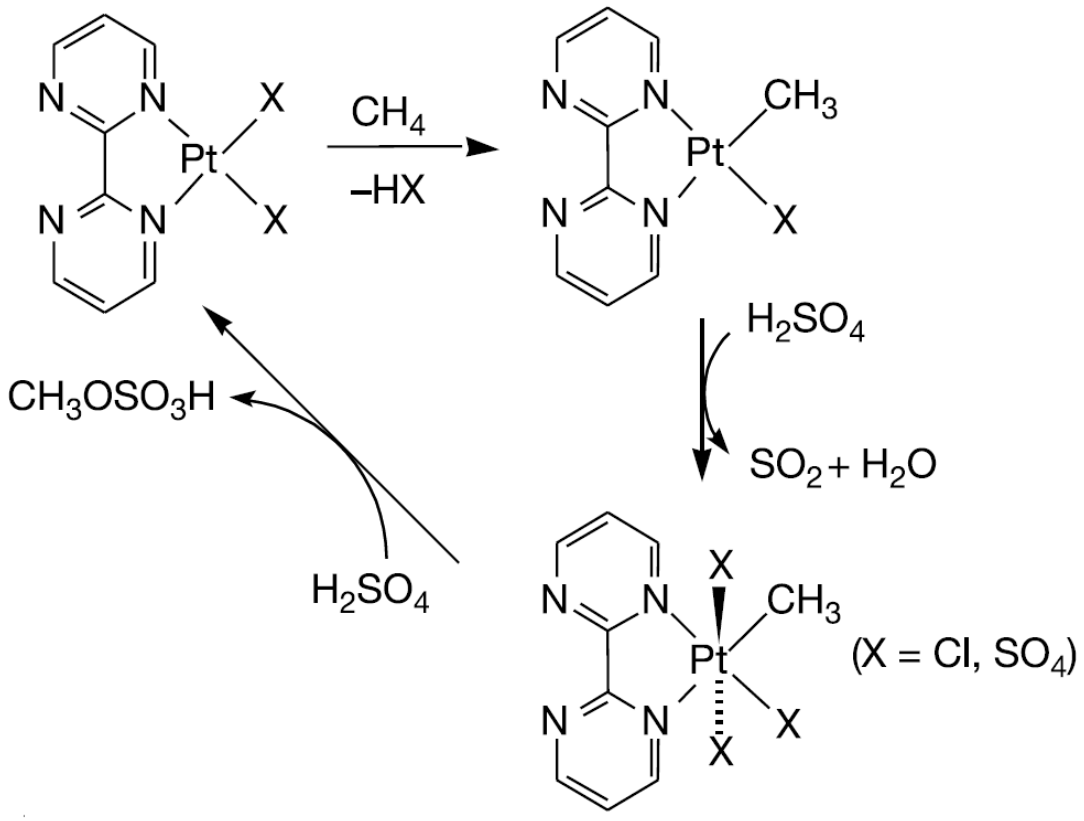

Figure 1.5 The Periana system for the formation of methyl bisulphate adapted from ref [54, 55].

This improved system led to a one pass yield of 72% with high activity (up to 90%) to methyl bisulphate with 81% selectivity at 220 °C in oleum (SO_3/H_2SO_4), which can then be further reacted to a more useful product, in our case methanol. From kinetic studies and control experiments on the oxidation of the resulting methyl bisulphate solution, it was found that the rate constant for oxidising methane is at least 100 times greater than the methyl bisulphate implying the ester is well protected by the bisulphate moiety.[54] There are also other limitations to the system such that the desired product will require an extra step to extract the methanol via a hydrolysis step. Methanol is also proven difficult to be separated from the acidic solvent therefore the use of expensive corrosive resistant materials cannot be avoided. This brings us back to another two-step process and it may not be competitive enough against the current syngas process. The overall equations for the overall Pt type catalyst with sulphuric acid chemistry is presented in equation 1.13 to 1.16.

The chemical equations for the Periana system.[54]

$$CH_4 + H_2SO_4 + SO_3 \rightarrow CH_3OSO_3H + H_2O + SO_2 \text{ [eq. 1.13]}$$

$$CH_3OSO_3H + H_2O \rightarrow CH_3OH + H_2SO_4 \text{ [eq. 1.14]}$$

$$SO_2 + 0.5\ O_2 + H_2O \rightarrow H_2SO_4 \text{ [eq. 1.15]}$$

$$Overall: CH_4 + 0.5\ O_2 \rightarrow CH_3OH \text{ [eq. 1.16]}$$

After the improvement made by Periana *et al.* by adding sulphuric acid, the Pt based catalyst was modified further by Palkovits *et al.*[54] in which the Pt catalyst existed as a solid catalyst. The catalyst was developed based on a type of high performance polymer framework that are formed by the trimerisation of aromatic nitriles in molten $ZnCl_2$. It utilises the 2,6-dicyanopyridine as monomer, a type of covalent triazine-based framework (CTF) with multiple accessible bipyridyl units that allows the incorporation of the Periana type platinum complex. More importantly the Pt centre retains those electrophilic activation features observed like the previously cases for methane oxidation. The structure of the Pt-CTF catalyst is shown in figure 1.6. Under the same reaction condition used in the Periana system, this Pt-CTF solid catalyst leads to a similar activity and selectivity to methanol. The great advantage of this heterogeneous system compare to homogeneous analogue is that the catalyst can be recycled and separated easily which could significantly shorten the process time. Moreover, it is found that the catalyst is very stable after several reactions achieving turnover number of at least 250 in multiple cycles.[56, 57]

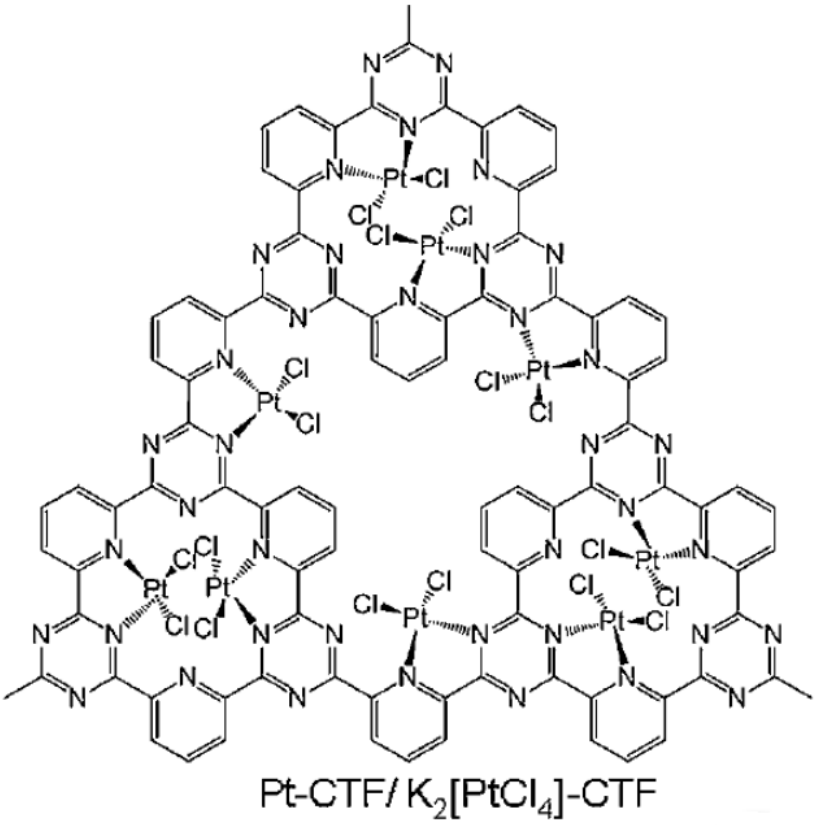

Figure 1.6 The Pt-CTF catalyst structure reported by Palkovits *et al.*[56]

The electrophilic approach for the methane oxidation to a range of different protected methanol derivatives was also reported using other transition metals. The use of Hg^{2+}, Pd^{2+}, Au^{+}, Au^{3+}, Co^{3+}, TI^{3+} were reported to be able to convert methane to other oxygenates such as methyl bisulfate, methane sulfonic acid or methyl triflouroacetate depending on the nature of the transition metal used.[56]

1.3.4 Enzymatic oxidation of methane

A powerful oxidant found in nature – the methanotrophic bacteria contains an enzyme named methane monooxygenases (MMOs) is able to catalyse the oxidation of methane to methanol under ambient conditions using oxygen with 100% selectivity.[58-60] MMOs can also avoid the over oxidation products such as carbon oxide and formic acid. This process is described in equation 1.17.

This enzymatic methane oxidation is well studied and concluded that the soluble MMO (sMMO)[61] and particulate MMO (pMMO)[62, 63] were the active enzyme found in the bacteria.[64-67] The pMMO contain serveral different metal centres in which all of them

consisted of a copper binding site. Furthermore, a dicopper site is suggested to be the active site of pMMO but the exact nature of the active site is still unknown.

The chemical equation of methane partial oxidation by MMO:

$$CH_4 + NADH + H^+ + O_2 \rightarrow CH_3OH + NAD^+ + H_2O$$

Eq. 1.17

On the other hand, the sMMO contains only one active diiron metal centre. It is reported that the diiron ions can present between +2 to +4 oxidation state during the methane oxidation redox process.[61, 68, 69] It starts with reductive activation of dioxygen using the $NADH^+$ co-factor to form peroxodiiron (III) intermediates, which breaks the oxygen-oxygen bond. After the bond cleavage, the peroxodiiron (III) is converted to compound Q[70-72] as shown in figure 1.7, which consist of a diiron (IV) centre before reacting with methane to break the strong C-H. The diiron (IV) then converted to a complex denoted T.[73] The structure of Compound Q is a crucial bit of information but has proven to be very difficult to reveal[74] as it is only form transiently and required specialised equipment and technique to capture the signal using resonance raman spectroscopy. Recently, Banerjee et al. has reported that compound Q consisted of a bis-μ-oxo diamond core structure using a time-resolved resonance Raman spectroscopy with fingerprinting of intermediates by their unique vibrational signatures through extended signal averaging for short-lived species.[75-80]

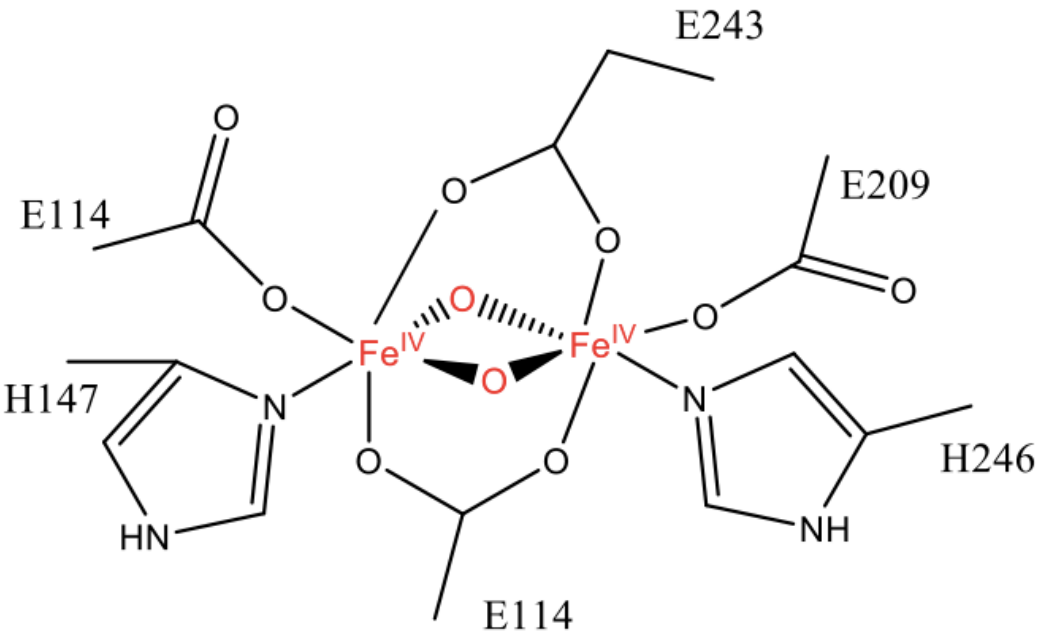

Figure 1.7 The structure of compound Q in sMMO.[74]

Although the nature found MMOs enzymes have shown unique ability to oxidise methane, this biological system is unlikely to be commercialised as the efficiency of molecular oxygen utilisation is proved to be the barrier. While the enzymatic system is difficult to scale up, the understanding of the metal centred active site is invaluable and has inspired scientists to synthesise catalysts, which later on lead to the development of a biomimetic approach for methane oxidation.

1.3.5 Biomimetic approach

As discussed previously in section 1.3.4, there are two types of metal centres found in MMOs and is reported to be a copper associated active site and the diiron based active site. The development of a biomimetic approach applied for instance using copper and iron based zeolite material is the substitution of bulky ligands around the active centre by a zeolite lattice structure.

Groothaert *et al.*[73] first reported the use of Cu-ZSM-5 for the selective oxidation of methane. The experimental procedure requires an oxygen pretreatment to the copper zeolite catalyst overnight at 450 °C before reacting with methane at 125 °C. The used catalyst is then stirred with a mixture of acetonitrile and water at room temperature to

extract the methanol produced over the catalyst. This system has achieved an impressive high selectivity of 98% to methanol by analysing the extracted mixture using ^{13}C NMR. The author reported that $[Cu_2(\mu\text{-}O)_2]^{2+}$, a bis (μ-oxo) dicopper core, is the active sites anchored on ZSM-5. It is capable of converting methane to methanol using oxygen. The work was supported through spectroscopic data from UV-Vis/EXAFS.

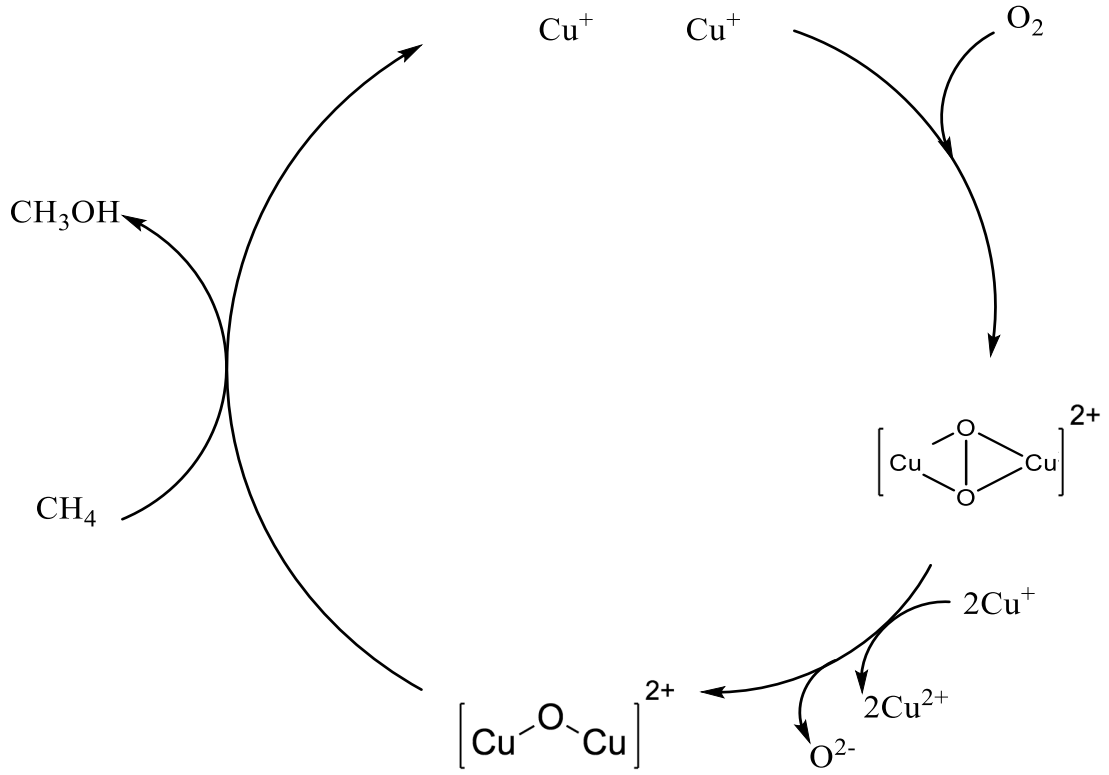

Figure 1.8 A proposed reaction pathway in Cu-ZSM-5 adapted from ref [81].

Haddad *et al.* reported the transformation of the active site precursor during the O_2 activation process occurred in Cu-ZSM-5 using time resolved UV-Vis spectroscopy.[82] This proposed reaction cycle, which facilitates the O_2 activation process and subsequent methane activation, is illustrated in figure 1.8. A side on bridged peroxo dicopper (II) precursor, $[Cu_2(O_2)_2]^{2+}$ is found to be converted directly into the bent $[Cu_2O]^{2+}$ species, which is responsible for the selective oxidation of methane to methanol. It is also suggested that spectator Cu^+ species formed during the ion exchange process could be

providing the electrons required to reduce the $[Cu_2(O_2)_2]^{2+}$ precursor to form the $[Cu_2O]^{2+}$ species.

The sMMO system has also inspired many works focusing on using the bi nuclear Fe centre embedded in different types of support. An interesting approach using a combination of Fe-ZSM-5 system with N_2O as the oxidant for the selective methane oxidation was first reported by Panov *et al.*[82] Panov and co-workers reported that methane was activated over Fe-ZSM-5 by α-oxygen species formed on the Fe centre when using N_2O as the oxidant.[83] The proposed schematic on the formation of the α-oxygen species over Fe-ZSM-5 is shown in figure 1.9. The catalyst is typically pre-treated under a range of temperature between 200 to 900 °C under oxygen pressure to convert the Fe^{3+} to Fe^{2+} state, also called the α-Fe sites. It follows a structural rearrangement to allow the α-oxygen to be generated by decomposing N_2O over the reversible redox α-Fe sites, which switch back to Fe^{3+}. An overall equation of this catalytic N_2O conversion is shown in equation 1.18.[83-89]

$$N_2O + (Fe^{2+})_\alpha \rightarrow (Fe^{3+} - O^{-})_\alpha + N_2 \quad \text{(eq. 1.18)}$$

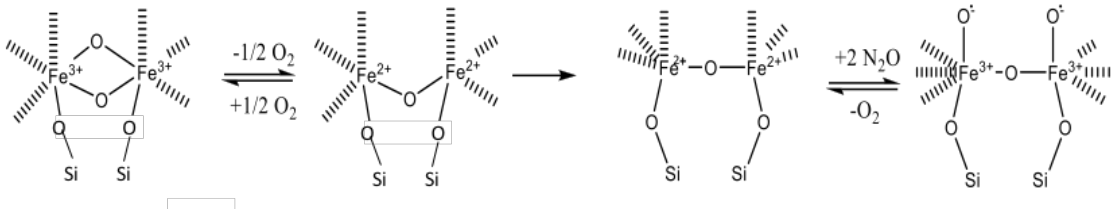

Figure 1.9 A proposed schematic on the formation of the α-oxygen species over Fe-ZSM-5.[89]

The α-oxygen is stabilised by the zeolite structure and the reverse oxidation with oxygen became thermodynamically unfavourable.[84, 90] It is reported that the thermal stability of α-oxygen is up to approximately 350 °C before recombining to form molecular oxygen. The radical anionic nature of the α-oxygen species allows the cleavage of the methane C-H bond *via* the hydrogen abstraction mechanism to occur at room temperature.[91] However, it is reported that the surface α-oxygen species cannot

be generated using molecular oxygen due to the strong stabilisation of the parent ZSM-5 zeolite.[92]

From their early work, Panov *et al.* have shown a three step process which involves: Step 1, N_2O pre-treatment over Fe-ZSM-5 to set up α-oxygen; step 2, switch over to methane to perform stoichiometric methane to methanol oxidation and; step 3 methanol extraction from the methane treated catalyst. It is reported that the methoxy and hydroxyl groups formed are subsequently adsorbed on the α-Fe sites even at room temperature, which can yield methanol directly on the surface of the zeolite.[89, 91] This process is quasi-catalytic as methanol must be extracted from the catalyst surface *via* hydrolysis using a solvent system consisted of a mixture of acetonitrile and water and achieved 94% selectivity to methanol.[89] The proposed reaction cycle of this α-oxygen driven methane oxidation is illustrated in figure 1.10. More recently, the same group has reported a one step process that operates between 275 to 300 °C by reacting N_2O and CH_4 simultaneously over Fe-ZSM-5 and a catalytic cycle was achieved.[89]

The nuclearity of the α-active site is still debatable considered to comprise of either mono-nuclear Fe^{4+}=O (or Fe^{3+}-O^{-}) or di-nuclear Fe as an oxo-bridged $Fe^{3+}O^{2-}Fe^{3+}$ species[87]. Synder *et al.*[93] recently reported that using magnetic circular dichroism spectroscopy, a mononuclear α-Fe^{2+} in an extra-lattice site probed using Fe-beta zeolite (BEA). A high spin Fe^{4+}=O was described as the reactive intermediate with the confinement of the zeolite lattice facilitates the reactivity was observed. Furthermore, Dubkov *et al.*[94] employed Mössbauer spectroscopy to reveal that the active oxygen species with adjacent Fe^{2+} atoms behaved as mono nuclear sites upon decomposition of N_2O in Fe-ZSM-5.

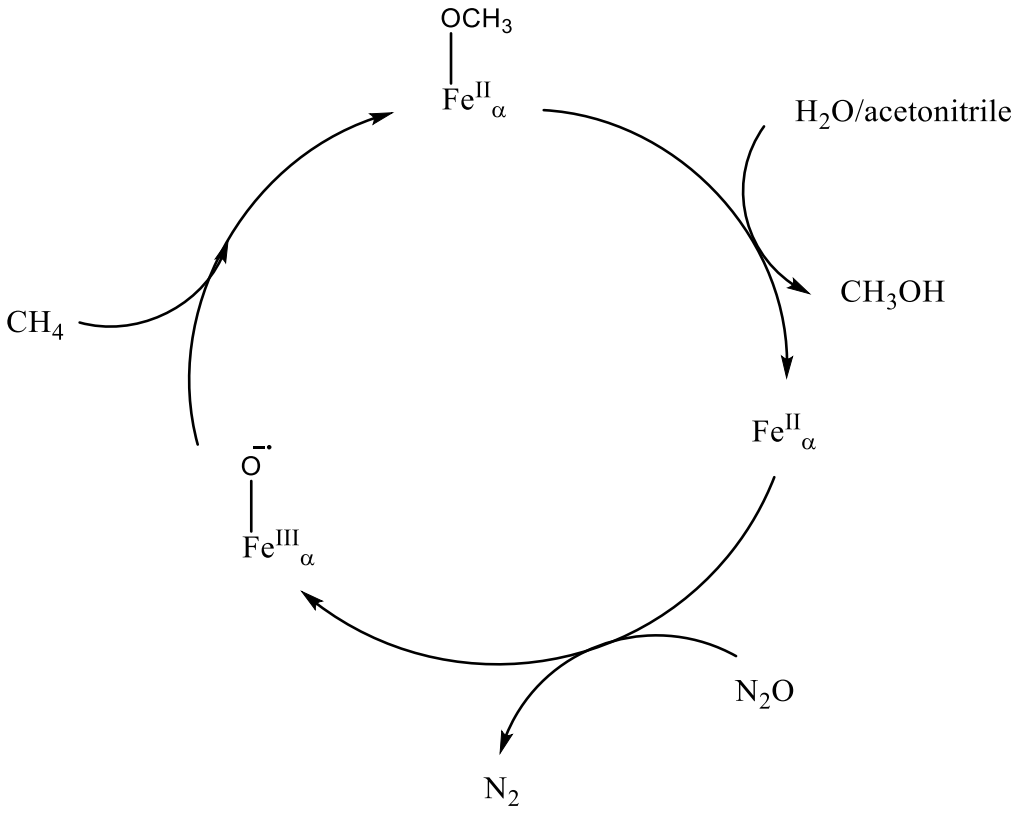

Figure 1.10 Proposed reaction path for the methane oxidation over Fe-ZSM-5.

Panov and co-workers' pioneer work on using the combination of Fe-ZSM-5 and N_2O as an oxidant to generate the active Fe-O species has led to numerous publications on the selective oxidation of different hydrocarbons.[85] The special properties of the elegant α-oxygen chemistry was applied to selectively oxidise benzene to phenol[87, 89, 95-99], epoxidation of propene[100] and most importantly, it is able to carry out methane activation even at room temperature.[101] Although it is shown that high selectivity to methanol can be achieve from this system operating under quasi-catalytic mode, methanol remains strongly bound to the catalyst surface and an extraction step must be added which would bring in additional cost to the process. If this system were to operate to approximately 300 °C, a one-step continuous process can be achieved in which methanol is desorbed into the reaction outlet but only result in poor selectivity with <2% reported from the same author.[89] Therefore, further investigation on this work especially to pinpoint the type of active component required and the kinetics for the formation of methanol would help understand this process better.

1.4 Zeolite

1.4.1 Introduction

Zeolites consist of repeating SiO_4 and AlO_4^- tetrahedral units; these aluminosilicate crystals are the building blocks to many different types of zeolite framework structure.[87] The tetrahedra (T = Si, Al) are linked up by bridging oxygen atoms and arranged in regular dimensions from 3 to 12 Å that could be 1D, 2D or 3D system of channels and cages.[102] A graphical representation of the tetrahedral unit is shown in figure 1.11. The tetravalent Si atoms can be substituted by 3^+ or 5^+ atoms and extraframework cations are required to compensate the overall charge of the framework.[103] This allows us to modify and incorporate a range of different cation such as H^+, NH_4^+, Na^+ or metallic ions into the framework which give rise to its Brønsted and Lewis acidity.[104]

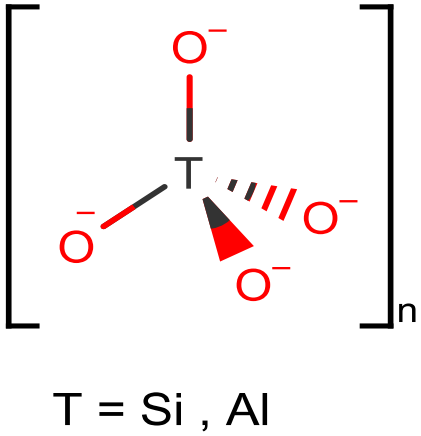

Figure 1.11 The structure of a basic zeolite tetrahedral unit.

The ratio of Si to Al can be adjusted (Si:Al ratio = 1 - ∞) in order to obtain different framework compositions. The upper limit of Si:Al ratio = 1 is described by Lowenstein rules that it is forbidden to have two adjacent AlO_4^- tetrahedra due to the electrostatic repulsion, therefore the two AlO_4^- must be separated by at least one bridging SiO_4 unit.[105] The thermal stability of the zeolite is dependent on the Si:Al ratio, where lower Si:Al ratio zeolite are stable to approximately 700 °C and high Si content material such as silicalite (pure silica MFI framework) stable to approximately 1400 °C. As the Si:Al ratio increases, both the hydrothermal stability and hydrophobicity increase.[106]

1.4.2 Zeolite synthesis

Zeolite growth process can be summarised in 4 steps; hydrolysis of zeolite precursor, condensation, the association of small clusters and, finally the precipitation to form crystals. The schematic diagram of the crystallisation process is shown in figure 1.12.[107] The synthetic approach for making zeolite is through hydrothermal synthesis. For aluminosilicate, there are four key components, including a silicon source (i.e. SiO_2, tetraethyl orthosilicate), aluminium source (i.e. $Al(NO_3)_3$, $AlCl_3$), a structure directing agent or template (i.e. tetrapropylammonium hydroxide for ZSM-5) and a solvent, mineralising agent (i.e. OH^- or F^-) which are reacted together to form a sol-gel before crystallisation takes place in a pressurised hydrothermal autoclave under a desired temperature.

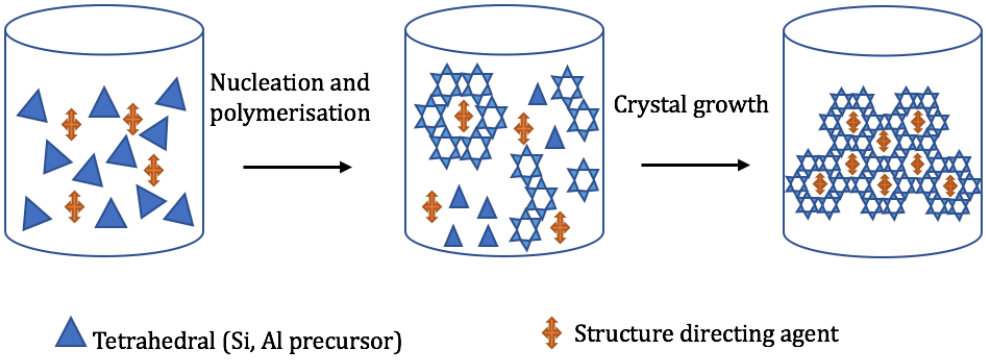

Figure 1.12 The crystallisation process during zeolite synthesis.[108]

The appearance of the precursor mixture can vary from a clear colloidal suspension to a dry solid-like dense gel depending on the condition of mixing and the type of precursor used. This can be a result of the silica or alumina suspension being partially or completely dissolved in the formation of the mixture.[108] The structure directing agent is used to stabilise the zeolite framework and the choice of template determines the size, morphology and chemical composition of the resulting zeolite. The solvent is typically water in combination with alcohols or ammonia and is multifunctional in zeolite synthesis such that it acts as a hydrolyser and accelerator of the chemical reactions.[109] The SiO_2 and AlO_4^- are the building blocks that undergo polymerisation at high temperature and pressure and grow into the desired structure, guided by the structure directing agent, before nucleating and crystal growth taking place to complete the

crystallisation process. There are numerous factors to take into consideration in order to achieve the desire results: From the type and impurities of the precursors used; order of mixing; agitation of the mixture; ageing time to the crystallisation time; and synthesis temperature during the crystallisation process.[109]

The sodalite cage is a type of common building block which gives rise to a wide range of different zeolite topology. The tetrahedral, 4 to 8 TO_4 units, (T = Si, Al) are linked together to form a 4 to 8 membered ring structure. These tetrahrdral rings can further combine together to form larger rings and cages, such as sodalite cages and pentasil units, before transforming into more complex framework structures; such as faujasite from sodalite cages and ZSM-5 from pentasil units. A schematic of the formation and transformation of sodalite cages into different complex framework is shown in figure 1.13.

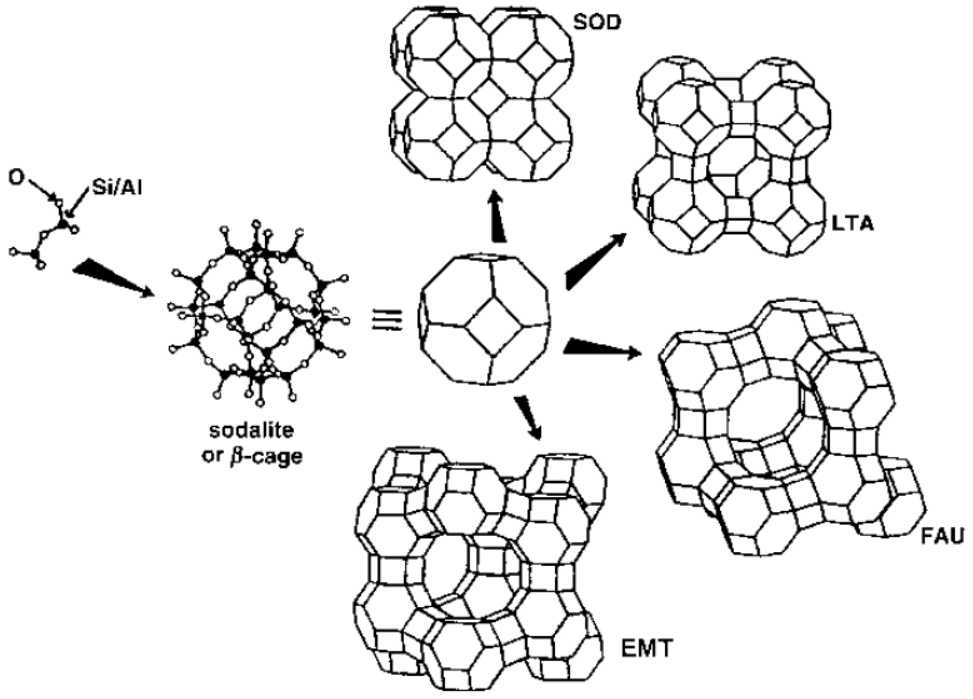

Fig 1.13 The formation of sodalite cages from tetrahedra units and its transformation to framework type FAU, LTA and EMT)

The Structure Commission of the International Zeolite Association (IZA-SC) is responsible for approving zeolite framework types and frameworks are assigned a

three-letter code. These framework types are often called the IZA structures and the IZA-SC has approved 227 distinct zeolite framework types to date.

1.4.3 Zeolites in catalysis.

Zeolite frameworks possess highly ordered structure and consist in repetitive units of uniform pores and channels. The crystalline multidimensional network may offer selective molecular adsorption and exclude the passages of bulky molecules. Therefore the shape and size selectivity features attract interest from industry for different type of industrial catalytic processes.[110] Zeolites have been widely used as a primer to produce various catalysts. The first industrial application used as a catalyst in the 1950s for cracking alkane in the oil refinery industry due to their thermal and mechanical stability and is still in use.[111] UOP and Norsk Hydro have developed the methanol to light olefin process for the production of ethene and propene using a chabazite framework zeolite (SAPO-34). The small pore channel provided by this topology has given its advantage to target light olefin.[104] The largest commercialised zeolite application is used as a detergent in which zeolite is exploited as an ion exchange reagents to remove Ca^{2+} and Mg^{2+} in hard water. The consumption of zeolites as a catalyst is estimated to be 27% of the world zeolite market value and the overall zeolite catalyst consumption is approximately 241 thousand metric tons per year.[112] As the zeolite structure database are growing rapidly, this signifies the potential of zeolites and could open up many opportunities for many different areas of chemistry.

Recent development of zeolite based heterogeneous catalysts has been inspired from nature's MMOs and is making remarkable breakthroughs on selective methane oxidation as discussed in previous chatper (1.3.5). There are different approaches that uses different type of zeolite framework for methane partial oxidation. Grundner *et al.* reported that the using Cu exchanged mordenite zeolite, methanol can be produced in a step-wised gas phase approach. The Cu-mordenite catalyst is activated upon a heat treatment at 450 °C using flowing oxygen. This activation step causes a Cu species transformation from a binuclear $[Cu\text{-}(\mu\text{-}O)Cu]^{2+}$ to the active trinuclear $[Cu_3(\mu\text{-}O)_3Cu]^{2+}$. This tricopper species is proposed to have a similar steric constraint environment that is found in the subunit formed in pMMO.[111] The temperature was then decreased to 190 °C before introducing a 90 % methane flow

mixture in He for 4h. An extraction step is followed by using equimolar mixture of steam and He for 30 min at 135 °C to extract the surface methanol.[113, 114] Wulfers *et al*. reported a series of testing using different types of Cu-exchanged chabazite. The methanol producing catalyst are Cu-SSZ-13, Cu-SSZ-16, Cu-SSZ-39 and Cu-SAPO-34 which all of them contained a small 8 membered ring pore. The reports has shown that those catalyst can produces a higher methanol per Cu active site than commonly used framework such as ZSM-5 and mordenite, which may imply that zeolite with small pore pocket/channel could favour the formation of methanol.[115] Moreover, Hutchings *et al.* has reported the bimetallic Fe and Cu containing zeolite catalyst (Cu-Fe-ZSM5) has the ability to oxidise methane to methanol in a one-step batch reaction using an aqueous reaction medium when hydrogen peroxide is used as the oxidant.[116]

This unprecedented subject could lead to an increase of the concentration between the interacting molecular orbitals, which would potentially enhance its catalytic activity.[117] However, this effect is not the only factor that contributes to the overall catalytic activity observed in the reaction between methane and Fe/ZSM-5. After the iron is incorporated into the ZSM5 framework, the Fe species in the extra framework have proven to be responsible for the high activity and high carbon/hydrogen based selectivity.[118]

1.4.4 Ion exchange process for metal incorporation

Upon the isomorphous incorporation of Al^{3+} (to form AlO_4^- tetrahedral) into the framework Si^{4+}, the aluminosilicate zeolite requires positively charged ions to maintain the overall neutral charge of the framework. The cationic species sit in the extraframework position of the zeolite, making this cation accessible to exchange; thus allowing a wide range of different type of cations to be incorporated such as Na^+, H^+ and transition metal ions.[119] This exchange process occurs without altering the crystalline structure of the solid.[117]

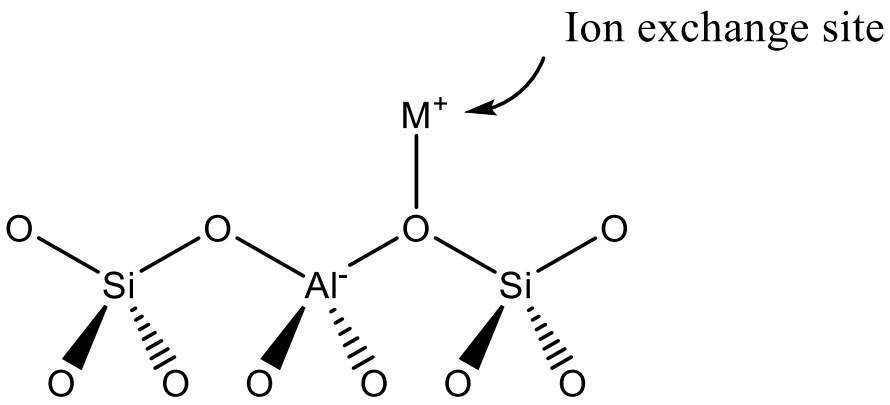

Figure 1.14 The exchange site present in the zeolite framework.

The incorporation of metal ions into the zeolite is possible either during zeolite synthesis or through a post synthetic method. The post synthetic ion exchange method to introduce metal ions to the Al-associated negatively charged exchange sites can be achieved through a range of different treatments to the parent zeolite support. Some common treatments for examples are solid-state ion change, aqueous phase ion exchange and chemical vapour impregnation.[106] The principal of these preparation methods is to bring the metal precursor and commercial zeolite to high temperature in order to remove any surface bound water and to ensure the deposition of the metal ion to the exchange site.[120-122]

There are different advantages and disadvantages to each exchange method, the aqueous phase ion exchange involves simply mixing and stirring the metal containing precursor solution and the commercial zeolite together, bringing it to the deposition temperature before drying the sample at a desired temperature and time. However, this approach often needs to be repeated multiple times to ensure a complete ion exchange process. This is due to the fact that OH^- and/or H^+ ions that arise from the hydrolysis of the cation; impurities from metal precursor that selectively build up in the zeolite; and other undesired excess salt that prohibit the desires metal ion to be coordinated to the exchange site.[93] It also requires large amounts of water and large amounts of nitrate or chloride waste are produced from the metal precursors.

The solid state ion exchange process involves physically mixing the metal precursor and the chosen zeolite using pestle and mortar. The problem associated with solid state approach is that the commercial zeolite has to be dehydrated in the best possible way

to ensure a complete ion exchange process. However, this approach is a very simple technique and could be used to anchor the desired metal onto the zeolite framework.

The chemical vapour impregnation (CVI) method is applied to most of the catalysts prepared in this study. This approach is based on the sublimation of the metal precursor and zeolite under vacuum condition. The early work of this application was demonstrated by Haruta and co-workers who used dimethylgold (III) acetylacetonateon as the gold precursor to disperse very small (<2 nm) active gold nanoparticles on various metal oxide support for CO oxidation.[123] The idea of using acetylacetonate based metal precursor is applied in this study for exchanging with the zeolite support is due to the ease of the preparation, preventing the formation of aqueous waste and also the catalyst can be scaled reliably as reported by Forde et al.[124]

Introduction of a metal ion to the zeolite framework can also be achieved by adding the metal ion precursor into the sol-gel mixture during zeolite synthesis. Along with the elementary silica precursors, structure directing agent and mineralising agent; the metal precursor is added to substitute the alumina precursor prior to the crystallisation process. In the formation of Fe-silicalite-1, the Fe precursor $Fe(NO_3)_3$ can form stable FeO_4^- tetrahedral units as an Al analogue. The synthesis control is important for Fe-silicalite-1, as the zeolite sol-gel is highly alkaline the insoluble $Fe(OH)_3$ species can be formed readily and prevent the incorporation of the metal into the framework.[120] The $Fe(NO_3)_3$ is reacted with oxalic acid to form the oxalate complex prior to mixing with the sol-gel, which is used to tackle the insolubility issue.[125] This synthesis approach offers greater control over the geometry of the Fe species formed for the ferrosilicate but requires careful control of reaction condition, (i.e. solubility of reagents in the mixing step, pH of the sol-gel and stirring temperature) whereas the post ion exchange allows a much more convenient process for introducing the metal ion and does not require the expensive hydrothermal autoclave reactor for zeolite synthesis.

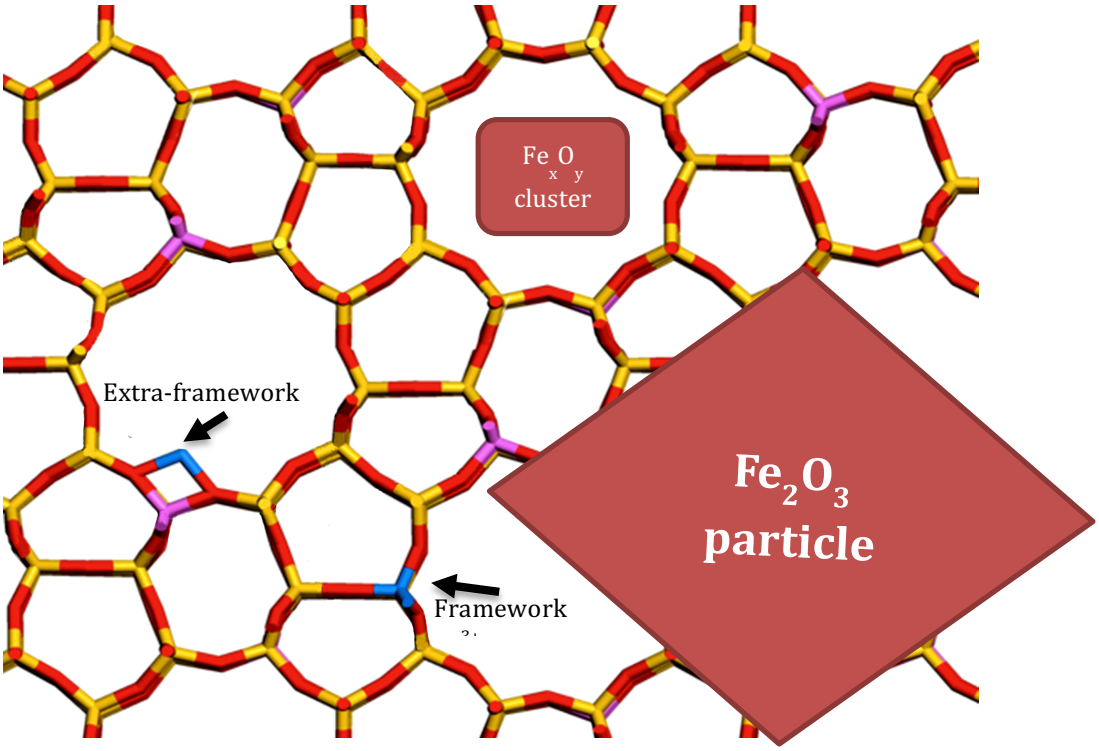

Figure 1.15 The location of the Fe species after the ion exchange process taken place using ZSM-5.[126]

1.4.5 Zeolite acidity

The catalytic activity of the zeolite depends on the presence of the hydroxyl groups, which can generate carbenium ion reactions. The acidity of the zeolite is reported to be essential for a wide range of applications. Since the recognition of its acidic properties, zeolites have been employed as selective hydrocarbon cracking catalyst by US and European refiners in the 1960s.[127] For example, Borges et al. reported that the n-hexane cracking reaction over H-ZSM-5 is known to be associated with the Bronsted acid site where lower reaction activation energy is observed associated with acid sites with greater strength.[93]

The complex formal charge of a zeolite, containing structural units [Si(OH)Al] (where a proton is attached to the oxygen atom that bridges skeletal tetrahedrally coordinated Si and Al atoms) can behave as a Bronsted acid. The strength of the zeolite acidity is a combination of both acid site strength and density.[128] The strength of the acid sites increases as the density of the acid sites decrease (i.e. the aluminium content is lowered). Therefore the acidity and strength of the zeolite can be tuned by changing the pre-treatment condition, preparation of the zeolite; post treatment of the resulting zeolite such as acid treatment; calcination temperature; performing ion exchange; altering the Si:Al ratio or isomorphously substituting the Si with Al.[129]

Lewis acidity is another important feature observed with zeolite. Zeolite can generate Lewis acid sites by dehydration by high temperature treatment which leads to the dehydroxylation of the Brønsted sites.[130, 131] The Lewis acids sites can also be generated by mild steam treatment which causes the migration of aluminium from their regular framework position.[132] The incorporation of other metal ions into the extraframework position (exchangeable sites) would also induce Lewis acidity. Zahmakiran reported that the increase Lewis acidity of ruthenium nanoclusters formed in the zeolite cavity enhances the catalytic activity for hydrogen generation.[133]

1.4.6 Confinement effect

The confinement effect of zeolite on the diffusing and adsorbing species through the micropore framework structure was first introduced by Prof. Eric G. Derouane.[134] The surface curvature of their internal surface allows the non-covalent interaction between zeolite framework and the chemical species passing through its intercrystalline space.[135, 136] This creates two types of interaction: 1) The repulsive force in the short range interaction and; 2) Van der Waal's type of attractive interaction in long range. It is these interactions that make zeolites unique and allows zeolites to behave like solid solvents.[136]

Barthomeuf first reported the effect on alkane under the electric field gradient created by aluminium and cation distribution.[137] The confined molecule can be polarised to different extents depending on the type of confining cages under the influence of this field gradients, altering the HOMO and LUMO energy levels[138], induce dipole and mutipoles and also be able to weaken or strengthen the C-C bonds.[118]

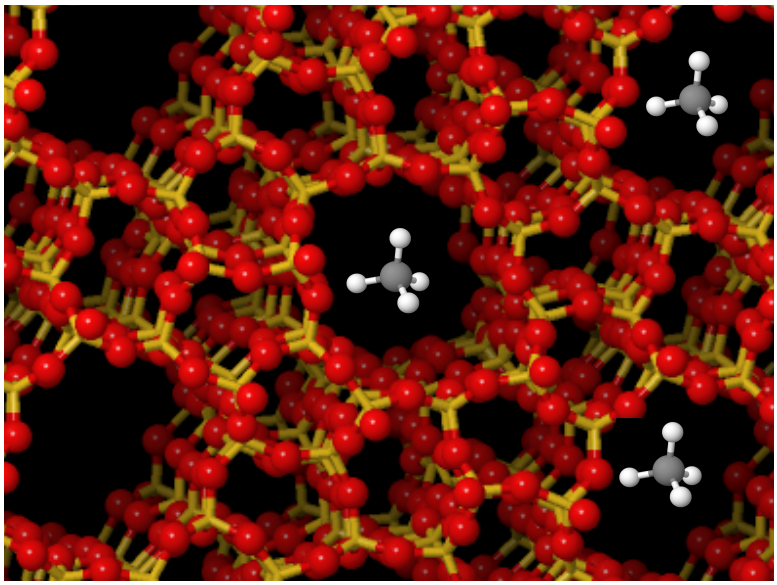

Figure 1.16 Confined molecules in a zeolite micropore environment.

Derouane reported that the Van der Waal's energy of a spherical molecule confined in a micropore depends on the relative size of the confined molecule and the micropore. Suppose there are two extreme cases: A) a molecule with the same size as the pore and; B) a molecule that has a flat surface. The adsorption energy due to the Van der Waal's force within the pore for scenario A would be up to 8 times larger.[137] The force acting over the confined molecule equals to zero so that the attractive force is cancelled out by the repulsive force and achieves supermobility. This allows the resulting molecule to have a much higher diffusivity in the intercages of the zeolite meaning the energy barrier of such molecule to go through the cages would be little to none. Yashonath and Santikary reported that a sharp increase of intercage diffusivity was observed on the sorbates and the relatively low energy barrier associated with them when the size of the confined molecules approaches the cage size using zeolite Y.[135]

The shape selective function given by the unique channel property of zeolite can be exemplified by the dehydrocylisation of n-hexane into benzene using a potassium exchanged zeolite L where the selectivity was reported to be >90%. The non binding interaction between n-hexane and the specific cavity shape of the zeolite L leads to the preorganisation of the n-hexane to a pseudo-cycle. The resulting intermediate is then transformed into cyclic compounds before selectively yielding benzene.[139] The regular crystalline channels with uniform pore size can also allow only molecules that are

below certain size to diffuse to the active site. Therefore, the catalytic activity can also depend on the size of the reactant to the zeolite pore.[140]

1.5 Research objectives

There are numerous challenges for the direct oxidation of methane. The reaction condition use in this study must be able to activate methane and should also minimise the over oxidation step. A large number of reports have demonstrated the catalytic ability of both Fe and Cu containing zeolite for methane oxidation. However, most of the studies were carried out in multiple steps which involves steam extraction and limited progress is made for the continuous gas flow system. Therefore this work would provide an insight in this area. In order to gain a better understanding into the partial oxidation of methane, under a continuous gas phase regime, the research objectives detailed below have been studied.

1) To develop Fe based zeolite catalyst for the gas phase methane oxidation to target valuable partial oxidants (ideally a direct synthesis of methane to methanol) using mild oxidants such as N_2O and O_2.
2) To carry out systematic study using Fe-Zeolite on how the zeolite acidity influence the performance of methane activation and the product selectivity. Parameters such as the temperature of the catalyst heat treatment, oxidising/ reducing environment applied and Fe loading used were investigated.
3) To identify and carry out characterisation on active sites required and to hypothesize plausible reaction pathways occur for the methane oxidation using porous zeolite materials. This would allow more efficient catalyst to be designed to target desire products.
4) To investigate how the incorporation of water in the gas phase methane oxidation affects the performance of the catalyst.
5) To perform kinetic studies to work out the product rank of the complex reaction network.

1.6 References

1. J. R. Webb, T. Bolano and T. B. Gunnoe, *Chemsuschem*, 2011, **4**, 37-49.
2. BP, Natural gas reserves., https://www.bp.com/en/global/corporate/energy-economics/statistical-review-of-world-energy/natural-gas/natural-gas-reserves.html, (accessed 22 March, 2018).
3. M. A. Qyyum, K. Qadeer and M. Lee, *Industrial & Engineering Chemistry Research*, 2017.
4. A. I. Olivos-Suarez, A. Szecsenyi, E. J. M. Hensen, J. Ruiz-Martinez, E. A. Pidko and J. Gascon, *Acs Catalysis*, 2016, **6**, 2965-2981.
5. D. Liederman, S. M. Jacob, S. E. Voltz and J. J. Wise, *Industrial & Engineering Chemistry Process Design and Development*, 1978, **17**, 340-346.
6. M. Stocker, *Microporous and Mesoporous Materials*, 1999, **29**, 3-48.
7. U. Olsbye, S. Svelle, M. Bjorgen, P. Beato, T. V. W. Janssens, F. Joensen, S. Bordiga and K. P. Lillerud, *Angewandte Chemie-International Edition*, 2012, **51**, 5810-5831.
8. P. Tian, Y. X. Wei, M. Ye and Z. M. Liu, *Acs Catalysis*, 2015, **5**, 1922-1938.
9. Z. Zakaria and S. K. Kamarudin, *Renewable & Sustainable Energy Reviews*, 2016, **65**, 250-261.
10. K. Aasberg-Petersen, I. Dybkjaer, C. V. Ovesen, N. C. Schjodt, J. Sehested and S. G. Thomsen, *Journal of Natural Gas Science and Engineering*, 2011, **3**, 423-459.
11. N. D. Parkyns, C. I. Warburton and J. D. Wilson, *Catalysis Today*, 1993, **18**, 385-442.
12. B. A. Arndtsen, R. G. Bergman, T. A. Mobley and T. H. Peterson, *Accounts of Chemical Research*, 1995, **28**, 154-162.
13. B. Ruscic, *Journal of Physical Chemistry A*, 2015, **119**, 7810-7837.
14. H. Schwarz, *Angewandte Chemie-International Edition in English*, 1991, **30**, 820-821.
15. J. A. Labinger, *Journal of Molecular Catalysis a-Chemical*, 2004, **220**, 27-35.
16. D. F. McMillen and D. M. Golden, *Annual Review of Physical Chemistry*, 1982, **33**, 493-532.

17. N. Dietl, M. Schlangen and H. Schwarz, *Angewandte Chemie-International Edition*, 2012, **51**, 5544-5555.
18. T. Mokrani and M. Scurrell, *Catalysis Reviews-Science and Engineering*, 2009, **51**, 1-145.
19. J. Baltrusaitis and W. L. Luyben, *Acs Sustainable Chemistry & Engineering*, 2015, **3**, 2100-2111.
20. G. Jones, J. G. Jakobsen, S. S. Shim, J. Kleis, M. P. Andersson, J. Rossmeisl, F. Abild-Pedersen, T. Bligaard, S. Helveg, B. Hinnemann, J. R. Rostrup-Nielsen, I. Chorkendorff, J. Sehested and J. K. Norskov, *Journal of Catalysis*, 2008, **259**, 147-160.
21. C. H. Collett and J. McGregor, *Catalysis Science & Technology*, 2016, **6**, 363-378.
22. J. R. Rostrup-Nielsen, *Catalysis Today*, 2000, **63**, 159-164.
23. Y. X. Pan, P. Y. Kuai, Y. A. Liu, Q. F. Ge and C. J. Liu, *Energy & Environmental Science*, 2010, **3**, 1322-1325.
24. S. Arora and R. Prasad, *Rsc Advances*, 2016, **6**, 108668-108688.
25. G. C. Chinchen, K. Mansfield and M. S. Spencer, *Chemtech*, 1990, **20**, 692-699.
26. S. S. Bharadwaj and L. D. Schmidt, *Fuel Processing Technology*, 1995, **42**, 109-127.
27. X. M. Liu, G. Q. Lu, Z. F. Yan and J. Beltramini, *Industrial & Engineering Chemistry Research*, 2003, **42**, 6518-6530.
28. M. S. Spencer, *Catalysis Letters*, 1998, **50**, 37-40.
29. A. Galadima and O. Muraza, *Journal of Natural Gas Science and Engineering*, 2015, **25**, 303-316.
30. M. J. Brown and N. D. Parkyns, *Catalysis Today*, 1991, **8**, 305-335.
31. S. S. Verma, *Energy Conversion and Management*, 2002, **43**, 1999-2008.
32. M. C. Alvarez-Galvan, N. Mota, M. Ojeda, S. Rojas, R. M. Navarro and J. L. G. Fierro, *Catalysis Today*, 2011, **171**, 15-23.
33. M. J. Gradassi and N. W. Green, *Fuel Processing Technology*, 1995, **42**, 65-83.
34. Q. J. Zhang, D. H. He, J. L. Li, B. Q. Xu, Y. Liang and Q. M. Zhu, *Applied Catalysis a-General*, 2002, **224**, 201-207.

35. A. Galadima and O. Muraza, *Journal of Industrial and Engineering Chemistry*, 2016, **37**, 1-13.
36. J. H. Lunsford, *Catalysis Today*, 2000, **63**, 165-174.
37. K. Takanabe, *Journal of the Japan Petroleum Institute*, 2012, **55**, 1-12.
38. K. Oshima, K. Tanaka, T. Yabe, E. Kikuchi and Y. Sekine, *Fuel*, 2013, **107**, 879-881.
39. J. A. Labinger and K. C. Ott, *Journal of Physical Chemistry*, 1987, **91**, 2682-2684.
40. V. J. Ferreira, P. Tavares, J. L. Figueiredo and J. L. Faria, *Industrial & Engineering Chemistry Research*, 2012, **51**, 10535-10541.
41. V. H. Rane, S. T. Chaudhari and V. R. Choudhary, *Journal of Natural Gas Chemistry*, 2008, **17**, 313-320.
42. M. Yildiz, U. Simon, T. Otremba, Y. Aksu, K. Kailasam, A. Thomas, R. Schomacker and S. Arndt, *Catalysis Today*, 2014, **228**, 5-14.
43. S. Y. Peng, Z. N. Xu, Q. S. Chen, Z. Q. Wang, Y. M. Chen, D. M. Lv, G. Lu and G. C. Guo, *Catalysis Science & Technology*, 2014, **4**, 1925-1930.
44. J. H. Lunsford, *Angewandte Chemie International Edition in English*, 1995, **34**, 970-980.
45. P. G. Hinson, A. Clearfield and J. H. Lunsford, *Journal of the Chemical Society-Chemical Communications*, 1991, 1430-1432.
46. J. A. Labinger, *Catalysis Letters*, 1988, **1**, 371-375.
47. M. Peplow, *Nature*, 2017, **550**, 26-28.
48. Y. J. Lee, H. Yi, W. J. Kim, K. Kang, D. S. Yun, M. S. Strano, G. Ceder and A. M. Belcher, *Science*, 2009, **324**, 1051-1055.
49. K. T. Nam, D. W. Kim, P. J. Yoo, C. Y. Chiang, N. Meethong, P. T. Hammond, Y. M. Chiang and A. M. Belcher, *Science*, 2006, **312**, 885-888.
50. E. C. Scher, F. R. Zurcher, J. M. Cizeron, W. P. Schammel, A. Tkachenko, J. Gamoras, D. Karshtedt and G. Nyce, *Journal*, 2013.
51. E. S. a. G. B. S. p. Aleksandr, *Russian Chemical Reviews*, 1987, **56**, 442.
52. J. A. Labinger and J. E. Bercaw, *Nature*, 2002, **417**, 507-514.
53. G. A. Luinstra, L. Wang, S. S. Stahl, J. A. Labinger and J. E. Bercaw, *Journal of Organometallic Chemistry*, 1995, **504**, 75-91.

54. R. A. Periana, D. J. Taube, S. Gamble, H. Taube, T. Satoh and H. Fujii, *Science*, 1998, **280**, 560-564.
55. R. A. Periana, D. J. Taube, E. R. Evitt, D. G. Loffler, P. R. Wentrcek, G. Voss and T. Masuda, *Science*, 1993, **259**, 340-343.
56. R. Palkovits, M. Antonietti, P. Kuhn, A. Thomas and F. Schuth, *Angewandte Chemie-International Edition*, 2009, **48**, 6909-6912.
57. R. Palkovits, C. von Malotki, M. Baumgarten, K. Mullen, C. Baltes, M. Antonietti, P. Kuhn, J. Weber, A. Thomas and F. Schuth, *Chemsuschem*, 2010, **3**, 277-282.
58. S. Mukhopadhyay and A. T. Bell, *Journal of Molecular Catalysis a-Chemical*, 2004, **211**, 59-65.
59. S. Mukhopadhyay and A. T. Bell, *Advanced Synthesis & Catalysis*, 2004, **346**, 913-916.
60. G. R. Williams, S. T. Kolaczkowski and P. Plucinski, *Catalysis Today*, 2003, **81**, 631-640.
61. C. D. Blanchette, J. M. Knipe, J. K. Stolaroff, J. R. DeOtte, J. S. Oakdale, A. Maiti, J. M. Lenhardt, S. Sirajuddin, A. C. Rosenzweig and S. E. Baker, *Nature Communications*, 2016, **7**.
62. A. C. Rosenzweig, C. A. Frederick, S. J. Lippard and P. Nordlund, *Nature*, 1993, **366**, 537-543.
63. A. C. Rosenzweig, P. Nordlund, P. M. Takahara, C. A. Frederick and S. J. Lippard, *Chemistry & Biology*, 1995, **2**, 409-418.
64. R. L. Lieberman and A. C. Rosenzweig, *Nature*, 2005, **434**, 177-182.
65. A. S. Hakemian, K. C. Kondapalli, J. Telser, B. M. Hoffman, T. L. Stemmler and A. C. Rosenzweig, *Biochemistry*, 2008, **47**, 6793-6801.
66. S. M. Smith, S. Rawat, J. Telser, B. M. Hoffman, T. L. Stemmler and A. C. Rosenzweig, *Biochemistry*, 2011, **50**, 10231-10240.
67. S. Sirajuddin, D. Barupala, S. Helling, K. Marcus, T. L. Stemmler and A. C. Rosenzweig, *Journal of Biological Chemistry*, 2014, **289**, 21782-21794.
68. C. Hammond, M. M. Forde, M. H. Ab Rahim, A. Thetford, Q. He, R. L. Jenkins, N. Dimitratos, J. A. Lopez-Sanchez, N. F. Dummer, D. M. Murphy, A. F. Carley, S. H. Taylor, D. J. Willock, E. E. Stangland, J. Kang, H. Hagen, C. J. Kiely and G.

J. Hutchings, *Angewandte Chemie-International Edition*, 2012, **51**, 5129-5133.

69. S. Sirajuddin and A. C. Rosenzweig, *Biochemistry*, 2015, **54**, 2283-2294.
70. K. Yoshizawa, A. Suzuki, Y. Shiota and T. Yamabe, *Bulletin of the Chemical Society of Japan*, 2000, **73**, 815-827.
71. K. Yoshizawa and T. Yumura, *Chemistry-a European Journal*, 2003, **9**, 2347-2358.
72. K. Yoshizawa, *Accounts of Chemical Research*, 2006, **39**, 375-382.
73. A. C. Rosenzweig, *Nature*, 2015, **518**, 309-310.
74. R. Banerjee, Y. Proshlyakov, J. D. Lipscomb and D. A. Proshlyakov, *Nature*, 2015, **518**.
75. S. K. Lee, B. G. Fox, W. A. Froland, J. D. Lipscomb and E. Munck, *Journal of the American Chemical Society*, 1993, **115**, 6450-6451.
76. L. J. Shu, J. C. Nesheim, K. Kauffmann, E. Munck, J. D. Lipscomb and L. Que, *Science*, 1997, **275**, 515-518.
77. B. D. Dunietz, M. D. Beachy, Y. X. Cao, D. A. Whittington, S. J. Lippard and R. A. Friesner, *Journal of the American Chemical Society*, 2000, **122**, 2828-2839.
78. W. G. Han and L. Noodleman, *Inorganica Chimica Acta*, 2008, **361**, 973-986.
79. P. E. M. Siegbahn, *Journal of Biological Inorganic Chemistry*, 2001, **6**, 27-45.
80. G. Q. Xue, D. Wang, R. De Hont, A. T. Fiedler, X. P. Shan, E. Munckt and L. Que, *Proceedings of the National Academy of Sciences of the United States of America*, 2007, **104**, 20713-20718.
81. M. H. Groothaert, P. J. Smeets, B. F. Sels, P. A. Jacobs and R. A. Schoonheydt, *Journal of the American Chemical Society*, 2005, **127**, 1394-1395.
82. M. S. Haddad, S. R. Wilson, D. J. Hodgson and D. N. Hendrickson, *Journal of the American Chemical Society*, 1981, **103**, 384-391.
83. G. I. Panov, A. K. Uriarte, M. A. Rodkin and V. I. Sobolev, *Catalysis Today*, 1998, **41**, 365-385.
84. E. V. Starokon, M. V. Parfenov, S. S. Arzumanov, L. V. Pirutko, A. G. Stepanov and G. I. Panov, *Journal of Catalysis*, 2013, **300**, 47-54.
85. K. A. Dubkov, N. S. Ovanesyan, A. A. Shteinman, E. V. Starokon and G. I. Panov, *Journal of Catalysis*, 2002, **207**, 341-352.

86. G. I. Panov, K. A. Dubkov and Y. A. Paukshtis, *Catalysis by Unique Metal Ion Structures in Solid Matrices: from Science to Application*, 2001, **13**, 149-163.
87. M. V. Parfenov, E. V. Starokon, L. V. Pirutko and G. I. Panov, *Journal of Catalysis*, 2014, **318**, 14-21.
88. E. V. Starokon, K. A. Dubkov, L. V. Pirutko and G. I. Panov, *Topics in Catalysis*, 2003, **23**, 137-143.
89. E. V. Starokon, M. V. Parfenov, L. V. Pirutko, S. I. Abornev and G. I. Panov, *Journal of Physical Chemistry C*, 2011, **115**, 2155-2161.
90. E. V. Starokon, K. A. Dubkov, L. V. Pirutko and G. I. Panov, *Topics in Catalysis*, 2003, **23**, 137-143.
91. V. I. Sobolev, O. N. Kovalenko, A. S. Kharitonov, Y. D. Pankrat'ev and G. I. Panov, *Mendeleev Communications*, 1991, **1**, 29-30.
92. E. V. Starokon, M. V. Parfenov, S. E. Malykhin and G. I. Panov, *Journal of Physical Chemistry C*, 2011, **115**, 12554-12559.
93. A. Zecchina, M. Rivallan, G. Berlier, C. Lamberti and G. Ricchiardi, *Physical Chemistry Chemical Physics*, 2007, **9**, 3483-3499.
94. B. E. R. Snyder, P. Vanelderen, M. L. Bols, S. D. Hallaert, L. H. Bottger, L. Ungur, K. Pierloot, R. A. Schoonheydt, B. F. Sels and E. I. Solomon, *Nature*, 2016, **536**, 317-321.
95. F. M. Zhang, X. Chen, J. Zhuang, Q. Xiao, Y. J. Zhong and W. D. Zhu, *Catalysis Science & Technology*, 2011, **1**, 1250-1255.
96. M. A. Rodkin, V. I. Sobolev, K. A. Dubkov, N. H. Watkins and G. I. Panov, in *Studies in Surface Science and Catalysis*, eds. A. Corma, F. V. Melo, S. Mendioroz and J. L. G. Fierro, Elsevier, 2000, vol. 130, pp. 875-880.
97. R. Bulanek, B. Wichterlova, K. Novoveska and V. Kreibich, *Applied Catalysis a-General*, 2004, **264**, 13-22.
98. N. Hansen, A. Heyden, A. T. Bell and F. J. Keil, *Journal of Physical Chemistry C*, 2007, **111**, 2092-2101.
99. B. Imre, J. Halasz, K. Frey, K. Varga and I. Kiricsi, *Reaction Kinetics and Catalysis Letters*, 2001, **74**, 377-383.
100. G. I. Panov, G. A. Sheveleva, A. S. Kharitonov, V. N. Romannikov and L. A. Vostrikova, *Applied Catalysis a-General*, 1992, **82**, 31-36.

101. G. I. Panov, E. V. Starokon, M. V. Parfenov and L. V. Pirutko, *Acs Catalysis*, 2016, **6**, 3875-3879.
102. S. L. Suib, *Science*, 2003, **302**, 1335-1336.
103. J. Cejka, G. Centi, J. Perez-Pariente and W. J. Roth, *Catalysis Today*, 2012, **179**, 2-15.
104. R. Xavier and A. v. S. Rutger, in *Handbook of Zeolite Science and Technology*, CRC Press, 2003.
105. W. Loewenstein, *American Mineralogist*, 1954, **39**, 92-96.
106. R. C. Deka, *Indian Journal of Chemical Technology*, 1998, **5**, 109-123.
107. P. Pramatha and K. D. Prabir, in *Handbook of Zeolite Science and Technology*, CRC Press, 2003.
108. S. Ramsharan and K. D. Prabir, in *Handbook of Zeolite Science and Technology*, CRC Press, 2003.
109. J. Grand, H. Awala and S. Mintova, *Crystengcomm*, 2016, **18**, 650-664.
110. S. P. Zhdanov, in *Molecular Sieve Zeolites-I*, AMERICAN CHEMICAL SOCIETY, 1974, vol. 101, ch. 2, pp. 20-43.
111. B. Yilmaz and U. Muller, *Topics in Catalysis*, 2009, **52**, 888-895.
112. D. Lauriente and Y. Inoguchi, in *The Chemical Economics Handbook*, SRI consulting, 2005, ch. 14, pp. 6-8.
113. S. I. Chan, V. C. C. Wang, J. C. H. Lai, S. S. F. Yu, P. P. Y. Chen, K. H. C. Chen, C. L. Chen and M. K. Chan, *Angewandte Chemie-International Edition*, 2007, **46**, 1992-1994.
114. K. Y. Ng, L. C. Tu, Y. S. Wang, S. I. Chan and S. S. F. Yu, *Chembiochem*, 2008, **9**, 1116-1123.
115. S. Grundner, M. A. C. Markovits, G. Li, M. Tromp, E. A. Pidko, E. J. M. Hensen, A. Jentys, M. Sanchez-Sanchez and J. A. Lercher, *Nature Communications*, 2015, **6**.
116. M. J. Wulfers, S. Teketel, B. Ipek and R. F. Lobo, *Chemical Communications*, 2015, **51**, 4447-4450.
117. C. Hammond, N. Dimitratos, R. L. Jenkins, J. A. Lopez-Sanchez, S. A. Kondrat, M. H. ab Rahim, M. M. Forde, A. Thetford, S. H. Taylor, H. Hagen, E. E. Stangland, J. H. Kang, J. M. Moulijn, D. J. Willock and G. J. Hutchings, *Acs Catalysis*, 2013, **3**, 689-699.

118. A. Corma, H. Garcia, G. Sastre and P. M. Viruela, *Journal of Physical Chemistry B*, 1997, **101**, 4575-4582.
119. P. J. Smeets, J. S. Woertink, B. F. Sels, E. I. Solomon and R. A. Schoonheydt, *Inorganic Chemistry*, 2010, **49**, 3573-3583.
120. M. M. Forde, R. D. Armstrong, R. McVicker, P. P. Wells, N. Dimitratos, Q. He, L. Lu, R. L. Jenkins, C. Hammond, J. A. Lopez-Sanchez, C. J. Kiely and G. J. Hutchings, *Chemical Science*, 2014, **5**, 3603-3616.
121. S. Shwan, M. Skoglundh, L. F. Lundegaard, R. R. Tiruvalam, T. V. W. Janssens, A. Carlsson and P. N. R. Vennestrom, *Acs Catalysis*, 2015, **5**, 16-19.
122. R. P. Townsend, *Pure and Applied Chemistry*, 1986, **58**, 1359-1366.
123. K. Seff, *Journal of Physical Chemistry C*, 2010, **114**, 13295-13299.
124. M. Haruta, T. Kobayashi, H. Sano and N. Yamada, *Chem. Lett.*, 1987, 405-408.
125. P. Ratnasamy and R. Kumar, *Catalysis Today*, 1991, **9**, 329-416.
126. R. V. Prikhod'ko, I. M. Astrelin, M. V. Sychev and E. J. M. Hensen, *Russian Journal of Applied Chemistry*, 2006, **79**, 1115-1121.
127. N. Y. Chen, J. Mazuik, A. B. Schwartz and P. B. Weisz, *Oil and Gas J.*, 1968, **66**.
128. P. Borges, R. R. Pinto, M. Lemos, F. Lemos, J. C. Vedrine, E. G. Derouane and F. R. Ribeiro, *Journal of Molecular Catalysis a-Chemical*, 2005, **229**, 127-135.
129. L. E. Sandoval-Diaz, J. A. Gonzalez-Amaya and C. A. Trujillo, *Microporous and Mesoporous Materials*, 2015, **215**, 229-243.
130. G. T. Haller, *Catalysis Reviews-Science and Engineering*, 1981, **23**, 477-504.
131. J. W. Ward, *Journal of Catalysis*, 1970, **17**, 355-358.
132. A. P. Bolton and M. A. Lanewala, *Journal of Catalysis*, 1970, **18**, 1-11.
133. R. M. Lago, W. O. Haag, R. J. Mikovsky, D. H. Olson, S. D. Hellring, K. D. Schmitt and G. T. Kerr, in *Studies in Surface Science and Catalysis*, eds. Y. Murakami, A. Iijima and J. W. Ward, Elsevier, 1986, vol. 28, pp. 677-684.
134. M. Zahmakiran and S. Ozkar, *Langmuir*, 2009, **25**, 2667-2678.
135. E. G. Derouane, J. M. Andre and A. A. Lucas, *Journal of Catalysis*, 1988, **110**, 58-73.
136. E. G. Derouane, *Journal of Molecular Catalysis a-Chemical*, 1998, **134**, 29-45.
137. G. Sastre and A. Corma, *Journal of Molecular Catalysis a-Chemical*, 2009, **305**, 3-7.

138. D. Barthomeuf, *The Journal of Physical Chemistry*, 1979, **83**, 249-256.

139. S. Yashonath and P. Santikary, *Journal of Physical Chemistry*, 1994, **98**, 6368-6376.

140. W. L. Dai, S. S. Zhang, Z. Y. Yu, T. T. Yan, G. J. Wu, N. J. Guan and L. D. Li, *Acs Catalysis*, 2017, **7**, 3703-3706.

2

Experimental

2.1 Materials

The chemicals listed below were used in this study. Reagents were used as received unless stated otherwise.

- Methane (99.999% BOC gases)
- Nitrous oxide (99.997% BOC gases, AA grade)
- Argon (BOC gases)
- Oxygen (BOC gases)
- Iron Acetylacetonate, Fe $(acac)_3$, (99.9%, Sigma Aldrich)
- Copper Acetylacetonate, Cu $(acac)_3$ (99.9%, Sigma Aldrich)
- NH_4-ZSM-5 (SiO_2: Al_2O_3 molar ratio = 23, 30, 50, 80, 280, Zeolyst)
- TS-1 (SiO_2: TiO_2 molar ratio $\geq$ 25, ACS Material)
- Iron (III) nitrate nonahydrate, Fe $(NO_3)_3.9H_2O$ (99.99%, Sigma Aldrich)
- Tetraethylorthosilicate, TEOS (99.999%, Sigma Aldrich)
- Tetrapropylammonium hydroxide, TPAOH (40 wt% in H_2O, SACHEM ZeoGen)
- Methanol (99.9 %, Alfa Aesar)
- Oxalic acid (98 %, Sigma Aldrich)
- Potassium bromide (IR grade, Sigma-Aldrich)

2.2 Definitions

2.2.1 Conversion

CH_4 and N_2O conversion was calculated as follows

$$\mathrm{CH_4\ conversion\ (\%)} = \frac{\mathrm{CH_{4\,in} - CH_{4\,out}}}{\mathrm{CH_{4\,in}}} \times 100$$

where, $CH_{4\ in}$ and $CH_{4\ out}$ represent the molar fraction of CH_4 at the inlet and outlet, respectively.

$$\mathrm{N_2O\ conversion\ (\%)} = \frac{\mathrm{N_2O_{in} - N_2O_{out}}}{\mathrm{N_2O_{in}}} \times 100$$

Where, N_2O_{in} and N_2O_{out} represent the molar fraction of N_2O at the inlet and outlet, respectively.

2.2.2 Methanol Productivity

$$\mathrm{STY} = \mu\mathrm{mol}_{\text{product formed}}\ \mathrm{g}_{\text{catalyst}}^{-1}\ \mathrm{h}^{-1}$$

2.2.3 Product selectivity

The selectivity for product i (S_i) was calculated as follows, coke assumed to be the remainder;

$$S_i\ (\%) = \frac{\text{amount of product (i) produced (mol carbon)}}{\mathrm{CH_4\ converted\ (mol\ of\ carbon)}} \times 100$$

2.3 Catalyst preparation

The commercially available zeolite materials used in this study were activated by converting to the acidic protonated form prior to use by high temperature calcination. An example using ZSM-5 is listed as follows.

NH_4-ZSM-5 (SiO_2:Al_2O_3 molar ratio = 30, 3g) was transferred into a ceramic combustion boat and placed inside a quartz tube within a combustion furnace. The glass tube was then sealed and air was flowed over the catalyst. The furnace was heated to the desired temperature (typically 550 ^oC at 20 $^oC\ min^{-1}$) and held for the desired period

of time (typically 3h). The sample was allowed to cool to room temperature under flowing air prior to any testing or other modifications such as ion exchange with a metal precursor.

A series of catalysts prepared using an ion exchange procedure are listed in the following section. A commercial zeolite material was exchanged once with the desired metal precursor in different synthetic approaches.

2.3.1 Chemical vapour exchange (CVI)

Zeolyst^{TM} H-ZSM-5 (SiO_2:Al_2O_3 molar ratio = 23-280) were used in all catalysts prepared by chemical vapour exchange (CVI). The full procedure for 2 wt. % Fe/ZSM-5 (30) is outlined below.

The desired amount of H-ZSM-5 (1.98 g) and Fe (III) acetylacetonate ($Fe(acac)_3$) (Sigma Aldrich, 99.9% purity, 2.53g) were mixed together thoroughly and transferred to a Schlenk flask. The dry powder mixture was heated to sublimation deposition temperature (150 °C) and heated under continuous vacuum condition (*ca* 10^{-3} mbar) for typically 2 h. The catalyst was then allowed to cool to room temperature before calcining for 3 h at 550 °C at 20 °C min^{-1} under static air.

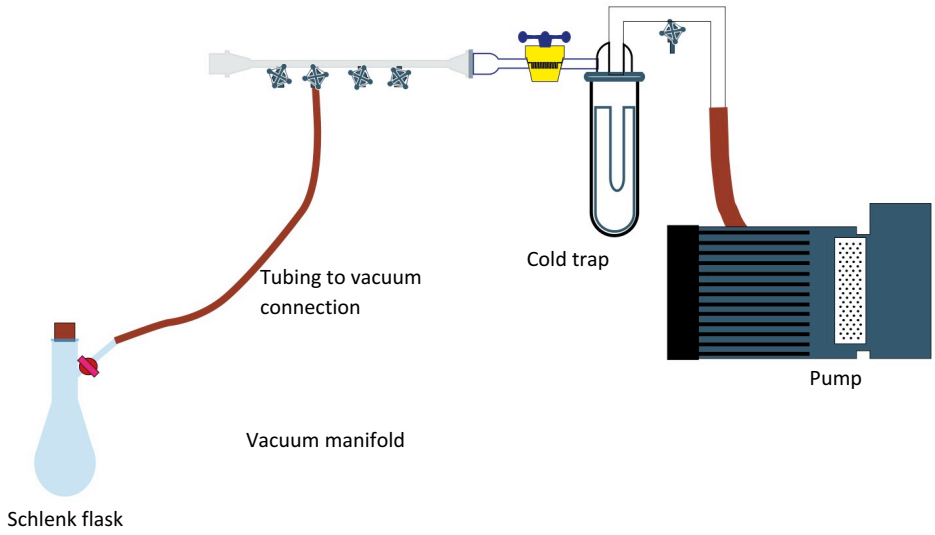

Figure 2.1 The schematic of a CVI set up used in this study.

The Schlenk line system used in this study is shown in figure 2.1. The vacuum manifold system is adopted to carry out the heat treatment of the dry mixture of the metal acetylacetonate precursor and the zeolite support. A mechanical pump is used to provide the vacuum condition (*ca.* 10^{-3} mbar in this set up), which is connected to the vacuum manifold and has a removable stopper at the other end to close the system. This allows easy access to remove any impurities trapped in the Schlenk line. There is a cold trap placed in between the pump and vacuum manifold to prevent any volatile or corrosive vapour from entering the pump that can cause damage and reduce the suction efficiency. Under standard operation, a liquid nitrogen filled Dewar flask is placed directly underneath the cold trap to facilitate its function. The liquid nitrogen forces the vapour and gases from the Schlenk line to condense in the trap and the residue can be later removed and cleaned after use.

Once the pump is turned on and all taps are opened, the Schlenk flask is connected to the vacuum. The tap is then opened gradually to allow a slow reduction of pressure, otherwise the sudden drop in pressure would cause the dry mixture to disperse all over the Schlenk flask and disrupt the ion exchange process.

2.3.2 Solid state ion exchange (SSIE)

The desired amount of metal acetylacetonate was added to H-ZSM-5 (SiO_2/Al_2O_3 molar ratio = 30) and ground with a pestle and mortar for 20 minutes. The dry mixture was then calcined under static air (550 °C, 20 °C min^{-1}) for 3 h.

2.3.3 Impregnation (Incipient wetness) ion exchange

The catalyst was prepared by impregnating H-ZSM-5 (*Zeolyst*^{TM}, SiO_2:Al_2O_3 molar ratio = 30) with an appropriate volume of a $FeCl_3$ solution until incipient wetness (IW) was achieved. The sample was dried for 18 h in an oven at 120 °C and then calcined at 550 °C at 20 °C min^{-1} under static air for 3 h prior to testing.

2.3.4 Hydrothermal synthesis

2.3.4.1 Preparation of silicalite-1 (molar ratio template/Si = 1)

Silicalite-1 was prepared according to Tarramasso *et al.*[1] tetraethyl orthosilicate (20.48 g, 98.8 mmoles) was added dropwise to tetrapropylammonium hydroxide (40 wt. % in H_2O, 25.4 g, corresponding to 10.16 g TPAOH, 49.9 mmoles) while stirring vigorously. The resulting gel was stirred for 5 h at 60 °C. Then the gel was transferred to a Teflon-lined stainless-steel autoclave and crystallised. (175 °C, 48 h). The sample was later recovered by centrifugation, washed with deionised water (1 L) and air-dried (110 °C, 16 h). The dried silicalite was calcined (550 °C, 24 h, 1 °C min^{-1}) in flowing air in order to remove the residual organic template.

2.3.4.2 Preparation of Fe-silicalite-1 (SiO_2/Fe_2O_3 mole ratio = 130 to 500)

Fe-Silicalite-1 was prepared according to Prikhod'ko *et al.*[2] The procedure for a sample with SiO_2/Fe_2O_3 ratio = 260 is exemplified as follows.

Tetrapropylammonium hydroxide (40 wt. % in H_2O, 15 g, corresponding to 6.0 g TPAOH, 30.8 mmoles) was stirred vigorously (25 °C, 1 h), and to this solution tetraethyl orthosilicate (20.48 g, 98.8 mmoles) was added dropwise. The clear gel obtained was subsequently stirred (60 °C, 3 h). At this time, a 10 mL aqueous solution of $Fe(NO_3)_3.9H_2O$ (0.294 g, 0.76 mmoles) and oxalic acid (0.304 g, 2.50 mmoles) was added dropwise to obtain a homogeneous, ferrisilicate gel with the following composition:

SiO_2: Fe_2O_3: $H_2C_2O_4$: TPAOH
1 0.00385 0.013 0.312

The resulting gel was subsequently crystallised in a Teflon-lined stainless steel autoclave (175 °C, 120 h). The as-synthesised materials were later recovered by centrifugation, washed with deionised water (1 L) and air-dried (110 °C, 16 h). The sample was heat treated (550 °C, 8 h, 1 °C min^{-1}) in a flow of nitrogen (5 h) and later air (3h).

2.4 Catalyst characterisation

In this section, the techniques used for materials characterisation are described in detail, in addition to stating the experimental conditions implemented.

2.4.1 Powder X-ray diffraction (XRD)

XRD is perhaps the most widely used technique that allows one to identify the bulk crystal structure of a compound and also estimate the crystallite sizes. X-rays are generated in an X-ray tube by bombarding a target material (Cu, Fe, Mo, Cr) using accelerated high-energy electrons. The electrons located on the inner orbitals of the metal are excited, producing characteristic X-ray spectra when the electrons on the higher valence band drop back to occupy the inner orbital.[3, 4] The wavelengths of the X-rays generated from the metal source are then filtered by crystal monochromaters (nickel filter) to produce the monochromatic X-rays required for diffraction. These X-rays are collimated and hit the sample, which are then scattered by the atomic plane present in the sampling material.

A movable sample detector is used to measure the intensity as a function of angle (θ) of the diffracted radiation at which constructive interference occur.[5] The sample was kept rotating in circular motion during measurement with the intention to maximise the number of particles that contribute to the diffraction. Upon constructive interference, diffraction pattern is produced and from that it is possible to calculate the lattice spacing (d) of the sampling crystallite using Bragg's equation shown as (eq. 2.1).

Bragg's equation:

$$n\lambda = 2d\sin\theta$$

eq. 2.1

where;

n = the order of the reflection (an integer)

λ = the X-rays wavelength

d = the distance between two lattice plane

θ = the angle between the incoming X-rays and the normal to the reflecting lattice plane

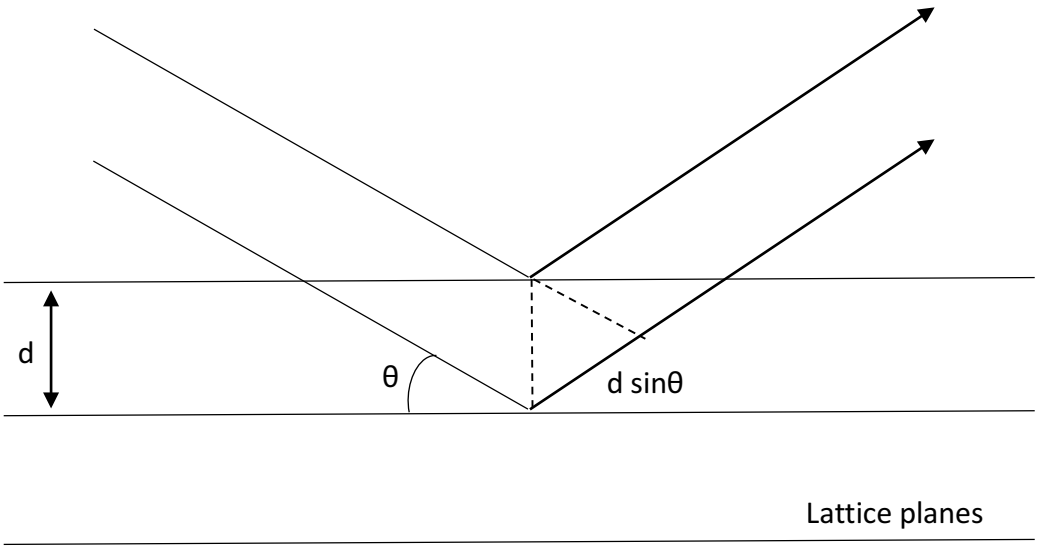

Figure 2.2 The X-rays diffraction on a lattice plane when a constructive interference occurred.

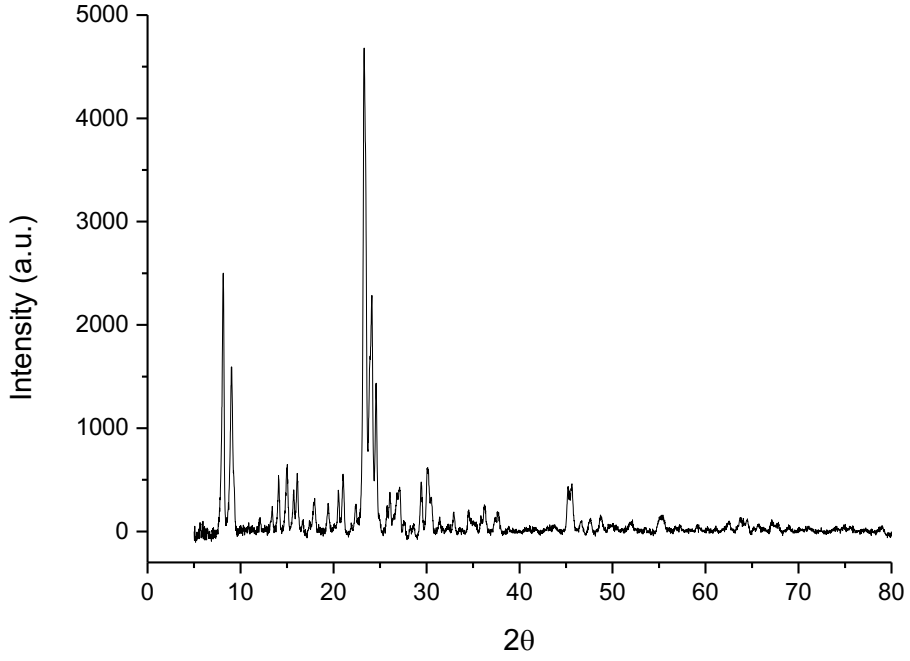

Figure 2.3 Powder XRD pattern of a commercially available zeolite, ZSM-5 (SiO_2:Al_2O_3 = 30) obtained from *Zeolyst*^{TM}.

In this study, XRD is applied for structural determination of zeolites and to identify any loss of structural integrity after series of calcination treatment at high temperature. An illustrative XRD pattern of ZSM-5 (SiO_2:Al_2O_3 = 30) obtained from *Zeolyst*^{TM} is shown in fig. 2.3. Powder X-ray diffraction was performed using a PANalytical X'PertPRO X-ray diffractometer, with a CuKα radiation source = 1.5418Å (40 kV and 40 mA) and Ni filter. Diffraction patterns were recorded in a range of 5 - 80 degrees, 0.0167 ^{o} step size (time / step = 150 seconds). A typical XRD preparation procedure was carried out using a back filled sample holder or with a layer of sample dispersed on a silicon wafer when limited sample was available.

2.4.2 Ultraviolet-Visible spectroscopy (UV-Vis)

UV-Vis involves transitions between energy states upon photon absorption of a molecule in the ultraviolet and visible region of the electromagnetic spectrum. This induces electronic excitation from its ground state to an excited state. This technique is

particularly useful to look at the electronic transitions such as d-d transitions, metal to ligand charge transfer (MLCT) and the ligand to metal charge transfer (LMCT) of a transition metal centre, i.e. Fe species in this study. The Beer-Lambert law stated in equation 2.2 shows that the absorbance of the electromagnetic radiation is affected by both the concentration and path length. As the absorbance is correlated to the concentration of the Fe ions, this could provide quantification of the species providing a known extinction coefficient.

$$A = \varepsilon.[c].l$$

eq. 2.2

Where, A = absorbance

ε = molar extinction coefficient

[c] = concentration

l = path length of the sample cell

There are different types of Fe species present in the Fe-exchanged zeolite catalyst. The information provided by UV-Vis spectroscopy can be used to identify the geometry and the agglomeration of Fe species in the sample. The UV absorption for the isolated Fe^{3+} species at the framework (tetrahedral) and extraframework (octahedral) position appears between 200 to 300 nm.[6, 7] The formation of oligomeric Fe_xO_y clusters is commonly observed through high temperature calcination, which is observed between 300 to 450 nm.[8] The absorption band of > 450 nm represents the bulk iron oxide when high loadings of Fe is used in the ion exchange process.[9]

UV-Vis analysis of powdered sample was performed on an Agilent Cary 4000 UV-Vis Spectrophotometer with a Harrick Scientific Diffuse Reflectance set-up, praying mantis. Samples were scanned between 200 and 800 nm at a scan rate at 400 nm min^{-1}. Prior to analysis, all samples were ground to fine powder using agate pestle and mortar.

2.4.3 Thermogravimetric analysis (TGA)

Thermogravimetric analysis (TGA) is a powerful tool to monitor the compounds that partially decompose and determine the amount and rate of change in the mass of a sample as a function of temperature under a range of different condition (oxidising, reducing and inert environment). The technique analyses the mass gain or loss in samples that undergoes decomposition or oxidation and from which the thermal stability, sample life time and oxidative ability can be determined.

This technique was used to monitor the retained organic species accumulated during methane oxidation. The coke deposited on the catalyst would be oxidised into CO/CO_2 during the TGA run. TGA was performed using a PerkinElmer TGA 4000. Approximately 20-30 mg of the sample was loaded into ceramic crucibles sample holder, heated to 900 °C (at 5 °C/min) under flowing air (50 ml/min) and held for 10 minutes before cooling. For each batch run, a blank $CaCO_3$ run was first carried out to ensure the accuracy of the data.

2.4.4 Brunauer Emmett Teller (BET) isotherm analysis

BET analysis is a commonly used analytical technique to measure the surface area and the pore size of the solid sample by gas adsorption.[10, 11] The catalyst is first degassed under desired condition to remove surface impurities or water bound to the surface before exposing the sample to an inert gas (typically nitrogen) at 77 K. Some of the inert gas will adsorb onto the solid surface and some remains unadsorbed. Adsorption isotherm is used to describe the relationship between the pressure of the inert gas and amount of gas adsorbed on to the surface. The BET equation is as follows in equation 2.3.[12]

$$\frac{P}{V(P_0 - P)} = \frac{C - 1}{V_m C}\frac{P}{P_0} + \frac{1}{V_m C}$$

eq. 2.3

Where;

P = Pressure

P_0 = saturation pressure of the gas

V = volume

V_m = volume of the gas required to form a unimolecular adsorbed layer

C = BET constant

From the BET equation, a plot of $P/ V(P_0-P)$ against P/ P_0 would give a straight line, the intercept will equal to $1/ V_mC$ and the slope of the line of best fit equals $(C - 1)/ V_m C$. This allows the volume of the gas required to form a unimolecular adsorbed layer (V_m) to be determined. V_m is then used to calculate the surface area by multiplying by the area of adsorbed molecule.

Nitrogen adsorption isotherms were collected on a Micromeritics 3Flex. Samples (*ca.* 0.020 g) were degassed (150 °C, 6 h) prior to analysis. Analyses were carried out at 77 K with P_0 measured continuously. Free space was measured post analysis with He. Pore size analysis was carried out using Micromeritics 3Flex software, N_2-Cylindrical Pores Oxide Surface DFT Model.

2.4.5 Scanning electron microscopy (SEM)

Scanning electron microscopy provides information on the size, composition and topology of a sample. An image is produced by scanning a high energy beam of electrons over the catalyst surface which interacts with atoms at various depth within the sample. The electron beam is generated from a field emission gun (FEG) which is composed from fine single crystal of tungsten. The resulting interaction leads to different signals to be produced including secondary electrons, reflected or back-scattered electrons, characteristic X-rays and light (cathodoluminescence) (CL), absorbed current (specimen current) and transmitted electrons. SEM is commonly equipped with a secondary electron detector which is used to analyse the secondary electrons for constructing images of the sample.

Energy Dispersive X-ray (EDX) analysis is used in combination with SEM to obtain information on elemental composition and their distribution. SEM was performed on a

Tescan Maia3 field emission gun scanning electron microscope (FEG-SEM) fitted with an Oxford Instruments XMAXN 80 energy dispersive X-ray detector (EDX). The sample was dispersed as a powder onto carbon Leit discs mounted onto aluminium stubs. The stubs were then sprayed with a 8nm Au:Pd (80:20 ratio) coating before scanning. Images were taken using the secondary electron and backscattered electron detectors at varying magnification and field view.

2.4.6 Temperature programme desorption (TPD)

Temperature-programmed desorption (TPD) is a technique used to study surface reactions and molecular desorption between the catalyst surface and the probe molecule. The experiment involves saturating the sample surface with the probe molecule at ambient temperature and heating the sample in a controlled manner (linear temperature ramp rate). The molecule desorbed from the surface of the sample into the gas phase is monitored simultaneously.

Adsorption of base molecules such as ammonia, quinolone and pyridine are often used to measure the concentration and strength of the acid sites on solid zeolite catalysts which are reflected in the peak area and desorption temperature, respectively.[13] The relative number and strength of acid sites on different catalysts were estimated following the same TPD experimental conditions.

TPD of ammonia for the zeolites was carried out in a conventional flow apparatus (Chembet TPR/TPD Chemisorption analyser, Micromeritics Inc.). The sample (0.05 g) was loaded in a U-type tube and sandwiched between quartz wool. The samples were pretreated at 550 °C with a He flow of 145 mL min^{-1} for 1 h to remove residual water and was allowed to cool to room temperature. Ammonia adsorption was carried out by flowing 5% NH_3 in Ar to the sample tube for 15 min. The physisorbed ammonia and excess in the sample tube was removed by heat treating the sample tube to 100 °C at 15 °C min^{-1} under a flow of helium (145 mL min^{-1}) for 1h. The TPD signal for the desorption of chemisorbed ammonia was recorded while ramping from 100 to 900 °C at 10 °C min^{-1} under a flow of helium (145 mL min^{-1}) with a thermal conductivity detector (TCD).

2.4.7 Diffuse Reflectance Infrared Fourier Transform Spectroscopy (DRIFTS)

Fourier transform infrared spectroscopy is a commonly used vibrational spectroscopy and is used to determine the force constraints and bond length of a molecule.

IR active molecules (molecule associated with changes in dipole moment) can vibrate in different ways and the characteristic vibrational frequencies can be identified upon IR absorption. When IR radiation is passed through and being absorbed and transmitted by the sample, a molecular fingerprint spectrum of the sample is produced.[3] Different spectral fingerprints can be produced when molecular possess different chemical structure.

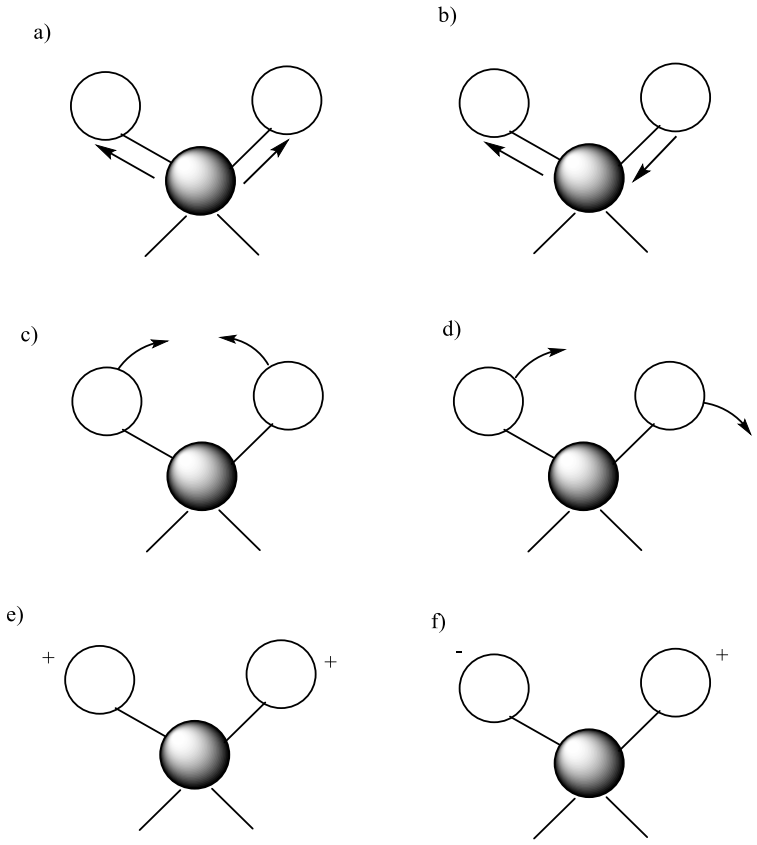

Figure 2.4 Vibrational modes occurs upon IR absorption: a) symmetric stretching, b) asymmetric stretching, c) scissoring, d) rocking, e) wagging and f) twisting.

The OH bond strength present in zeolite (i.e. Si-OH group) can be measured directly using IR which makes it a powerful tool for characterising the intrinsic strength of zeolite. Acidity of zeolite materials can be obtained from studies of using adsorbed molecules. Pyridine, quinolone, acetonitrile etc. are widely used sorbed molecules for determining both Lewis and Brønsted acid sites at the same time. DRIFTS allows fine

powder sample to be measured very easily due to very little to no sample preparation. It eliminates the requirement for KBr (typically used as a blank) to be pressed in a pellet form. The sample will be placed in a sample holder which allows fast sample changing/clean up.

Pyridine adsorption experiments were carried out as follows:

Samples were pretreated prior to acquisition by heating the sample in a Harrick Praying Mantis *in situ* cell to 550 ° C (20 ° C min^{-1}) under flowing nitrogen for 1 h to remove residual water. After the heat treatment, the sample was left to cool down to room temperature before pyridine was introduced to the cell for 5 min. The excess pyridine in the cell was removed by vacuum (10^{-3} mbar) for 5 min and IR spectra were recorded at different temperatures in the range of 30−600 °C under continuous vacuum. The scan was taken 5 min after reaching each of the desired set temperatures.

For *in situ* heat treatments a Harrick automatic temperature controller heater was used in heating the sample cell according to a predefined (20 °C min^{-1}) heating program. Gas flows were passed through the sample, with flow rates (60 mL min^{-1}) controlled by a Brooks MFC. IR spectra were collected on a Bruker Tensor 27 spectrometer (4000 cm^{-1} - 500 cm^{-1}, 4 cm^{-1} frequency, 64 scans) fitted with a liquid N_2 - cooled Mercury Cadmium Telluride (MCT) detector. The samples were placed within a Praying Mantis high temperature diffuse reflection chamber (HVC-DRP-4) *in situ* cell fitted with calcium fluride windows. Background scans were recorded using dry KBr.

2.4.8 Magic angle spin nuclear magnetic resonance (MAS-NMR)

MAS-NMR is a technique which provide information on the chemical environment and dynamics in solid materials. It studies molecules with a magnetic moment where the nucleus contains an uneven number of protons/neutrons. Unlike solution NMR where the anisotropic interaction is averaged by rapid tumbling of the molecules, the interactions such as chemical shift and dipolar coupling dominates in solid state NMR and give rise to broad nuclei spectral line width. This is overcome by rapidly rotating the solid sample around an axis and spun at the magic angle $\theta_m = 54.74°$ with the static field.[14] This allows high resolution spectra to be obtained in solid state.

^{27}Al MAS-NMR spectra were performed in this study to investigate the extent of dealumination of the FeZSM-5 after high temperature calcination. The samples were

measured at the Solid-State NMR Group, Durham University in England, by Dr David Apperley. The samples were run as-received on a 400 MHz Varian VNMRS spectrometer. Pencil rotors were used as sample holders and were spun on a bearing of dry air. ^{27}Al NMR spectra were recorded using a 4 mm probe at a resonance frequency of 104.198 MHz. The rotors were spun at a speed rate at 14049 Hz with pulse lengths of 1 μs and subtracted background signal from all sample spectra.

2.5 Catalyst testing

2.5.1 Set up of gas phase reactor

Catalyst testing for the oxidation of methane under continuous gas flow system using $N_2O/O_2/H_2O$ as oxidants was carried out in a custom-built gas phase reactor, the schematic of which is shown in figure 2.5.

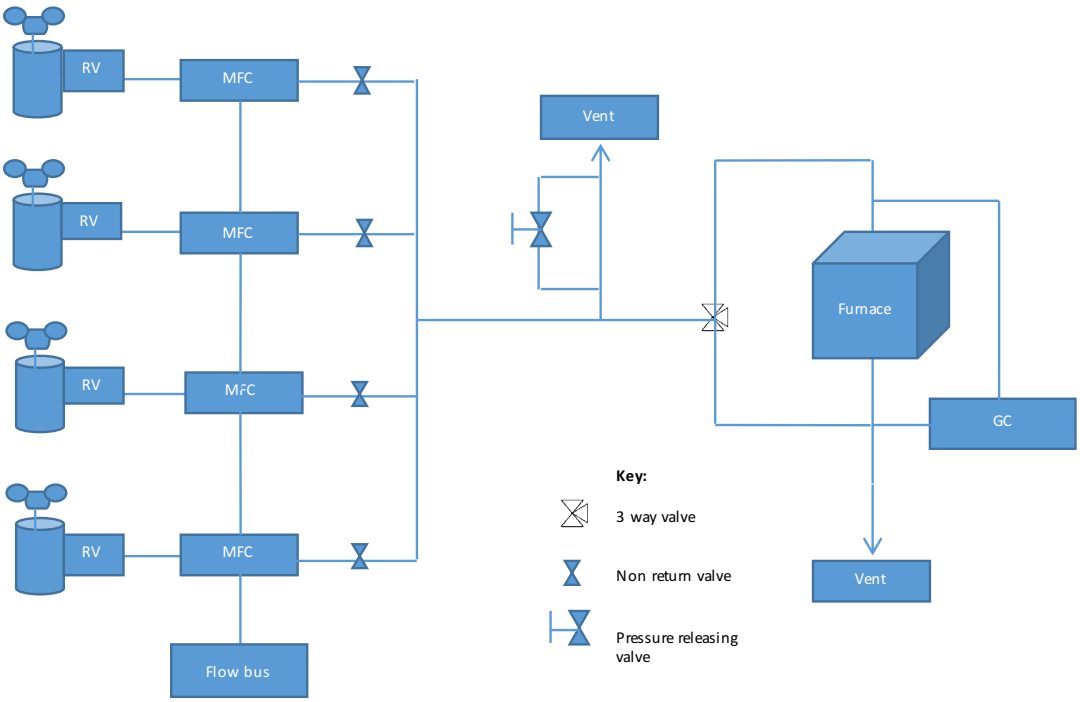

Figure 2.5 The schematic diagram of the custom-built gas phase reactor.

The custom-built continuous flow reactor was designed for methane oxidation using Swagelok fittings. The Swagelok reactor tubing has an internal diameter of 3/8 inch.

The gas flow for CH_4, Ar, N_2O and O_2 were controlled using four mass flow controllers (MFCs, Bronkhorst), which is all connected to a flow bus (central flow control station) that allows the digital communication between digital devices and a PC. The pressure of each flowing gas was maintained at 2 bar using backpressure regulators.

2.5.2 Oxidation of methane with N_2O

The specific reaction conditions were varied throughout the investigation. A typical reaction procedure is exemplified as follows: Prior to testing, the system is purged using argon for 30 min to remove any residual gas that could remain in the stainless steel tubing. The catalyst is first pelleted and sieved (20 - 40 mesh). The pelleted catalyst with desired volume (0.9 ml, typically 0.44 g) is then transferred into a stainless steel reactor tube and is held in the middle of the tube sandwiched by two pieces of quatz wool.

In a typical methane oxidation reaction the feed mixture comprised of 20 % CH_4 + 2 % N_2O with Ar balance (total flow rate = 55 mL min^{-1}, typically GHSV = 3600 h^{-1}) at 1 atm pressure. The reaction temperature (typically 300 °C) was controlled by an isothermal oven (± 1 °C) with a thermocouple located directly above the catalyst bed. The products from the reactions were analysed using a Agilent GC. The details of the methods used in production detection are given in Chapter 2.6. After each reaction, the reactor tube was clean thoroughly with deionised water and dry at 140 °C for 12 h before carrying out a new experiment.

2.5.3 Oxidation of methane with N_2O and H_2O

Methane oxidation reactions were also performed in a stainless steel conventional flow setup in the presence of water in a similar procedure described above. The desired amount (typically 0.44 g) of catalyst (20-40 mesh) was placed in a stainless steel tube sandwiched between two quartz wool plugs. The addition of water to the reaction stream was carried out using a syringe pump (Sono-Tek, Syringe Pump TI). The total flow rate of the feed mixture in the presence of water was kept at 55 $mLmin^{-1}$, containing 20 % CH_4 + 20 % H_2O + 2 % N_2O (Ar balance) at atmospheric pressure and were controlled by mass flow controllers (Bronkhorst UK Ltd).

2.5.4 Sequential oxidation of methane with N_2O and O_2

For the sequential methane oxidation reaction, a similar set up described in 2.5.2 was adopted. The starting reaction feed mixture comprised of 20 % CH_4 + 2 % N_2O with Ar balance (total flow rate = 55 mL min^{-1}, typically GHSV = 3600 h^{-1}) at 1 atm pressure in the first 120 min. Then the N_2O is substituted with the same volume percentage of O_2 in the same gas mixture with CH_4 and Ar at 55 $mLmin^{-1}$.

2.6 Product analysis and quantification

2.6.1 Gas chromatography (GC) - Introduction and theory

Gas chromatography (GC) is used for separating a mixture of chemicals and is widely used as an analytical tool that provides both qualitative and quantitative information on the individual component of the mixture. The sampling method often involves using an inert carrier gas such as helium or argon (mobile phase) to transfer a portion of the sample gas mixture into the packed column through a sample loop. If the sample is a liquid phase substance, it will be vaporised before going into the column. The column is known as the stationary phase that consists of a microscopic layer of varying polarity supported on an inert material. It is kept at a specific temperature by the oven.

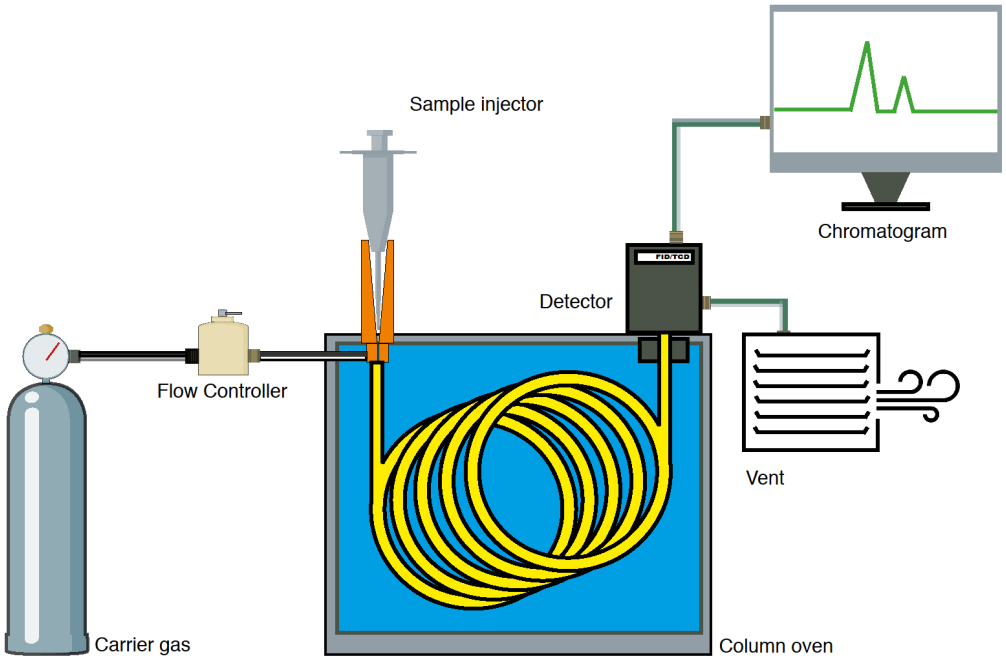

Figure 2.6 Schematic diagram of a typical chromatography system.

The separation of the sampling mixture is carried out through the column at different rate. The interaction between the individual compound and the stationary phase would allow component to be retained in the column for different amounts of time (retention time) and is characteristic to a certain molecule. The strong the interaction results in higher retention time and this allows the separation of the mixture into its individual constituents at a different rate.

The carrier gas flow rate affects how long the components remain in the column. Higher flow rates allow faster analysis but can also lower the separation between analytes. Packed column and capillary column are two types of commonly used separation columns. Packed column is made of glass/stainless steel tube that filled with finely divided inert support material coated with stationary phase. Capillary column is made of flexible material with internal diameter at a very small scale with its internal wall coated with stationary phase. This type of column offers higher efficiency, able to be used on smaller sample size and much longer for the length of the column. The oven temperature for the column is used to control the speed of the analysis. A lower oven temperature results in the greatest separation but requires long elution time and vice

versa. The flow rate of carrier gas, type of carrier gas used, column temperature, type of column used and oven temperature setting are the factors that can all be adjusted and optimised in order to achieve the most efficient separation of reaction mixture.

There are two types of detector used for the GC in this study, flame ionisation detector (FID) and thermal conductivity detector (TCD). FID detects compounds through pyrolysis, for instance, the separated compound passed through a flame that leads to the oxidation of the compound and forms fragments which can be detected between oppositely charged plates. This information is then plotted as chromatogram. The compound is identified through its retention time by comparing it to a standard and quantified by calculating the area of the trace against a calibration of the known concentrations of the compound. A TCD measures the difference in the thermal conductivity of the separating component and carrier gas. There are two sample cells in the detector, signal is produced when a difference in heat conductivities is detected from flowing pure carrier gas (reference cell) and component from the sample mixture (sample cell) passing through the TCD.

2.6.2 GC setup for gas analysis from methane oxidation reaction

GC analysis was performed using a customised Agilent 7890B analyser consists of two analytical channels. 1) A front capillary channel (Porabond 25 m in length, 0.32 mm inner diameter) with a FID sampling valve; and 2) A back permanent gas channel with a methaniser unit fitted with a FID and TCD detector. A schematic for the two channels are shown in figure 2.7 and 2.8.

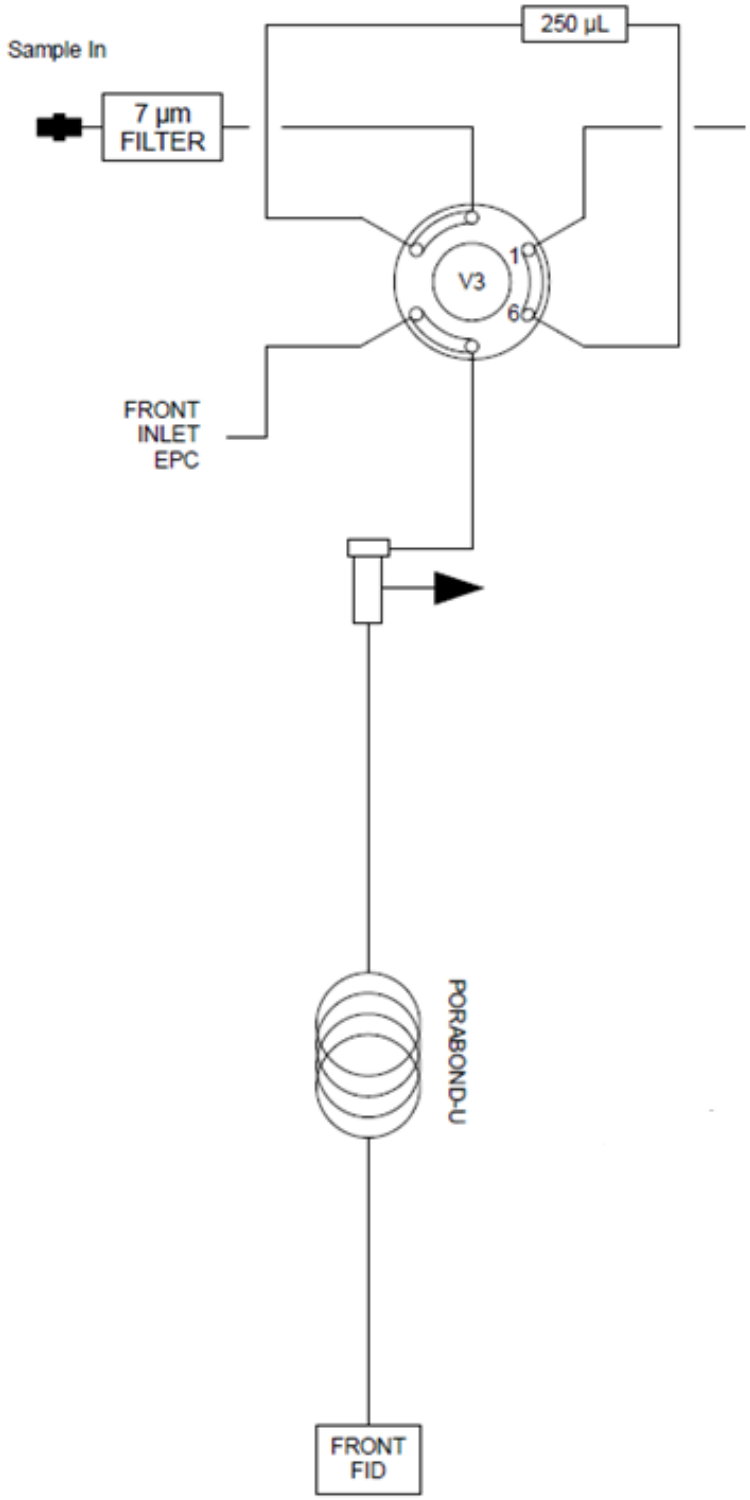

Figure 2.7 A schematic of the custom built gas chromatography setup (channel 1) used in this study.

Channel 1) Capillary Channel with Gas Sampling Valve (FID):

Channel 1 consists of the following components:
- Gas Sampling Valve (Valve 3)
- Inert Sample Loop (250 μL)
- Split Injector (Front)
- Front Inlet EPC (helium)
- Capillary column (Main GC oven)
- Flame Ionisation Detector (Front)

When Valve 3 is fired, the contents of the sample loop are sent to the split injector by the front inlet carrier flow. The carrier gas used in channel 1 is helium. The sample is split at the injector and transferred to the capillary column, separated and eluted to the FID.

The permanent gas channel columns are mounted in a separate oven in the side pneumatics compartment, the split ratio, column flow rate and main oven temperature program can be set as desired. The installed PoraBond capillary column can be replaced with different capillary column for other applications if required.

The total flow through the split injector is kept above 30 ml/min during the injection for a fast transfer of the sample from the loop to the column. Valve 3 in the on position for about 30 seconds after injecting.

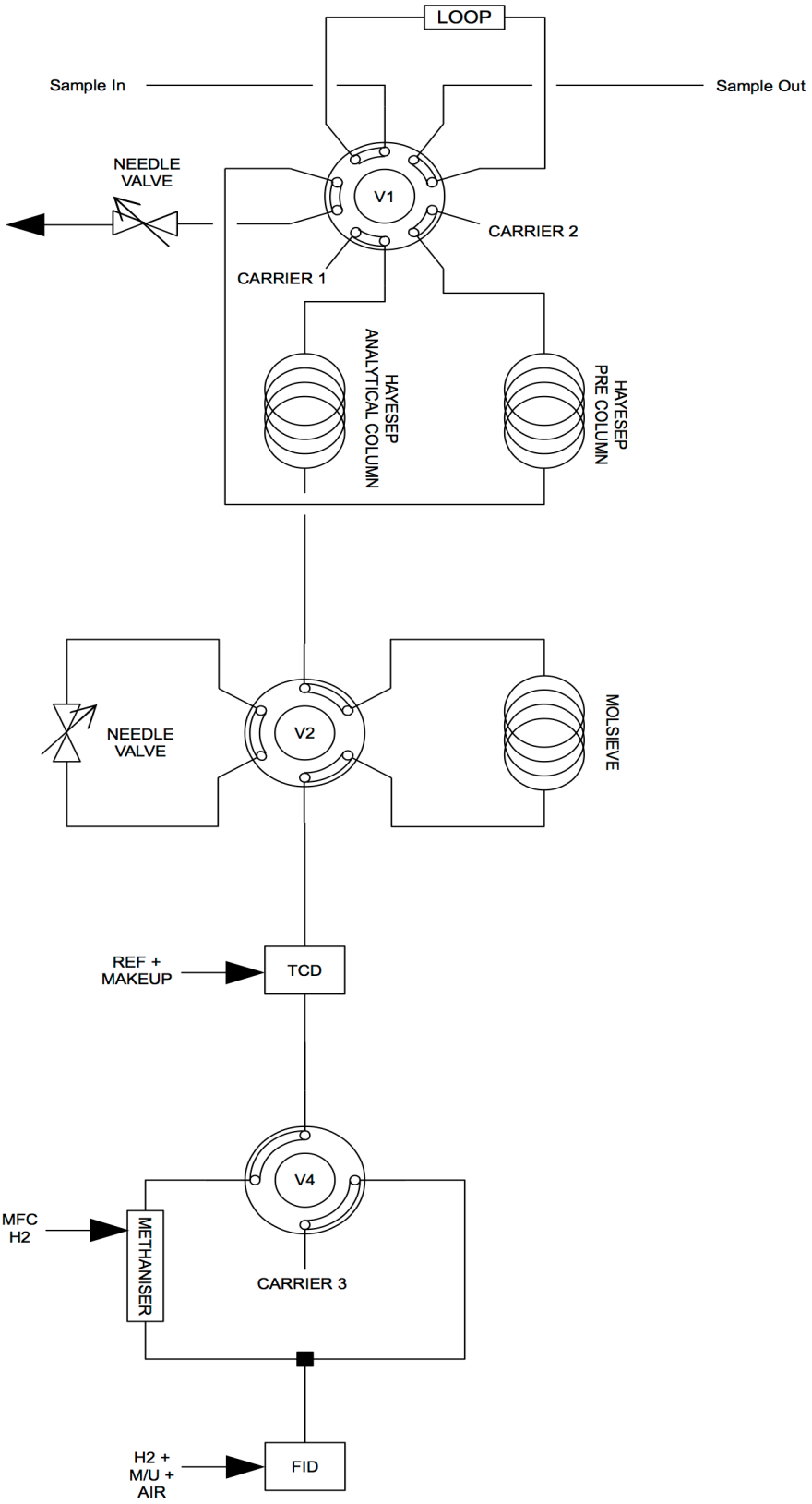

Figure 2.8 A schematic of the custom built gas chromatography setup (channel 2) used in this study.

Channel 2) Back permanent gas channel with a methaniser unit fitted with a FID and TCD detector.

This channel consists of the following components:
- Gas Sampling Valve with Backflush to Vent (Valve 1)
- Sample Loop (1000 μL)
- Aux EPC 1,2 and 3 (argon)
- Two Hayesep Packed Columns (on Valve 1)
- Series-Bypass Valve with Variable Restrictor (Valve 2 and VR 2)
- Molecular Sieve Packed Column
- Thermal Conductivity Detector (Aux/Side)
- Methaniser Bypass Valve (Valve 4)
- Methaniser (Back Injector Position)
- Flame Ionisation Detector (Back)

When Valve 1 is fired, sample is transferred from the sample loop to the first Hayesep column. Analytes of interest elute to the second Hayesep column. Valve 1 then switches off to backflush the heavier analytes to vent. The air, methane and carbon monoxide analytes elute to the Molecular Sieve column. Valve 2 then fires to isolate the Molecular Sieve, trapping the analytes. The remaining analytes elute from the second Hayesep column, bypassing the Molecular Sieve. Once theses analytes have been detected at the TCD, Valve 2 switches off and releases the trapped analytes which are now separated into molecular oxygen, nitrogen, methane and carbon monoxide. These analytes are also detected at the TCD. Analytes passing the TCD now either pass through or bypass the methaniser (nickel catalyst), depending on the position of Valve 4 (OFF = methaniser in line). The methaniser reduces carbon monoxide and carbon dioxide to methane allowing trace amounts to be detected.

The methaniser is only switched into flow when carbon dioxide and carbon monoxide are eluting to avoid unnecessary contact with potential water molecule in the line which would damage the lifetime of the methaniser. All analytes then elute to the FID detector. The FID have greater sensitivity for hydrocarbons than the TCD therefore the hydrocarbon signals used for data analysis came from FID.

The packed columns are mounted in the small side oven controlled by the external temperature controller on the front of the side compartment and is kept to 50°C at all times. The carrier gas used in channel 2 is argon.

All the detectable gases from the reaction outlet were quantified against a calibration curve constructed from commercial standards and a known quantity of gas pre-mixed using MFCs. An illustrative calibration curve for CO_2 is presented in figure 2.10.

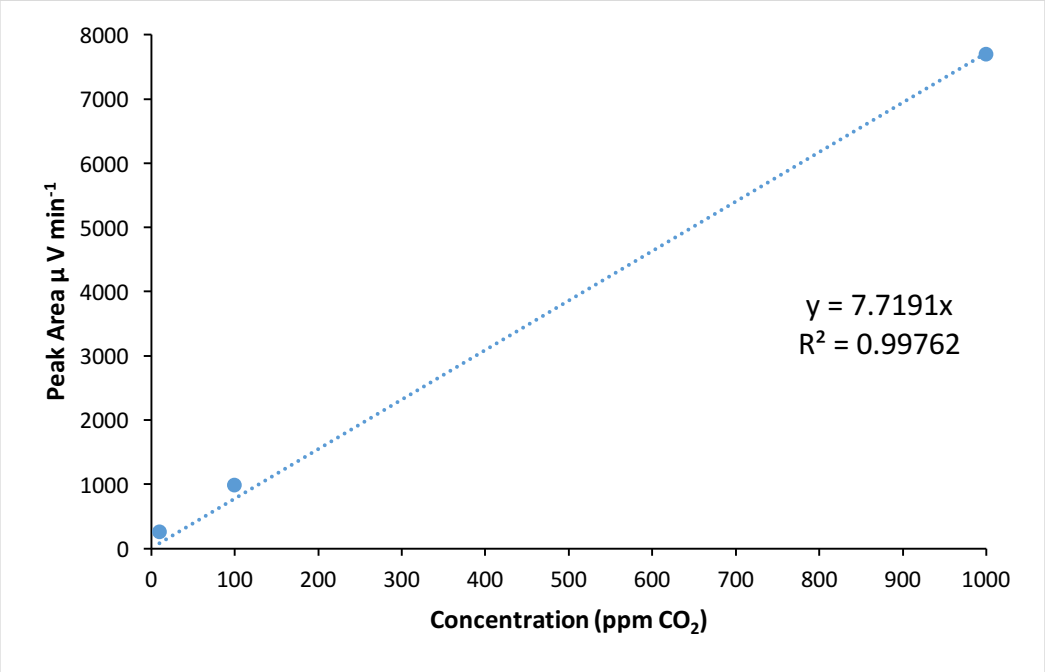

Figure 2.9 Illustrative calibration curve obtained for CO_2.

2.7 References

1. M. Taramasso, G. Perego and B. Notari, Preparation of porous crystalline synthetic material comprised of silicon and titanium oxides, United States Patent 4410501, 1982.
2. R. V. Prikhod'ko, I. M. Astrelin, M. V. Sychev and E. J. M. Hensen, *Russian Journal of Applied Chemistry*, 2006, **79**, 1115-1121.
3. J. W. Niemantsverdriet, *Spectroscopy in Catalysis: An Introduction*, Wiley, 2000.
4. G. C. Bond, *Heterogeneous catalysis : principles and applications*, Clarendon Press, Oxford [Oxfordshire]; New York, 1987.
5. J. W. Niemantsverdriet, in *Spectroscopy in Catalysis*, Wiley-VCH Verlag GmbH & Co. KGaA, 2007, pp. 147-177.
6. E. J. M. Hensen, Q. Zhu, M. M. R. M. Hendrix, A. R. Overweg, P. J. Kooyman, M. V. Sychev and R. A. van Santen, *Journal of Catalysis*, 2004, **221**, 560-574.
7. E. J. M. Hensen, Q. Zhu, R. A. J. Janssen, P. Magusin, P. J. Kooyman and R. A. van Santen, *Journal of Catalysis*, 2005, **233**, 123-135.
8. A. S. Kumar, J. Perez-Ramirez, M. N. Debbagh, B. Smarsly, U. Bentrup and A. Bruckner, *Applied Catalysis B-Environmental*, 2006, **62**, 244-254.
9. J. Perez-Ramirez, M. S. Kumar and A. Bruckner, *Journal of Catalysis*, 2004, **223**, 13-27.
10. G. Leofanti, M. Padovan, G. Tozzola and B. Venturelli, *Catalysis Today*, 1998, **41**, 207-219.
11. F. Rouquerol, J. Rouquerol and K. Sing, in *Adsorption by Powders and Porous Solids*, Academic Press, London, 1999, pp. 27-50.
12. S. Brunauer, P. H. Emmett and E. Teller, *Journal of the American Chemical Society*, 1938, **60**, 309-319.
13. R. C. Deka, *Indian Journal of Chemical Technology*, 1998, **5**, 109-123.
14. T. Poenova, R. Gupta and A. Goldbourt, *Analytical Chemistry*, 2015, **87**, 5458-5469.

3

Investigating the influence of acid sites in continuous methane oxidation with N_2O over Fe-MFI zeolite

The goal of this chapter is to firstly identify the different Fe species present in the intra-framework and extra-framework and secondly the role of the different acid sites (*i.e.* Lewis and Brønsted) which may be involved in the catalytic oxidation of methane in the presence of N_2O over Fe/ZSM-5. The utilisation of molecular oxygen from the industrial point of view is desirable as it is more economical. Therefore, the use of oxygen was investigated and compared to reactions with N_2O.

3.1 Introduction

Panov and co-workers are the pioneers who reported the use of Fe/ZSM-5 and N_2O to form active α-oxygen species to activate methane.[1, 2] The α-oxygen species were generated by decomposing N_2O over the reversible redox α-Fe sites, which switch from Fe^{2+} to Fe^{3+} as shown in equation 3.1.[3] The radical, anionic nature of the α-oxygen species allows the cleavage of the methane C-H bond *via* the hydrogen abstraction mechanism that occurs readily at room temperature (Eq. 3.2).[4]

$$N_2O + (Fe^{2+})_\alpha \rightarrow (Fe^{3+} - O^{-})_\alpha + N_2 \qquad \text{(Eq. 3.1)}$$

$$CH_4 + 2(O^{-})_\alpha \rightarrow (OH)_\alpha + (OCH_3)_\alpha \qquad \text{(Eq. 3.2)}$$

$$(Fe^{2+} - CH_3OH)_\alpha \rightarrow (Fe^{2+})_\alpha + CH_3OH_{ads} \qquad \text{(Eq. 3.3)}$$

The methoxy (CH_3O) and hydroxyl (OH) groups formed after cleaving the methane C-H bond are subsequently adsorbed on the α-Fe sites, which can yield methanol directly on the surface of the zeolite through the recombination of the two groups (Eq. 3.3). This process is quasi-catalytic at low temperatures, as methanol must be extracted from the catalyst surface *via* hydrolysis using solvent extraction.[2, 3] However, at temperature above 300 °C methanol desorbs and the process is catalytic.[5]

The true nature of the active site is still debated and is considered to be comprised of either mono-nuclear Fe^{4+}=O (or Fe^{3+}-O^{-}) or di-nuclear Fe containing oxo-bridged $Fe^{3+}O^{2-}Fe^{3+}$ species[6]. Synder *et al.*[7] recently reported mononuclear α-Fe^{2+} in an extra-lattice site within Fe zeolite beta (Fe/BEA) from magnetic circular dichroism spectroscopy. The reactive intermediate generated in Fe/BEA was described as having a high spin Fe^{4+}=O species, whereby the confinement of the zeolite lattice facilitates the reactivity observed. Hutchings and co-workers reported a di-nuclear Fe sites in Fe/ZSM-5, derived from EXAFS measurements and these Fe sites were considered to be the active component for methane oxidation using H_2O_2 under liquid phase reaction.[8, 9] Furthermore, Dubkov *et al.*[10] reported that adjacent Fe^{2+} atoms can behave as mono-nuclear sites when transformed to Fe^{4+}=O on the formation of the active oxygen species upon decomposition of N_2O on Fe/ZSM-5, using Mössbauer spectroscopy. Reports from similar research method on methane oxidation, have shown that carbon oxides were mainly formed and the desired oxygenates such as methanol, dimethyl ether (DME), acetaldehyde and other hydrocarbons such as ethane were also produced.[3, 5] Catalyst fouling resulting from coke formation were also observed in post-reaction samples.[5, 11] At temperature below 300°C, DME is observed in the gas phase. This secondary product was considered to form due to a prolonged binding period of methanol on the surface of Fe/ZSM-5.[5] However, under the catalytic regime at higher temperatures (*ap.* 300 °C) reported from the same groups, DME was not detected in the gas-phase and was proposed to be the precursor to catalyst fouling. Therefore, methanol can either desorb directly from Fe/ZSM-5 or accumulate on the zeolite surface

depending on the reaction temperature.[5] It was reported that the activation energy of the surface diffusion of adsorbed species is much lower than the activation energy of desorption on ZSM-5, implying that it is more favourable for the adsorbed methanol to diffuse across to other acid-sites on the zeolite and carry out further reactions to form coke.[5, 12]

The Brønsted and Lewis acid sites both play a role in methane oxidation. Narsimhan *et al.* reported the presence of Brønsted acid sites results in higher specific activity and space-time-yield (STY) for the Cu-containing zeolite with different topology such as ZSM-5 and mordenite. Furthermore, the apparent activation energy in the case of the protonated form of Cu/ZSM-5 was calculated to be approximately 30 $kJ.mol^{-1}$ higher from its Na analogue.[13] The Lewis acid sites are formed in the zeolite framework by exchanging with a metal precursor or through high temperature/steam treatment to cause dealumination.[14] This allows metal ions, for example the commonly used Fe, Cu, Co, to incorporate into the internal-framework position and/or extra-framework positions. The extra-framework Lewis acid species can increase the acid strength and the catalytic activity of zeolites due to an interaction with the Brønsted Si(OH)Al sites.[15, 16] It was reported that Lewis acid sites were required for the hydroxylation of benzene with N_2O yielding 70-80% phenol with high selectivity and regioselectivity.[17] The two types of acid sites, in the zeolite, catalyse a wide range of chemical reactions currently used in industry from alkylation and isomerisation of hydrocarbons, cracking and hydrocracking processes.[14]

In this chapter, the continuous methane oxidation over Fe exchanged MFI framework zeolites was investigated with various acidity profiles using N_2O as a mild-oxidant. The combination of Fe and Al are required to activate methane. However, the presence of Al also provides a competing reaction path which is similar to the methanol-to-olefin (MTO) type reaction mechanism. This undesired side reaction path converts methanol to ethene and active aromatic intermediates in zeolites. Characterisation carried out such as NH_3-TPD and pyridine adsorption techniques confirms the importance of acidity for the activation of methane, demonstrated by calcining a series of MFI-based zeolites at different temperatures. Furthermore, methanol control experiments and temperature programmed desorption (TPD) experiments were carried out to understand

the complex reaction mechanism present in the continuous, one step-oxidation of methane by N_2O.

3.2 The effect of Fe and Al in MFI structure

The influence of both Fe and Al on the reaction of CH_4 with N_2O was investigated by preparing several catalysts that possess the MFI zeolite structure. The performance of the tested catalysts (SIL-1, HZSM-5 (30), TS-1, 0.5 wt. % Fe/SIL-1, 2 wt.% Fe/ZSM-5 and 2 wt.% TS-1 along with a blank reaction carried out with no catalyst present are summarised in Table 3.1. The Fe-exchanged MFI zeolites have been reported to be successful in producing methanol from methane under both static[26] or continuous operation.[5] The Fe/MFI catalysts were compared to their corresponding parent zeolites (Table 3.1 and figures. 3.1 - 3.4) over 2 h.

Table 3.1: Comparison of MFI catalysts for methane oxidation with N_2O.

Catalyst	Conversion[a] (%)		Selectivity[a] (%)						STY[b] $_{MeOH}$ (μmol. g_{cat}^{-1} h^{-1})
	N_2O	CH_4	MeOH	CO	CO_2	C_2H_4	DME	Coke	
Blank tube	-	-	-	-	-	-	-	-	-
SIL-1	-	-	-	-	-	-	-	-	-
HZSM-5 (30)	2.3	0.15	0.6	56.3	14.4	8.8	-	19.9	0.55
TS-1	-	-	-	-	-	-	-	-	-
0.5 wt. % Fe/SIL-1	2.0	0.19	0.3	77.5	22.0	-	-	0.2	0.28
2 wt. % Fe/ZSM-5	21.5	1.8	1.1	24.3	9.5	3.5	-	62.6	6.4
2 wt. % Fe/TS-1	0.4	<0.05	-	17.7	82.3	-	-	<0.5	-

Reaction conditions: 0.44 g catalyst; Pellet Mesh size = 600 μm; V = 0.9 mL; 300 °C; 2 h; Feed mixture: 20%CH_4 + 2% N_2O with Ar balance; Flow rate = 55 mL.min^{-1}; P(total) = 1 atm; GHSV= 3600 h^{-1}. [a] Values after 1 h on-stream; [b] STY_{MeOH}: space time yield of methanol.

The parent SIL-1 and TS-1 zeolites were shown to be inactive for methane conversion. In the case of H-ZSM-5, a low conversion is observed which can be attributed to metal impurities, such as Fe introduced during the hydrothermal zeolite synthesis. Indeed, it is well known that the preparation of metal impurities-free zeolite is extremely difficult and it is common to find Fe impurities in "metal free" commercial zeolite support.[18] Metal impurities are present in the alumina precursor used for the synthesis.[8, 18] Fe-impurity can be present at approximately 100s ppm level and despite being located in framework positions it can activate C-H bonds in the presence of H_2O_2.[8]

The addition of Fe to the parent MFI zeolites clearly illustrates that the reaction environment has a significant impact on the activation of methane. For the Fe/SIL-1, the Fe was introduced during the zeolite synthesis stage and 0.5 wt. % loading is a compromise to obtain Fe containing samples with an MFI structure. There were numerous experiments carried out to try to incorporate higher Fe weight loading (*i.e*. 2 wt.%), however during the synthesis process, the so-gel appeared to turn into a solid gel as soon as higher concentration of Fe precursor (Iron III nitrate used) was mixed with the silica precursor. The subsequent crystallization process was prevented from taking place and may imply that there is a limited maximum number of Fe ions that can be allowed to be incorporated into the silicalite framework during the exchange-process.

In the case of Fe/ZSM-5 and Fe/TS-1 samples, the Fe was introduced post-synthesis *via* CVI with their corresponding commercially available zeolite. In each case, the samples were characterised by UV/vis spectrometry to assess the Fe speciation and location within the MFI structure (Fig. 3.5 – 3.6) For both, Fe/SIL-1 and Fe/TS-1, only very low degree of methane and N_2O conversion was recorded. Indeed, the activation of N_2O is a key marker to indicate the likely presence of either Fe^{4+}=O or $Fe^{3+}O^{2-}Fe^{3+}$ sites, which were reported to be part of the active methane oxidation sites.[9] The titanium silicate, TS-1 is comprised of TiO_4 and SiO_4 tetrahedral units. The absence of Al in the TS-1 sample indicate that there is no Brønsted acid sites presence, as TS-1 does not required the extra-proton to achieve the charge neutrality, and only contain Lewis acid sites. Table 3.1 illustrates that the TS-1 based materials are inactive for methane oxidation. Therefore, the combination of Fe and framework Al in the Fe/ZSM-5 catalyst can activate methane, although the selectivity to methanol was found to be low, *i.e.* 1.1 %, with the best tested catalyst *i.e.* 2 wt.% Fe/ZSM-5. Furthermore, it is found that the

poor mass balance with *ca.* 63 % selectivity to coke, strongly suggests that efficient desorption of reaction products is crucial in this reaction. It is reported that diluting the methane feed-stream with water vapour has been used to efficiently desorb methanol from the catalyst[5] and potentially react directly with adsorbed $*CH_3$.[19] Our results support this in the absence of water in the reaction mixture, CO_x products dominate the reactor effluent (Fig. 3.1) and the catalysts form coke rapidly. The time online data observed over HZSM-5 is shown in figure 3.1

a)

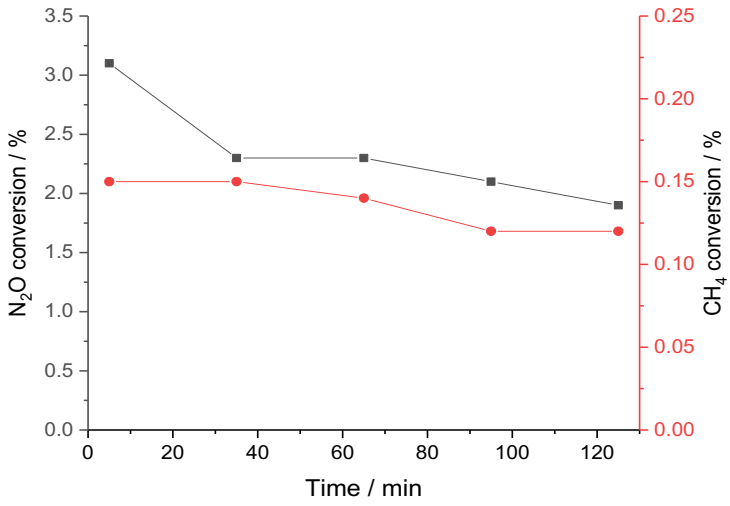

b)

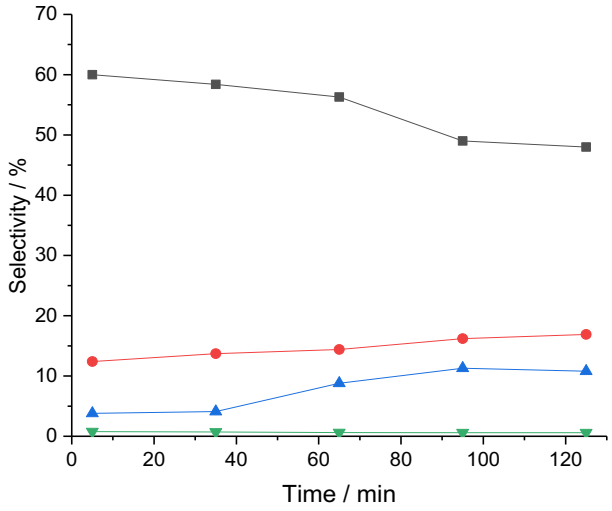

Figure 3.1 Time online data for methane oxidation at 300 °C for H-ZSM-5; (a) CH_4 (●) and N_2O (■) conversion and (b) Products selectivity in the gas phase: (■) CO; (●) CO_2; (▲) C_2 and (▼) MeOH

The low conversion observed over the parent H-ZSM-5 is shown in figure 3.1. It has been reported that the Fe impurities introduced during the zeolite synthesis can activate C-H bonds in the presence of H_2O_2.[8] Conversion of CH_4 and N_2O over H-ZSM-5 were found to be < 0.15% and *ca.* 2.5% respectively. Carbon monoxides are produced with a selectivity of 60 % during the first hour, which then lowered to 50 % until the end of the reaction. The selectivity toward C_2 starts to increase after 1 hour and reaches around 10%. The selectivity toward Methanol (MeOH) is *ca*. 0 %.

The time online data observed over 2 wt. % Fe/ZSM-5 is shown in figure 3.2.

a)

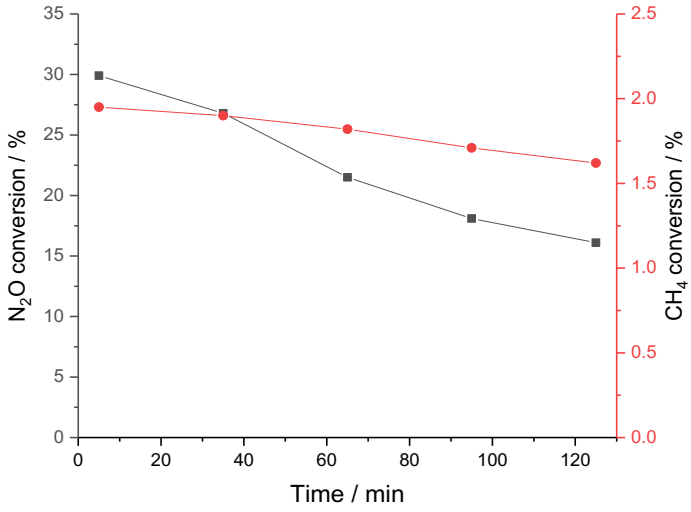

b)

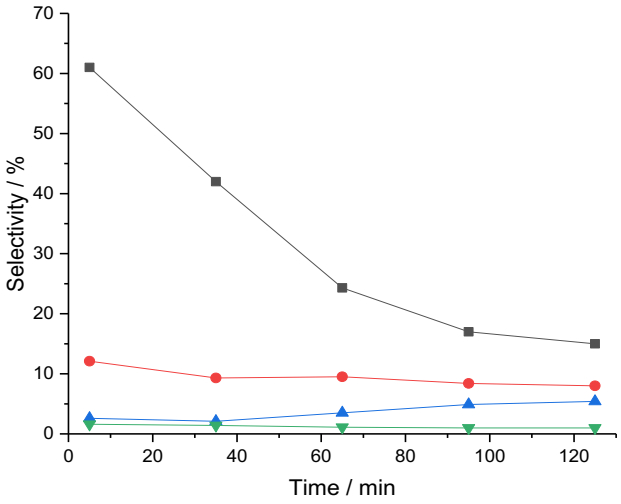

Figure 3.2 Time online data for methane oxidation at 300 °C for Fe/ZSM-5 (550°C); (a) CH_4 (•) and N_2O (■) conversion and (b) Products selectivity in the gas phase: (■) CO; (•) CO_2; (▲) C_2 and (▼) MeOH

Comparing it to the parent zeolite (*i.e.* H-ZSM5), the activity of 2 wt. % Fe/ZSM-5 is significantly increased, the respective conversion of CH_4 and N_2O increased to 1.75% and 25 %. Carbon oxides, C_2, MeOH and coke were produced from the reaction and it was observed that as the time-on-line increases the total moles of carbon in the gas outlet decreases and results in poor mass balance due to the formation of coke. The selectivity to coke reaches approximately 60 % by the end of a 2 h time online study. The selectivity toward methanol is again close to 0%.

The time online data observed over Fe/SIL-1 is shown in figure 3.3.

a)

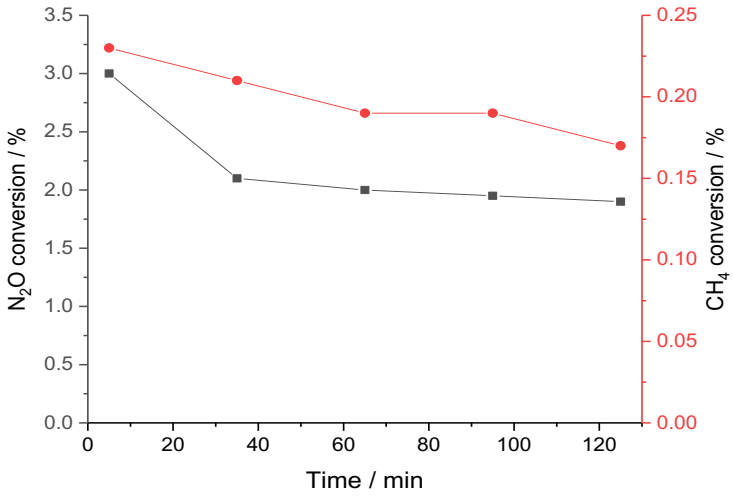

b)

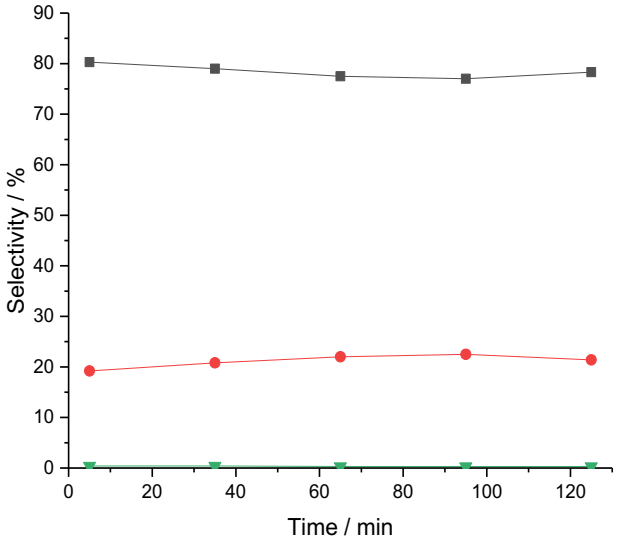

Figure. 3.3: Time online data for methane oxidation at 300 °C, over Fe/SIL-1 (550°C); (a) CH_4 (●) and N_2O (■) conversion and (b) Products selectivity in the gas phase: (■) CO; (●) CO_2; (▲) C_2 and (▼) MeOH.

The alumina-free MFI framework zeolite is showing *ca.* 0.15% and *ca.* 2.5% for CH_4 and N_2O conversion respectively. In this case the C_2 products are not detected in the effluent. Only a small amount of carbon oxides and MeOH at 300 °C are detected.

The time online data for Fe/TS-1 is shown in figure 3.4.

a)

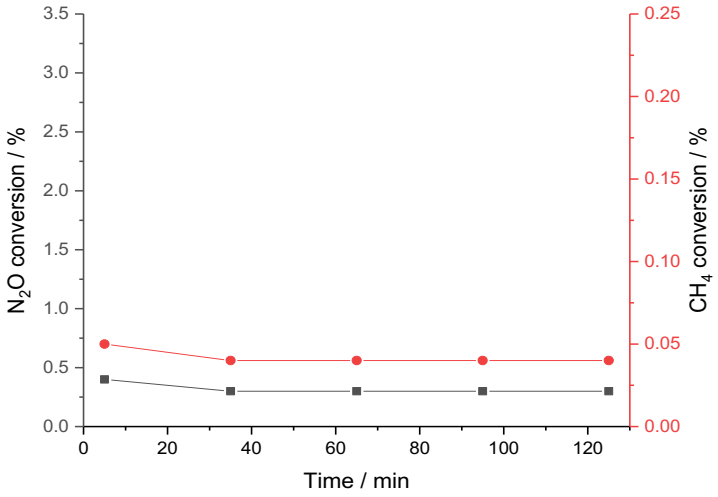

b)

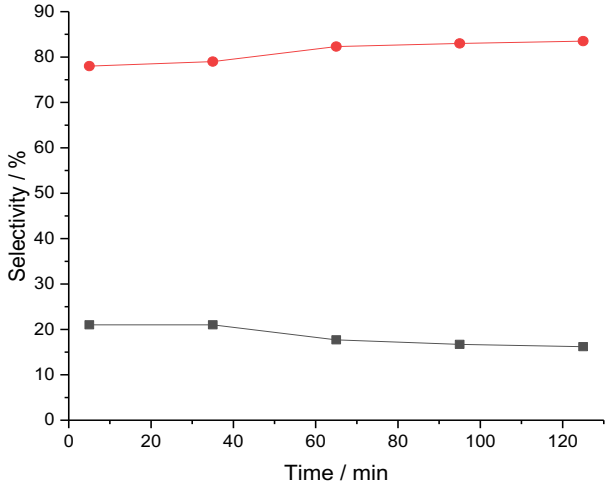

Figure 3.4: Time online data for methane oxidation at 300 °C, over Fe/TS-1 (550°C); (a) CH_4 (•) and N_2O (■) conversion and (b) Products selectivity in the gas phase: (■) CO and (•) CO_2.

The titanium silicate catalyst is essentially inactive showing *ca*. 0.05% and *ca*. 0.7% for CH_4 and N_2O conversion respectively and producing a small amount of carbon oxides

only at 300 °C. It is important to notice here that methanol is not detected in the gas effluent.

From all these experiments conducted on the different MFI supports it is interesting to observed that their composition and their structure plays an important role in the activation of the methane C-H bond and in the composition of the effluent stream. As discussed in the previous section these structures are characterised by different Fe species and also by the presence or absence of Brønsted and Lewis acid sites.

The aim of the next section is to investigate further on the effect of the Fe species position in the different MFI structures.

3.3 The influence of the position of the Fe in the MFI framework

The results from reactions over the metal-free SIL-1 and Fe/SIL-1 catalysts suggest that Fe has the potential to carry out C-H bond abstraction (Table 3.1). However, the Fe was introduced during the hydrothermal preparation and is likely to be situated in the tetrahedral-framework position. Two other analogue samples prepared by introducing Fe post-synthesis using physical grinding (SSIE) or sublimation (CVI) with the parent silicalite-1, prepared hydrothermally in house, was investigated to assess whether the location of the Fe species would facilitate improved C-H activation without the presence of aluminium. Using SSIE or CVI approaches should not produce any framework Fe species as the SiO_4 tetrahedral units are considered to be stable and will not permit metal ion exchange. The methane oxidation results presented in Table 3.2 indicate that the Fe/SIL-1 catalysts prepared by either CVI or SSIE are completely inactive.

Table 3.2: Methane oxidation at 300°C, over Fe/SIL-1 catalysts prepared with different Fe-deposition methods.

Catalyst	Conversion[a] (%)		Selectivity[a] (%)					STY[b] $_{MeOH}$ (μmol g_{cat}^{-1} h^{-1})
	N_2O	CH_4	MeOH	CO	CO_2	C_2H_4	DME	
SIL-1	-	-	-	-	-	-	-	-
0.5 wt.% Fe/SIL-1 (hydrothermal)	1.5	0.21	0.2	74.3	17.9	-	-	0.28
0.5 wt.% Fe/SIL-1 (CVI)	-	-	-	-	-	-	-	-
0.5 wt.% Fe/SIL-1 (SSIE)	-	-	-	-	-	-	-	-

[a] Values at 1 h; [b] STY_{MeOH}: space time yield of methanol; Reaction conditions: 0.44 g catalyst; Pellet Mesh size = 600 μm; V = 0.9 ml; 2 h; Feed mixture: 20% CH_4 + 2% N_2O with Ar balance; Flow rate = 55 ml min^{-1}; P(total) = 1 atm; GHSV= 3600 h^{-1}.

It is interesting to observe from these data that only the 0.5 wt.% Fe/SIL-1 catalyst prepared by hydrothermal synthesis demonstrates methane oxidation in the presence of N_2O. The other preparation methods deposit Fe on the external surface of the SIL-1 support and do not have any methane oxidation activity.

To understand the results obtained, UV/Vis analysis was performed to identify the Fe coordination environment (Fig. 3.5). The UV/Vis information provided on the speciation of different Fe is presented in Table 3.3.

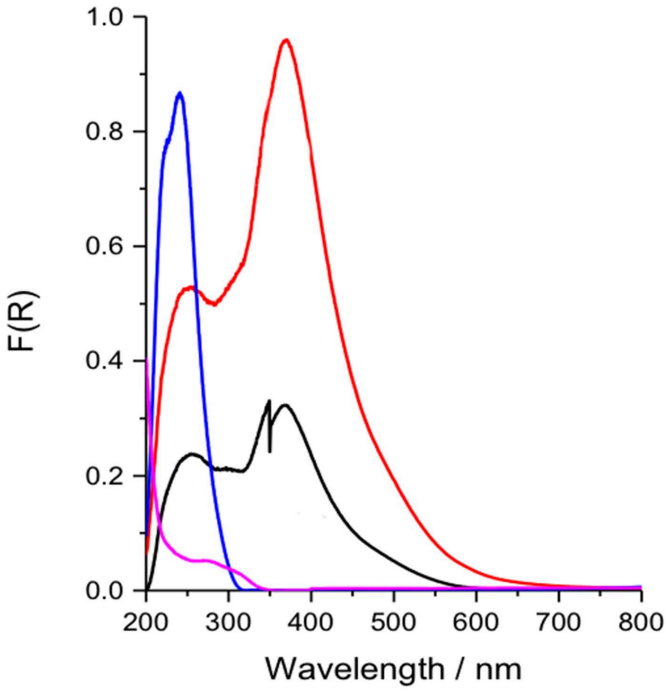

Figure 3.5: UV/Vis spectra of Fe/-SIL-1 materials prepared via different Fe loading methods. (Black – SSIE, red – CVI and blue – Hydrothermal synthesis).

Table 3.3: Nature of the absorbance bands present in the UV/Vis spectra of different the Fe species detected on the surface of the different catalysts.

Absorbance /nm	Fe species	References
200-250	Tetrahedral geometry	[20]
240-300	Octahedral geometry	[22]
300-450	Fe_x-O_y cluster	[23]
>450	Bulk iron oxide	[21]

Both Fe/SIL-1 samples, prepared by CVI and SSIE, possess a strong and broad absorbance stretch band between 310 to 600 nm which suggests that iron oxide clusters are dominant with possibility of the presence of bulky iron oxide. A weak absorbance at 250 nm potentially corresponds to extra-framework Fe species[20, 21]. This result in contradiction with the ones discussed in the previous section. Indeed, these species are

considered as part of the active sites which promote the activation of the C-H methane bond [9]. The results in Table 3.2 suggest that iron oxide clusters or bulk iron oxide on the SIL-1 are unable to facilitate N_2O conversion, as the first step to facilitate the C-H bond abstraction. Therefore, the proposed α-oxygen species does not seem to be generated from the Fe species over SIL-1 structure. The effect of calcination temperature or steaming under different temperatures was investigated to influence the coordination environment of the Fe in the 0.5 wt. % Fe/SIL-1 catalyst. The UV/Vis spectroscopy have been performed after these different treatments and the spectra are reported in figure 3.6.

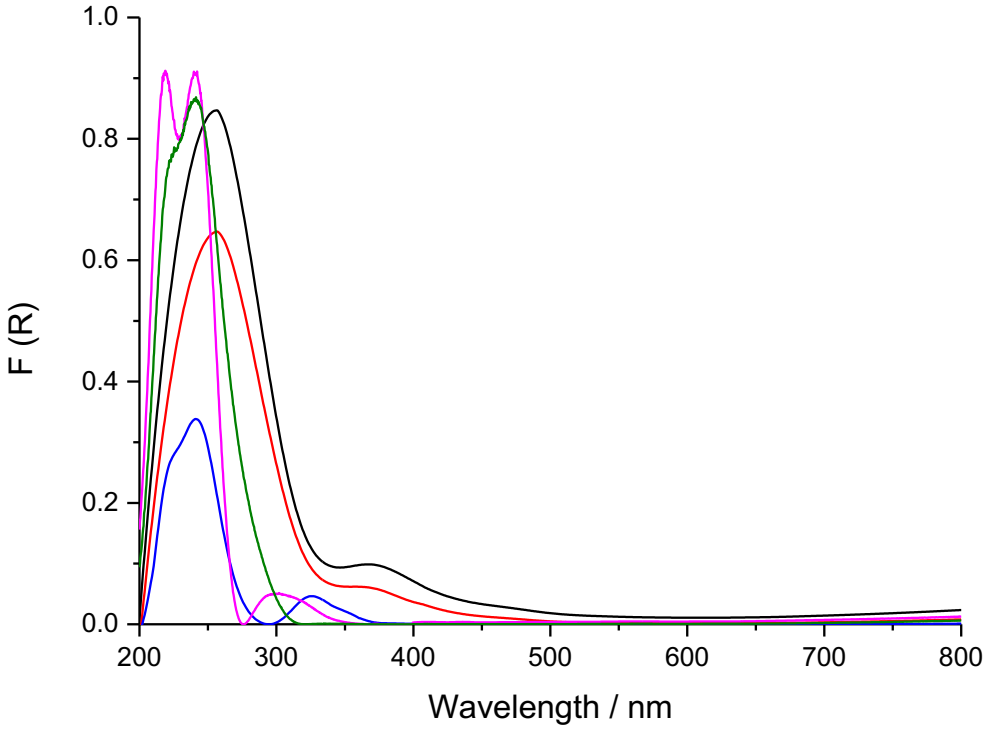

Figure 3.6: UV/Vis spectra for the as prepared 0.5 wt.% Fe/SIL-1 sample compared to those following heat treatments under different conditions; uncalcined (magenta), calcined 550 °C (green), steamed 550°C (blue), calcined 875°C (red) and steamed 875°C (black).

The distribution of the type of Fe species formed can be revealed from the UV/Vis spectra. For the uncalcined Fe/SIL-1, there were two major bands observed at 210 and

240 nm that correspond to the $t_1 \rightarrow t_2$ and $t_1 \rightarrow e$ transitions of the FeO_4 tetrahedral respectively. It suggests that the Fe species occupy the lattice positions[22, 23]. The sample was then treated at different temperatures at 550 °C and 875 °C, both under flowing air or steam as Fe can migrate out of the MFI intra-framework to the extra-framework position, that are reported to be more catalytically active using Fe/ZSM-5.[24] In the case of the Fe/SIL-1, samples calcined at 550 °C, the band at 210 nm has decreased which indicates at least a partial migration of Fe from the lattice position. The increasing signal absorbance from 240 to 300 nm indicates a minor level of migration of intra-framework tetrahedral Fe to extra-framework positions. After steaming the Fe/SIL-1 at 550 °C, all the absorption bands have significantly decreased. Following heat treatment at 875 °C under both steam and air, the UV-Vis analysis shows a larger degree of extra-framework Fe formed and can be linked to the catalytic activity for methane oxidation and other applications.[8, 25, 26] The UV/Vis spectra of the Fe/SIL-1 samples indicated that the surface was largely free from iron oxide clusters which are characteristic of higher wavelength absorption which are observed from 400 nm.

The Fe/SIL-1 samples treated under steam and air at 550 °C and 875 °C were tested for methane oxidation in order to reveal whether if the location of the Fe in the catalyst affects the C-H activation (Table 3.4).

Table 3.4: Methane oxidation over 0.5 wt.% Fe/SIL-1 materials prepared by different heat treatments

Catalyst (pre-treatment conditions)	Conversion[a] (%)		Selectivity[a] (%)						STY_{MeOH} [b] (μmol g_{cat}^{-1} h^{-1})
	N_2O	CH_4	MeOH	CO	CO_2	C_2H_4	DME	Coke	
SIL-1 (Metal-free)	-	-	-	-	-	-	-	-	-
Fe/SIL-1 (uncalcined)	-	<0.05	-	-	1.2	-	-	-	-
Fe/SIL-1 (calcined 550 °C)	2.0	0.19	0.3	22.0	77.5	-	-	-	0.28
Fe/SIL-1 (steamed 550 °C)	2.8	0.25	0.21	74.9	22.3	-	-	-	0.27
Fe/SIL-1 (calcined 875 °C)	1.7	0.19	0.3	73.2	26.5	-	-	-	0.33
Fe/SIL-1 (steamed 875 °C)	1.1	0.08	3.0	70.9	26.1	-	-	-	1.28
Fe/SIL-1 (calcined 875 °C) for 24h	1.5	0.05	2.3	74	23.6	-	-	-	1.1

[a] Values at 1 h; [b] STY_{MeOH}: space time yield of methanol; Reaction conditions: 0.44 g catalyst; Pellet Mesh size = 600 μm; V = 0.9 mL; 300 °C; 2 h; Feed mixture: 20%CH_4 + 2% N_2O with Ar balance; Flow rate = 55 mL.min^{-1}; P(total) = 1 atm; GHSV= 3600 h^{-1}.

The conversion of methane over the 0.5 wt. % Fe/SIL steamed at 550 °C was comparable to the calcined sample (*ca.* 0.2 %). This result suggests that the presence of Fe can potentially activate the methane C-H bonds in the same fashion as the H-ZSM-5 with the presence of unavoidable Fe impurities. Although, the uncalcined Fe/SIL-1 sample possesses framework Fe and is shown to be inactive for methane oxidation, the pores are likely to be inaccessible due to the TPAOH template (the zeolite structure directing agent used during synthesis) which would still be present in the zeolite structure as template removal requires heat treatment.[27] Following higher temperature treatment (875 °C) under steam or air, the activity of those samples decreased, despite possessing extra-framework Fe which is found to be able to oxidise methane. In this

case, the selectivity to methanol increased. However, as the methane conversion is not equivalent to those treated at lower temperatures (*i.e.* 550 °C) and it is difficult to compare directly. The active site is considered to be an extra-framework mono- or di-Fe species coordinated to a framework Al. [8, 10] According to the UV/Vis spectra (figure 3.6) and the methane oxidation results of the Fe/SIL-1 samples treated at 875 °C, the extra-framework Fe present is unable to activate N_2O (Table 3.4) compared to the case over Fe/ZSM-5 (Table 3.1), which are *ca.* 1% and 21% respectively. Therefore, despite the presence of extra-framework Fe, C-H bond activation was not observed. The hypothesis which can be proposed is that the Fe coordination environment is crucial to facilitate N_2O efficiently for methane oxidation. Considering this observation, the influence of the Brønsted acidity, which is present in the Fe/ZSM-5 sample should be explored.

3.4 The influence of the Brønsted acidity for methane oxidation

Under the high temperature treatment, zeolites undergo the loss of Brønsted acid sites through the migration of Al in the framework position.[28] Therefore, different heat-treatments have been performed for the 2 wt.% Fe/ZSM-5 catalyst with the aim to change the environment of the Fe situated on the extra-framework, considered as the active sites, and subsequently observe the effect on the methane C-H bond activation.

Starokon *et al.* reported that when Fe/ZSM-5 are treated under reducing atmosphere at high temperatures (900 °C), the number of active α-Fe sites would increase which led to a high activity for both N_2O and CH_4. This was reported to be due to an increase in the population of Fe^{3+}, formed after such treatment.[3]

The Fe/ZSM-5 sample was treated under static air or dilute, flowing hydrogen over a range of different temperatures from 550 to 950 °C. The samples recovered were tested for methane oxidation using N_2O as the oxidant (Table 3.5).

Table 3.5: Methane oxidation over 2 wt.% Fe/ZSM-5 prepared under different calcination conditions.

Calcination temperature (°C) and conditions	Conversion[a] (%)		Selectivity[a] (%)						STY_{MeOH}[b] (μmol g_{cat}^{-1} h^{-1})
	N_2O	CH_4	MeOH	CO	CO_2	C_2H_4	DME	Coke	
550 (static air)	21.5	1.8	1.1	24.3	9.5	3.5	-	61.6	6.4
550 (H_2/Ar)	26.0	2.0	0.7	13.4	8.2	3.8	-	73.9	7.1
750 (static air)	20.7	1.9	1.4	26.4	9.3	2.0	-	60.9	12.8
750 (H_2/Ar)	30.6	2.2	0.8	16.1	9.8	2.3	-	71	9.0
950 (static air)	4.4	0.2	13.7	76.8	4.9	-	4.6	-	18.7
950 (H_2/Ar)	29.5	1.4	1.6	25.1	14.0	4.2	-	55.1	13.6

[a] Values after 1 h on-stream; [b] STY_{MeOH}: space time yield of methanol; Reaction conditions: 0.44 g catalyst; Pellet Mesh size = 600 μm ; V = 0.9 mL ; 300 °C; 2 h; Feed mixture: 20% CH_4 + 2% N_2O with Ar balance; Flow rate = 55 ml min^{-1}; P(total) = 1 atm; GHSV= 3600 h^{-1}.

The samples treated at 550 and 750 °C under both air and hydrogen resulted in comparable methane conversions of *ca.* 2 %. In all cases the mass balance was low, as observed with the 2 wt.% Fe/ZSM-5 calcined at 550 °C. However, after heat treatment under air at 950 °C, the chemical environment appears to undergo an irreversible change and the result led to a significant loss in activity. Both the conversion of methane and N_2O are significantly lowered which saw a reduction of *ca.* 2 % to 0.2 % for methane and *ca.* >21 % to 4 % for N_2O conversion. However, the space-time-yield of methanol of the sample treated under air at 950 °C was calculated to be 18.7 μmol g_{cat}^{-1} h^{-1}. Conversely, over the 2 wt.% Fe/ZSM-5 calcined at 550 °C, the STY_{MeOH} was found to be significantly lower at 6.4 μmol g_{cat}^{-1} h^{-1}. The testing of the sample following treatment at the same temperature under the dilute hydrogen atmosphere suggests it did not undergo changes that would significantly supress the methane activation as observed using flowing air. The oxidising (flowing air) or reducing (flowing hydrogen)

environments of this catalyst pre-treatment steps will have different water content, which was found to be crucial to zeolite dealumination.[28]

The testing results presented in Table 3.5 suggest that the active site is stable to 750 °C and the formation of ethane observed in the reactor effluent indicates the surface Brønsted acidity is not compromised. In contrast, the presence of DME detected in the effluent over 2 wt.% Fe/ZSM-5 calcined at 950 °C under flowing air suggests that the high temperature calcination and the moisture present could alter the Brønsted acidity of the sample.

The Powder XRD spectra for the 2 wt. % Fe/ZSM-5 samples calcined at different temperatures (*i.e.* 550, 750 and 950 °C), at a ramp rate of 20 °Cmin^{-1} for 3 h under flowing air is shown in figures 3.7.

a)

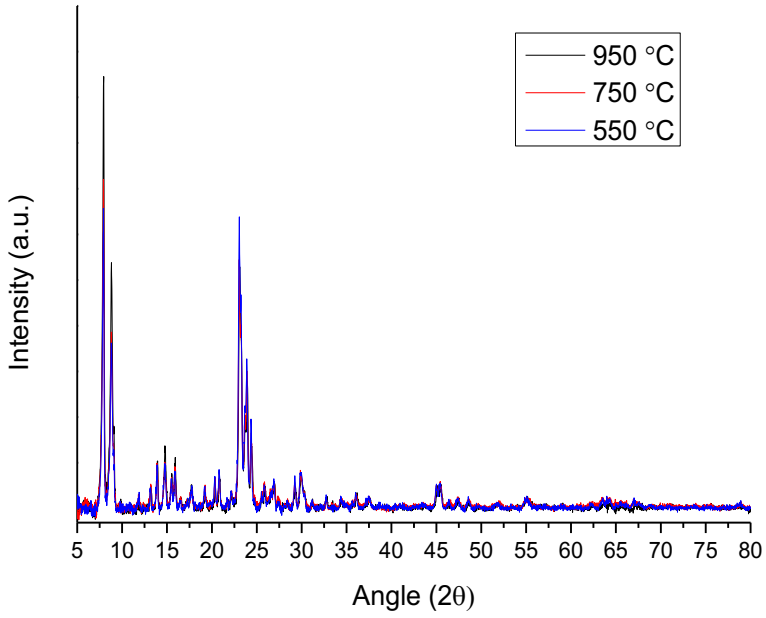

b)

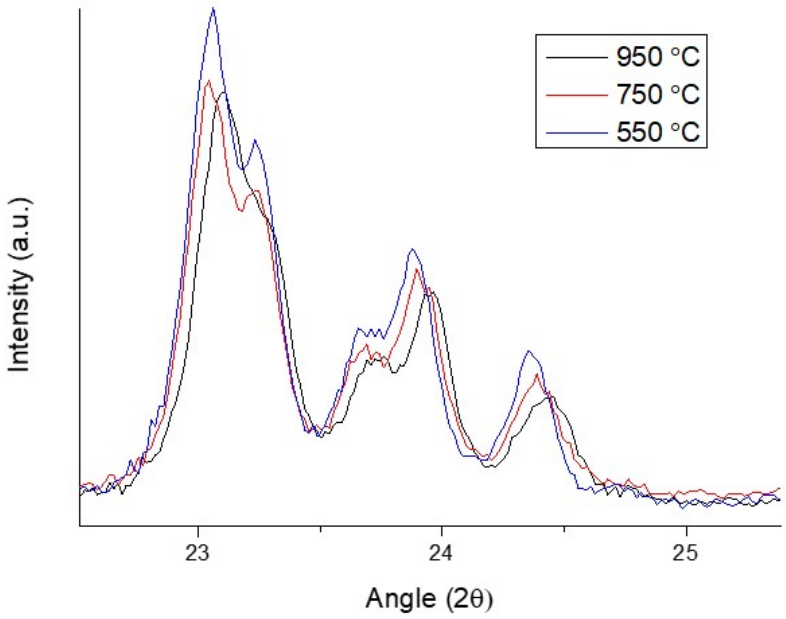

Figures 3.7 XRD spectra for the 2 wt. % Fe/ZSM-5 calcined at 550/750/950 °C; a) entire XRD spectra; b) scaled to the shifted in characteristic peaks of the MFI structure.

The spectra show that the XRD diffraction pattern of all three samples are very similar which indicates that the MFI crystallographic zeolite structure is retained even after treated at much higher temperatures. There is a progressive shift to higher angles for sample treated at higher temperatures in the characteristic peaks 2θ = 22.5 – 25 °, as shown at the bottom of figure 3.7. This observation suggests a small decrease in lattice space as the shift taken place is due to the shortening of the Si-O-Si bond. This result is concordant with the study of the thermal stability of H-ZSM-5 reported by Hoff *et al.*[28]

In figures 3.8 a, b and c are reported the STEM images of Fe/ZSM5 catalysts prepared by CVI across different area of the sample. The EDX spectra are also taken and shown underneath of the STEM images.

a)

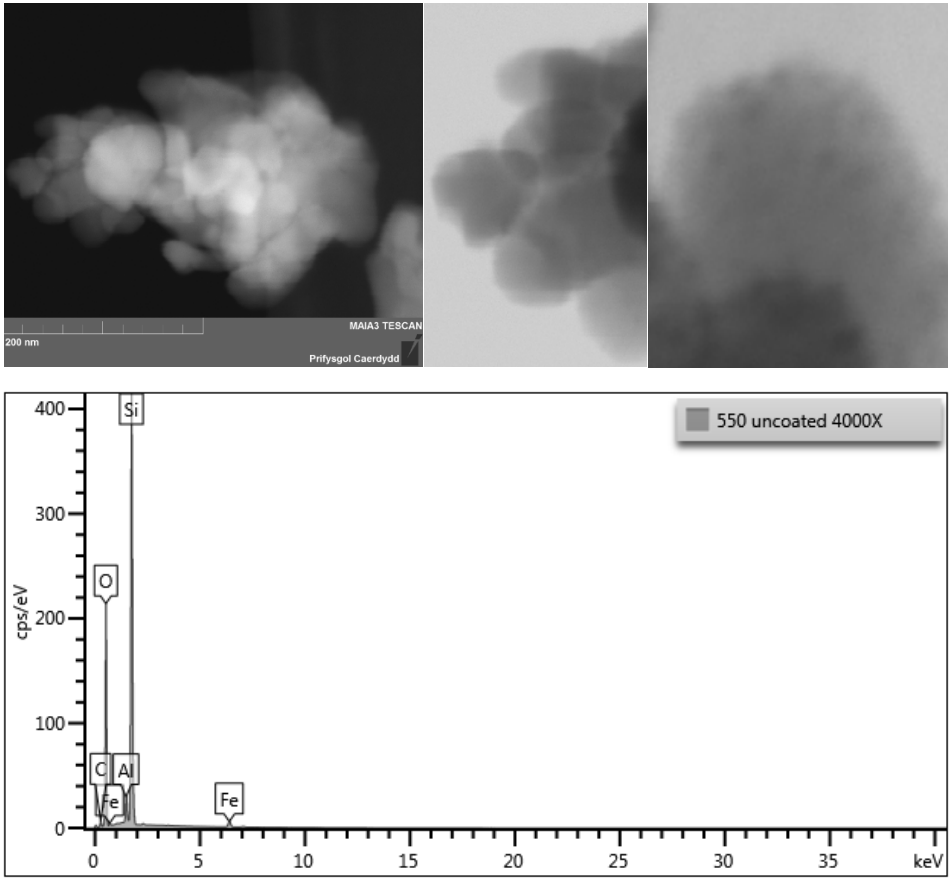

Figure 3.8 a Microscopic images and EDX spectrum of the 2 wt. % Fe/ZSM-5 prepared by CVI and calcined at 550 ⁰ C.

b)

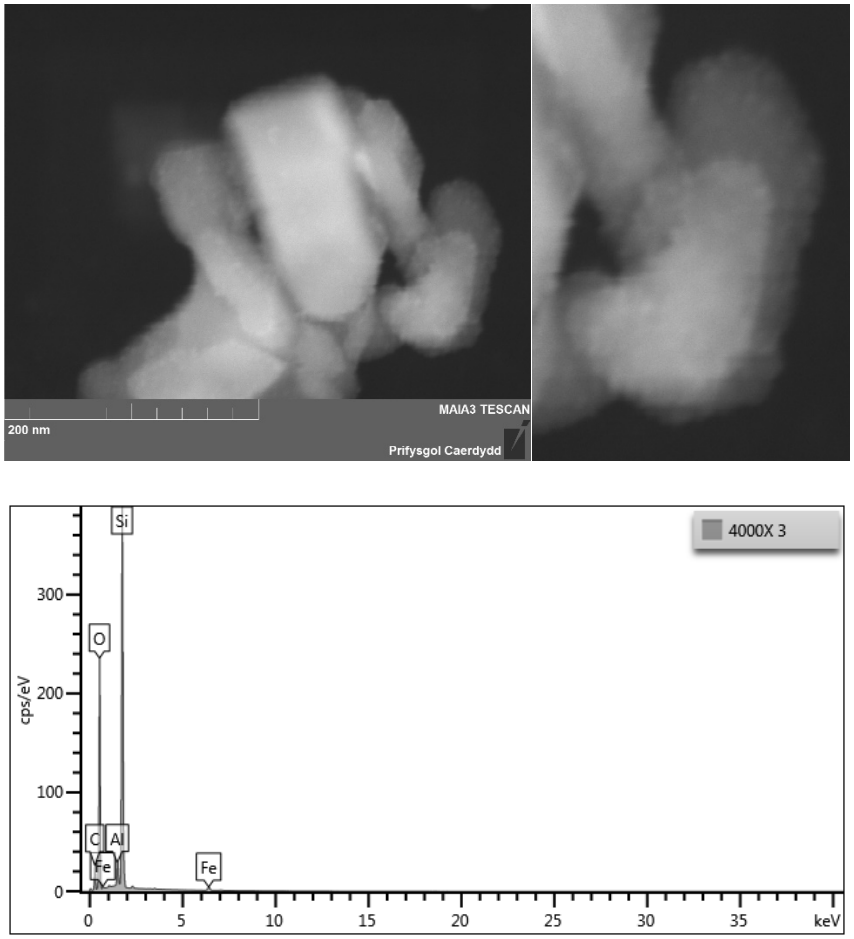

Figure 3.8 b Microscopic images and EDX spectrum of the 2 wt. % Fe/ZSM-5 prepared by CVI and calcined at 750 ⁰ C.

c)

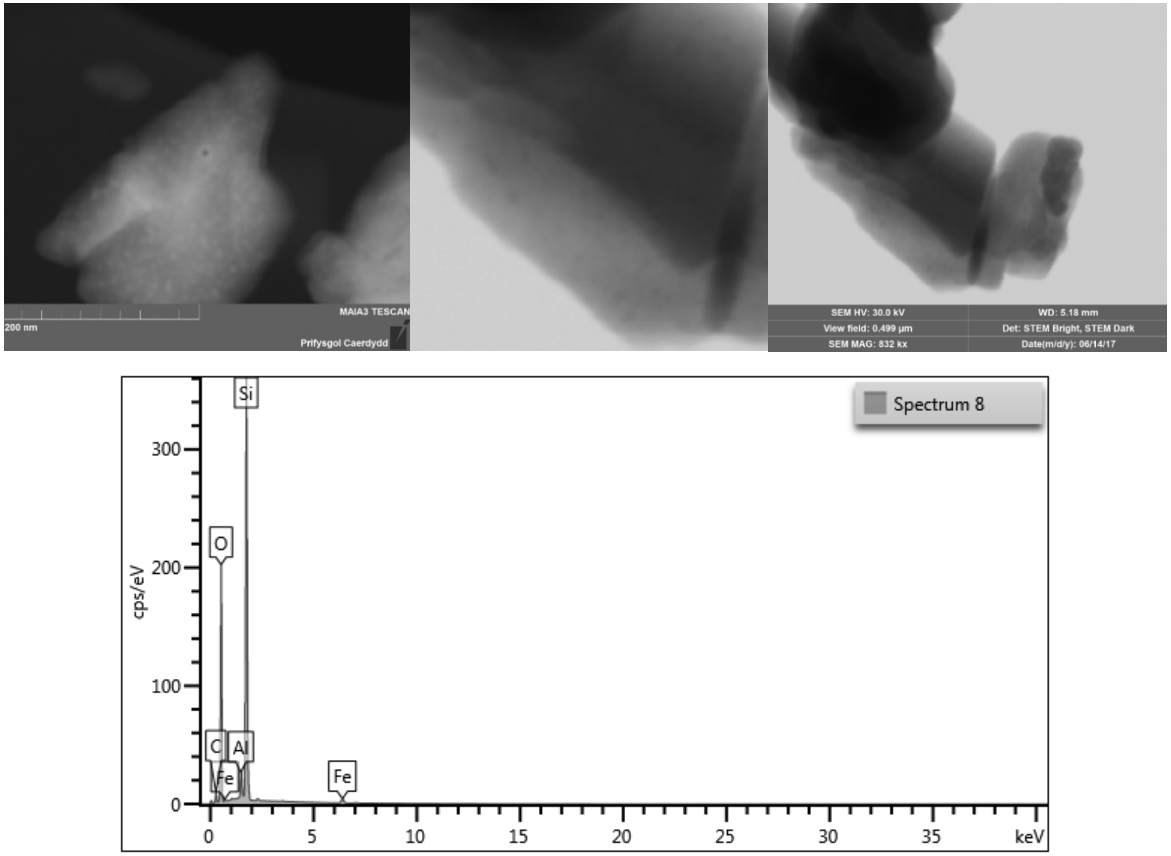

Figure 3.8 c Microscopic images and EDX spectrum of 2 wt.% Fe/ZSM-5 prepared by CVI calcined at 950 C.

The STEM images shown in figures 3.8a, b and c reveal that after Fe deposition and catalyst calcination, there are Fe nanoparticles present in the zeolite framework and are unevenly distributed. It is estimated that the size of those observed Fe nanoparticles are approximately below 5 nm. The morphology of these MFI structured zeolite is of coffin-shaped which are commonly observed for ZSM-5 zeolite.[29, 30]

EDX gives an elemental analysis of the Fe exchanged ZSM-5 samples and shows that all samples contain the expected elements of Si, Al, O, Fe signals from the samples and carbon signal from the sample holder. It is used to mainly look at the iron loadings in different region of the support. The iron weight content recorded is presented in Table 3.6.

Table 3.6: Fe content observed using EDX across different sampling regions of 2 wt% FeZSM-5.

EDX profile taken at different regions	Fe content (wt. %)
1	0.4
2	3.4
3	2.4
4	2.1
5	3.8
6	4.1
7	2.5
8	3.1

This set of results suggests that the Fe distribution are heterogeneously placed and the Fe content ranges between 0.5 to 4.1 wt. %, which also suggest that CVI may not be the best synthetic approach if one requires the metal ions to be highly dispersed and evenly across the parent zeolite.

Pyridine desorption experiments were carried out using DRIFTS, to monitor the changes of both the Lewis and Brønsted acidity as a function of temperature. In figures 3.9 are reported the IR spectra associated with the sample labelled a) H-ZSM-5 (for

comparison) and Fe/ZSM-5 calcined at b) 550 °C, c) 750 °C, d) 950 °C under static air and e) Reduced at 950 °C under H_2/Ar. In figure 3.9f illustrates the absorbance of the Brønsted acid sites and Lewis acid sites of the different ZSM-5 catalysts after different calcination temperatures.

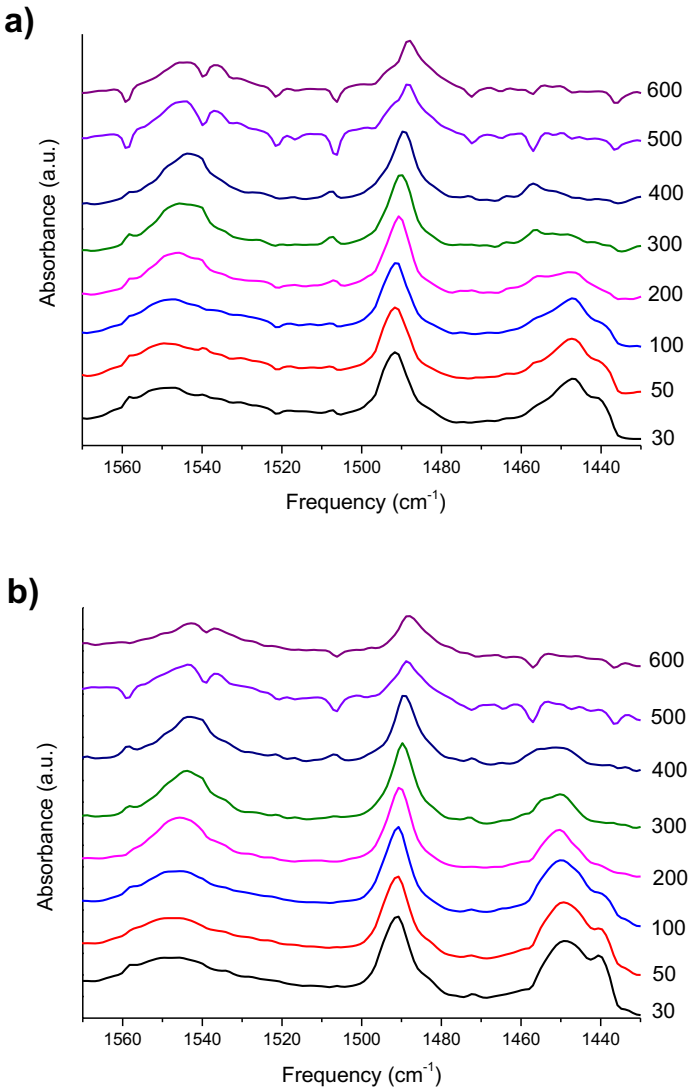

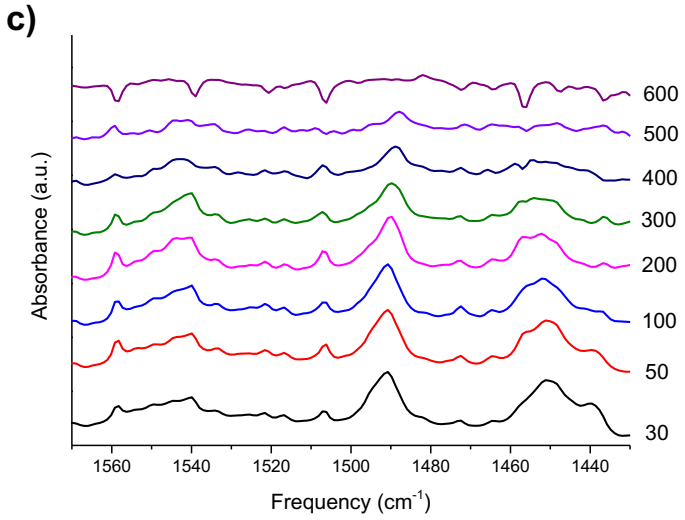
c)
Absorbance (a.u.)
600
500
400
300
200
100
50
30
1560
1540
1520
1500
1480
1460
1440
Frequency (cm-1)

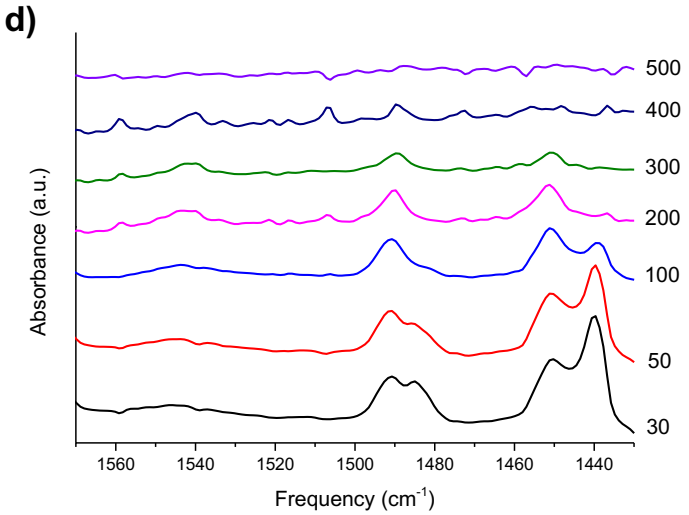
d)
Absorbance (a.u.)
500
400
300
200
100
50
30
1560
1540
1520
1500
1480
1460
1440
Frequency (cm-1)

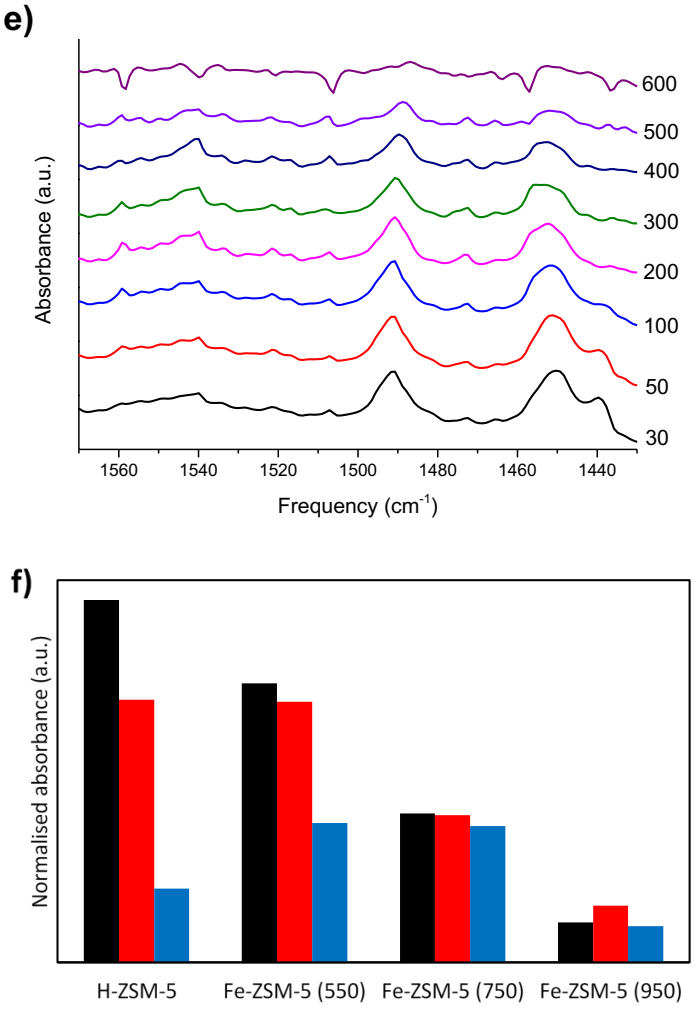

Figures 3.9 FTIR spectra of pyridine adsorbed on ZSM-5 materials recorded between 30 and 600 °C; a) H-ZSM-5; and Fe-ZSM-5 calcined at b) 550 °C, c) 750 °C, d) 950 °C under static air and e) calcined at 950 °C under H_2/Ar. f) The absorbance of the Brønsted acid sites (black), Brønsted + Lewis acid sites (red) and Lewis acid sites (blue) of the different ZSM-5 catalysts after different calcination temperatures. The area of the absorbance bands was normalised against the framework overtones at 2010 cm^{-1} at 300 °C.

The temperature of desorption, or the decrease in the intensity/loss of adsorption band, indicates the strength of the Lewis and Brønsted acid sites present in the samples. The pyridine absorbance at 1450 cm^{-1} corresponds to pyridine adsorption on a Lewis acid sites. The Brønsted acid sites can be observed by the band present at 1540 cm^{-1} which correspond to the C-C bond vibration of the pyridinium ion. The absorbance at 1490 cm^{-1} indicates the pyridine interaction of both Lewis and Brønsted acid sites.[31]

Comparison of the bands present over the samples studied at room temperature indicate that the high temperature calcination at 950 °C under air has clearly increased the number of Lewis acid sites as the band at 1450 cm^{-1} has significantly increased. This increase is considered to be due to the migration of aluminium forming greater Lewis acid sites within the pore channels.[14] However, these appear to be lower strength as pyridine is quickly lost from this site, as the corresponding reduction in the band at 1440 cm^{-1} over the measurements taken below 100 °C suggests. Furthermore, the intensity of the band is much lower after the desorption temperature was increased to >100 °C.

It is also reported that the pyridine desorption measurement taken below 200 °C may have signals arise from the overlapping of physisorbed and chemisorbed pyridine molecules [32, 33]. As the temperature of this sample is increased, the peak profile reduces until no pyridine remains adsorbed at 400 °C. In contrast, the pyridine remains adsorbed until at least 500 °C on the Fe/ZSM-5 samples heated at 550, 750°C and treated under H_2 at 950 °C. Despite retaining a degree of surface acidity, the Fe-ZSM-5 catalysts calcined under air at 950 °C was essentially inactive; Fe/ZSM-5 treated under H_2 at 950 °C is still shown to be active (1.4 % methane conversion) as shown in Table 3.6.

In figure 3.9f, the area of each absorbance band, normalised against the zeolite framework overtones at 2010 cm^{-1}, is presented. This method was previously adopted when comparing the acidity of H-ZSM-5 catalysts after high temperature calcinations at a similar range of temperature[28]. Figure 3.9f presents a comparison of the pyridine DRIFTS adsorption bands at 300 °C and clearly demonstrates that the addition of Fe led to a decrease of Brønsted acidity of the zeolite. This result is expected as we considered that the Fe is co-ordinated to the framework Al, thereby altering the Brønsted acid sites. Further heat treatment at 750 °C and 950 °C led to further decrease in Brønsted acidity, consistent with the de-alumination process which occurs with the zeolite. Interestingly, the addition of Fe to the H-ZSM-5 increased the size of the absorbance band associated with Lewis acidity, which did not appear to change significantly after calcination at 750 °C, but significantly decreased after calcination at 950 °C. The pyridine study can, therefore, conclude that the high temperature calcinations significantly decreased the number of Brønsted acid sites over Fe/ZSM-5.

The pyridine desorption experiments were complemented by NH_3-TPD analysis under similar conditions on the same set of catalysts to investigate the relative acid strength of the Fe-ZSM-5 after the heat treatment (Fig. 3.10).

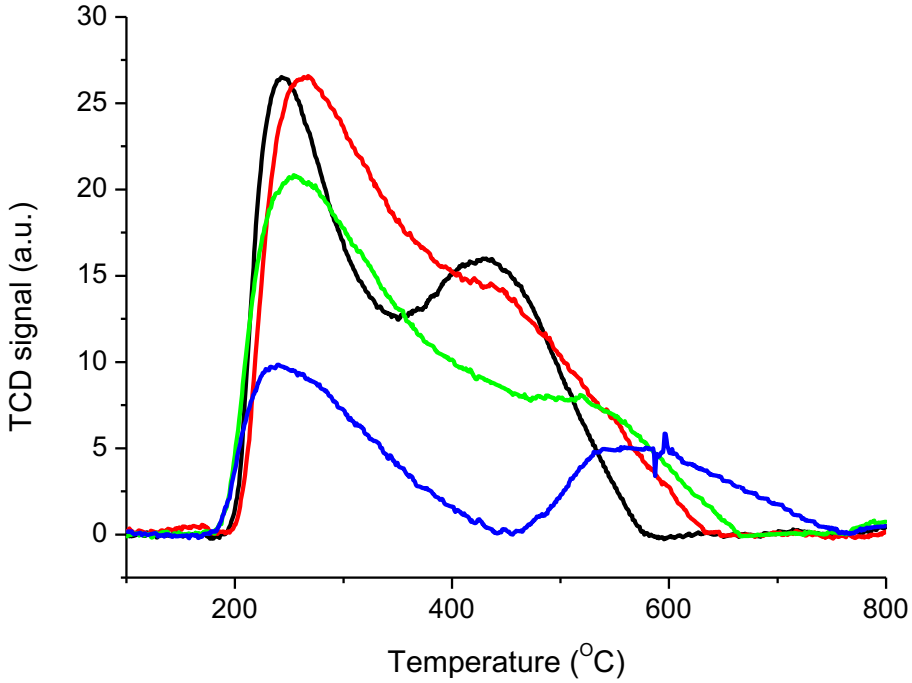

Figure 3.10 NH_3 – TPD profile obtained for the ZSM-5 based materials calcined at different temperatures under static air; black line: HZSM-5 (550 °C); red line: Fe/ZSM-5 (550 °C); green line: Fe/ZSM-5 (750 °C); blue line: Fe/ZSM-5 (950 °C).

There are two characteristic signals that are often observed and used for analysis in the NH_3-TPD spectra using MFI type zeolites. The desorption features are located at the temperature region of 260 °C and 450-550 °C, which represent the weak (low temperature desorption, LT) and strong acid sites (high temperature desorption, HT) respectively. The area of the HT desorption curve indicates the concentration of the acid sites and the temperature at which the HT peak maximum occurs give information on the overall acid strength of the sample.[34] The strong acid sites (HT) are generally considered instead of the weak acid sites to evaluate the acid strength of the zeolite catalysts. Indeed, the peaks of weak acid sites observed, represents the desorption from either non-acidic sites or physisorbed NH_3.[35] The addition of Fe to the H-ZSM-5 (support) framework modestly alters the strength of the strong acid sites (HT). In contrast, the calcination carried out at 750 and 950 °C causes a shift of the NH_3

desorption for the strong acid sites from 450 °C to 520 °C and 580 °C respectively. In addition, the overall number of NH_3 molecules adsorbed is lowered with these materials calcined at higher temperatures. Furthermore, the decrease in the overall number of acid sites observed with the sample calcined at 950 °C corresponds to an increase in the acid strength. This suggests that only the Brønsted acid sites have increased in strength following heat treatment, due to the observed increased adsorption of pyridine at low temperatures on Lewis acid sites, as previously shown in figure 3.10.

From the previous sections, it appears that the Fe coordination environment is crucial with respect to the activation of C-H bonds. The high temperature calcination under air at 950 °C has disrupted this environment *via* the migration of Al species as reported previously[28] and preventing efficient catalytic N_2O decomposition (see Table 3.6). Solid-state NMR (^{27}Al MAS SS-NMR) was used to monitor the tetrahedral and octahedral Al species present in the Fe/ZSM-5 samples after treatment at different calcination temperatures (Fig. 3.11).

a)

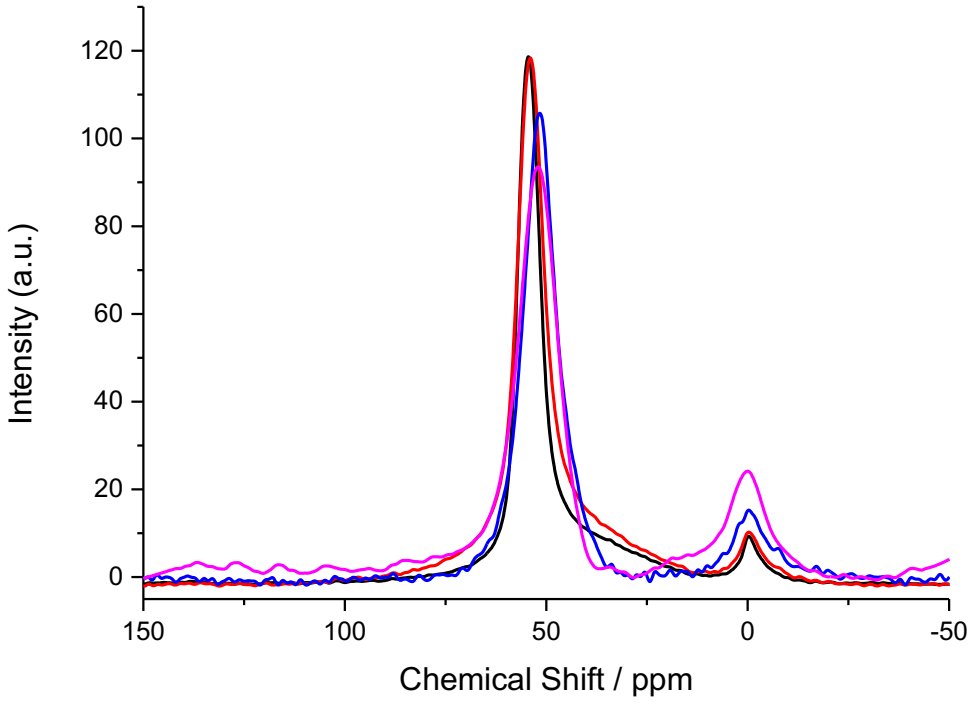

b)

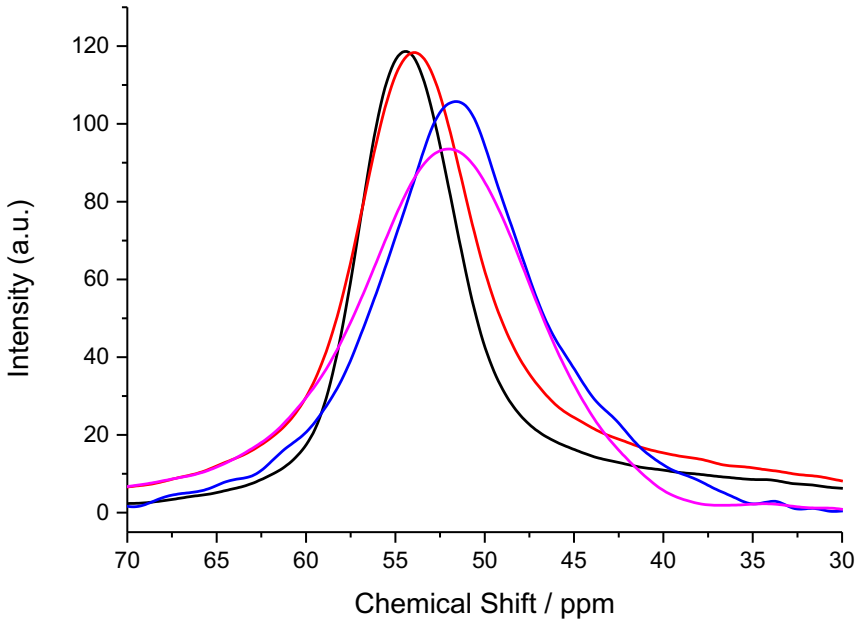

c)

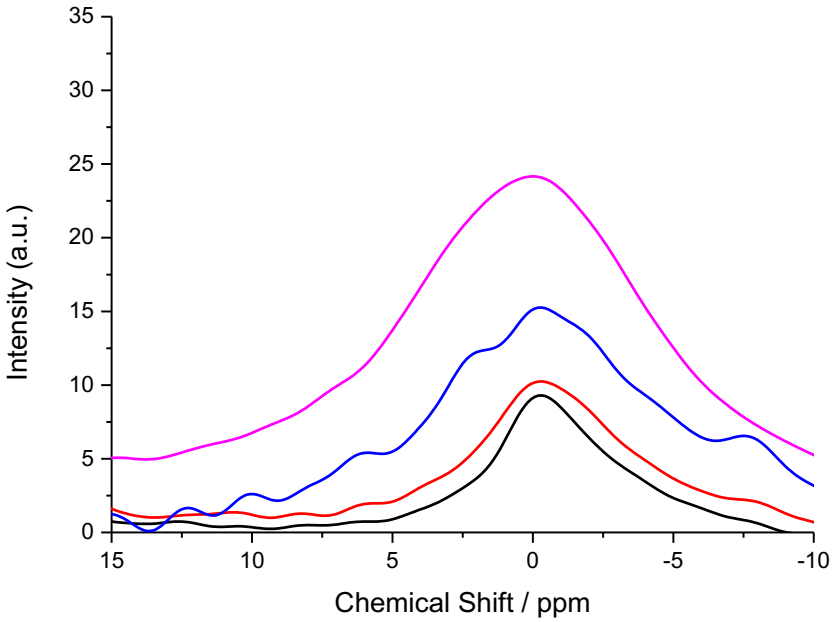

Figure 3.11 ^{27}Al solid-state nuclear magnetic resonance spectra of HZSM-5 (black) and 2 wt.%Fe/ZSM-5 calcined at 550 (red), 750 (blue) and 950 °C (magenta); a) entire spectrum; b) scaled to characteristic peaks of tetrahedral framework Al; c) scaled to characteristic peaks of octahedral extra-framework Al.

The results indicate that the dealumination process occurred and confirms the disruption of the framework Al. It was revealed that a decrease in the tetrahedral coordinated Al peak at approximately 55 ppm and an increase in the octahedrally coordinated Al positioned at 0 ppm, when the calcination temperature increases from 550 to 950 °C.

These results reienforce the importance of the acid sites and their concentration for the methane activation through the formation of the active α-oxygen species. The increase of acid strength and density of Lewis acid sites would cause a significant reduction of activity, which further suggests that Fe must be coordinated to the Al-framework for efficient formation of active oxygen species for the hydrogen abstraction step.

3.5 The influence of the Fe loadings at constant Fe:Al ratio for methane oxidation

The active Fe sites have been reported to be coordinated to the Al framework[36] and therefore the maximum number of active Fe sites is proportional to the number of Al present in the zeolite. A series of Fe/ZSM-5 catalysts were prepared that had the same Fe:Al ratio from parent H-ZSM-5 catalysts with varying SiO_2:Al_2O_3 ratios and were tested for methane oxidation using N_2O. The catalytic activity is summarised in Table 3.7.

Table 3.7: Methane oxidation over Fe/ZSM-5 catalysts (Si:Al of 23 to 280) at 300°C.

Fe content (wt.%) on ZSM-5 {Si:Al}	Conversion[a] (%)		TOF[b] (h^{-1})	Selectivity[a] (%)					STY_{MeOH}[c] ($\mu mol\ g_{cat}^{-1}.h^{-1}$)
	N_2O	CH_4		MeOH	CO	CO_2	C_2H_4	Coke	
2.7 {23}	27.2	2.5	3.1	0.3	10.5	6.4	3.2	79.6	4.9
2.0 {30}	22.5	1.7	3.8	0.8	19.3	8.6	4.4	66.9	6.6
1.2 {50}	11.9	0.9	3.3	0.8	36.0	12.8	1.9	48.5	3.9
0.3 {280}	3.4	0.5	3.8	0.9	38.6	11.9	1.9	46.7	2.4

[a] Values taken from average of 2 h; [b] moles of N_2O converted per moles of Fe present; [c] STY_{MeOH}: space time yield of methanol; Reaction conditions: 0.44 g catalyst; Pellet Mesh size = 600 μm ; V = 0.9 mL; 2 h; Feed mixture: 20% CH_4 + 2% N_2O with Ar balance; Flow rate = 55 $mL.min^{-1}$; P(total) = 1 atm; GHSV= 3600 h^{-}

An Fe:Al ratio of 0.47 was applied to the parent HZSM-5 catalysts with SiO_2:AlO_3 ratios of 23, 30, 50 and 280. This results in Fe/ZSM-5 catalysts with Fe loadings from 2.7 to 0.3 wt.%. Analysis of the Fe environment by UV/Vis was not carried out due to the high Fe loadings, which would easily obscure the identifiable features. It was found from our previous testing that the UV/Vis spectra show many overlapping bands from various form of Fe species that are produced during Fe introduction step.

Both the methane and N_2O conversion increases with increasing Al loading from 0.5 to 2.5 % and 3.4 to 27.2 %. However, the N_2O TOF as a function of Fe content remained comparable at *ca.* 3.5 h^{-1} across the samples therefore we assume the Fe environment is comparable across these samples. The selectivity to coke can be seen to be lowered according to the methane conversion and Al content which further suggests that the acidity of the MFI surface plays a role in the rate of products desorption. However, the reactions were not carried out at iso-conversion and comparison such as this is not ideal.

3.6 Methanol control experiments using MFI catalyst with various acidic profiles

The role of acidity and Fe location was further investigated with respect to the low methanol selectivity and low mass balances observed over catalysts such as the 2 wt.% Fe/ZSM-5 (calcined at 550 °C).

Control experiments were carried out with methanol diluted in an Ar stream containing N_2O, which is presumed to be a primary product. Methanol is known to react efficiently over HZSM-5 catalysts to form primarily DME and olefins in a process commonly known as the Methanol-to-Olefins process (MTO).[37] Methanol undergoes the hydrocarbon pool mechanism to form various hydrocarbons in the zeolite pores.[38] Wang *et al.* reported that in the case of HZSM-5, the methyl substituted 5-6 membered ring reactive carbenium intermediates such as pentamethylbenzenium ($PentaMB^+$), di/tri-methylcyclopentenyl cation (diMCP+, triMCP+) can be generated.[39] Those cyclic organic species confined in zeolite cages/intersection space could act as a co-catalyst for the formation of ethene *via* side chain elimination from MCP^+.[40] In addition, different type of MCP^+ can be formed depending on the parent zeolite used.

From the N_2O and methane reaction over Fe/ZSM-5 discussed in the present study, we were able to detect trace amount of aromatic species in the gas effluent including methyl benzene, toluene and xylene. This may explain the origin of ethene and coke generated from a competing reaction path (MTO). A simplified reaction network from N_2O and CH_4 over Fe/ZSM-5 is presented in figure. 3.12.

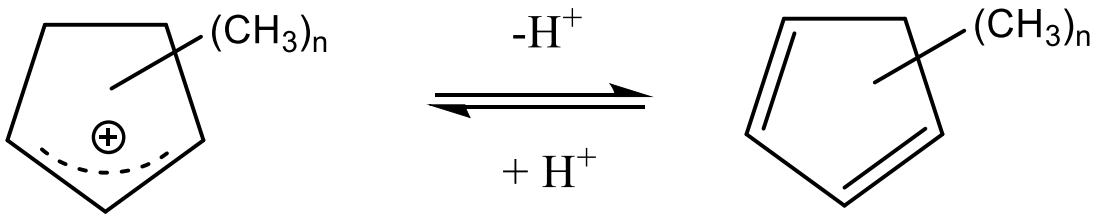

Figure 3.12 MCP^+ cations and its deprotonated analogue, methylcyclopentadienes which are often observed in MTO chemistry using HZSM-5, which may act as a precursor to coke.

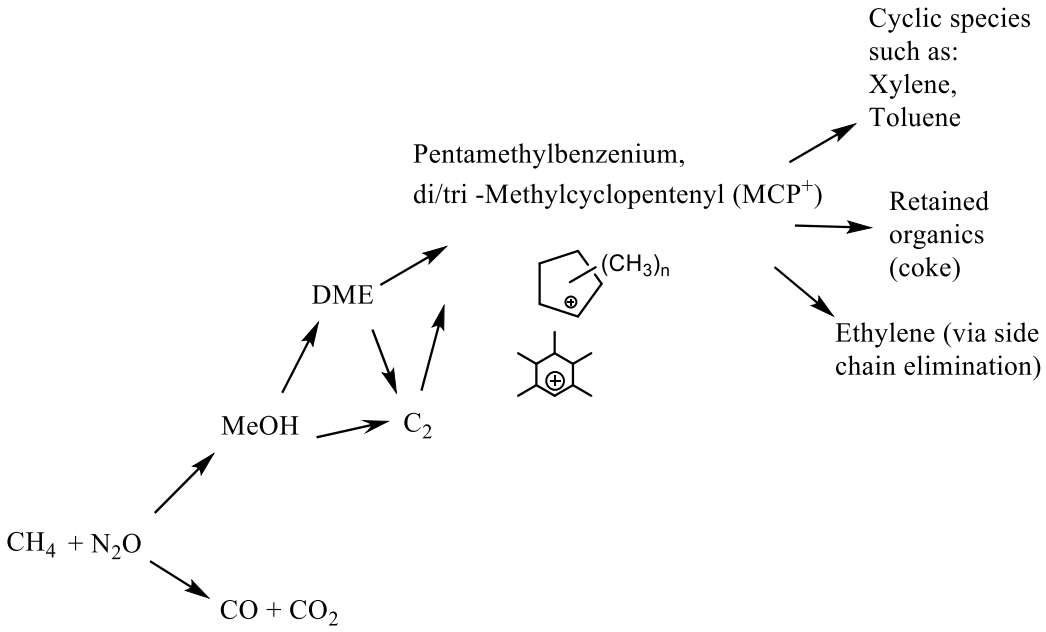

Figure 3.13 A basic schematic reaction path for the origin of coke formation.

The reaction path of methane is thought to occur according to the following steps: (1) the N_2O activated Fe/ZSM-5 initially converts methane to MeOH and carbon oxides, (2) the MeOH (through its methyl group) remains adsorbed on the catalyst surface and can undergo dehydration to form DME or may also directly transform to ethene via recombination of two methyl radicals, although this process is hotly debated[41, 42]. (3) There are bulky cyclic intermediates (MCP^+) which can be formed via the hydrocarbon pool mechanism in the zeolite pores, which result in the formation of aromatic molecules, ethene and organics deposits which remain strongly bounded to the catalyst to form coke. Diluted methanol vapour was passed over a series of MFI-based catalysts with N_2O presence to investigate the stability and reactivity of the target products under reaction conditions. The catalysts used in this MeOH control study were the SIL-1, TS-1, Fe-free H-ZSM-5 and their Fe containing analogues. The catalyst mass was adjusted to ensure comparable methanol conversions of *ca.* 15 % at 300 °C while maintaining a GHSV of 3600 h^{-1} by diluting the catalyst bed with SiC to maintain a constant space velocity. The results are summarised in Table 3.8 and the time online data for the active catalysts are presented in figures 3.14 - 3.19.

Table 3.8: Methanol control experiments over MFI catalysts calcined 550 °C unless otherwise stated.

Catalyst	Catalyst mass (g)	Conversion[a] (%)		Selectivity[a] (%)					Specific Activity [b] (mol. $g^{-1}.h^{-1}$)
		MeOH	N_2O	DME	CO	CO_2	C_2H_4	Coke	
H-ZSM-5	0.05	14.8	0.5	44.4	0.1	0.06	16.4	39.0	0.266
TS-1	0.4	-	-	-	-	-	-	-	-
SIL-1	0.4	-	-	-	-	-	-	-	-
2wt% Fe/ZSM5	0.05	16.1	6.5	54.3	0.5	0.2	8.0	37.0	0.290
2wt.% Fe/ZSM5 (calcined 950 °C)	0.05	12.8	1.3	88.1	0.2	0.06	1.6	10.0	0.230
2wt.% Fe/TS1	0.1	17.4	0.7	95.1	1.8	0.14	-	3.0	0.157
0.5wt.% Fe/SIL-1 (steamed 875 °C)	0.4	17.3	1.2	86.6	1.8	0.4	-	11.2	0.039

[a] Values at 65 min; [b] Moles of MeOH converted per g of catalyst per hour; reaction conditions: catalyst mass = varied between 0.05 – 0.4 g and diluted to 1 mL with SiC; GHSV 3600 h^{-1}, Pellet Mesh size = 600 μm; V = 0.9 ml ; 300 °C; 2 h; Feed mixture: 1.2% MeOH + 2% N_2O with Ar balance; Flow rate = 55 ml min^{-1}; P(total) = 1 atm.

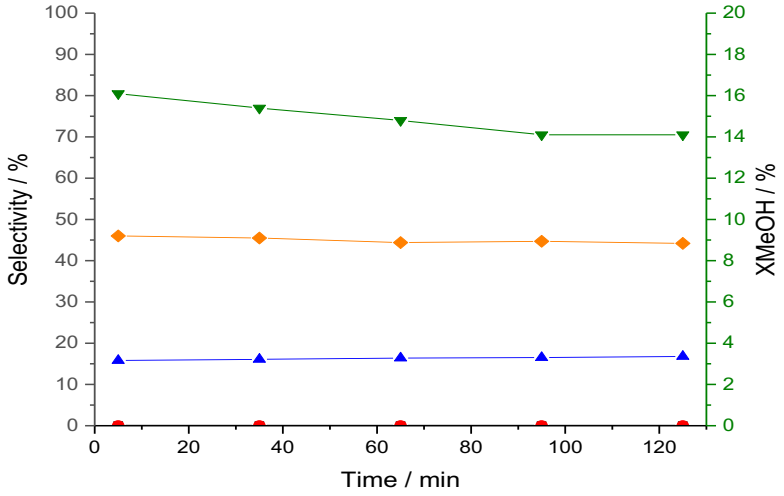

Figure 3.14: Time online data for MeOH control experiment at 300 °C for H-ZSM-5 (30). (▼) MeOH conversion and products selectivity in the gas phase: (●) CO_2; (▲) C_2 and (♦) DME.

Methanol was converted to DME as the major product without any addition of Fe species over HZSM-5. It appears that the zeolite framework containing Si-O-Al is effective to convert MeOH to DME and C_2 species along with small quantity of carbon oxides. However, it is also well-known that approximately ppm levels of Fe impurities are always present in the ZSM-5 sample from the zeolite framework precursor, and cannot be excluded from discussion.

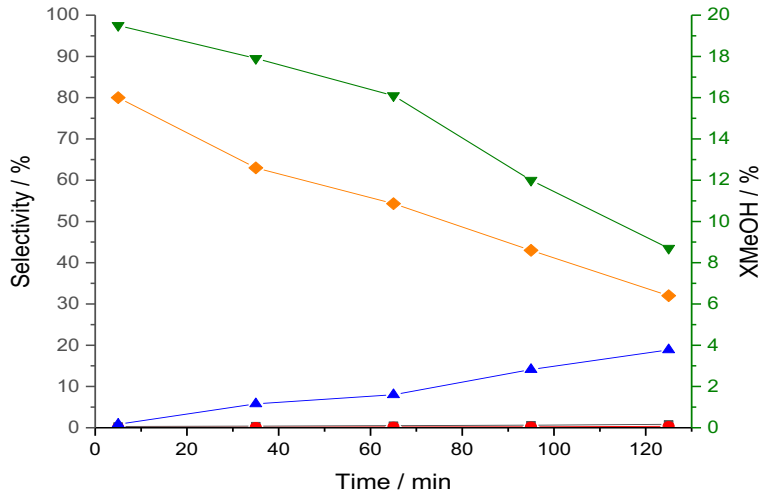

Figure 3.15 Time online data for MeOH control experiment at 300 °C for Fe/ZSM-5 calcined 550 °C. (▼) MeOH conversion and products selectivity in the gas phase: (●) CO_2; (▲) C_2 and (♦) DME.

In the MeOH control experiment using Fe/ZSM-5. It appears that MeOH primarily produces DME and as the reaction time increases, the selectivity to DME drops while C_2 selectivity increases over time which indicates the formation of ethene/ethane species which supress the DME formations. The formation of C_2 species also appears to contribute to the poor mass balance as a result of coking as reported through the MTO process. A small quantity of carbon oxide was also detected. It was observed that MeOH conversion has a decreasing trend as the reaction proceed over 2h. This shows the effect of retained organic species formed via the undesired MTO reaction and could be explained by the blockage of active sites and pore environment.

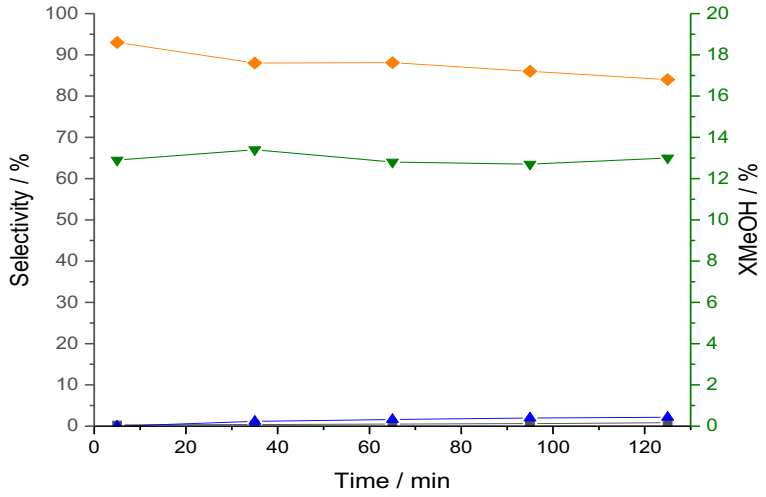

Figure 3.16: Time online data for MeOH control experiment at 300 °C for 2 wt.% Fe/ZSM5 calcined 950 °C. (▼) MeOH conversion and products selectivity in the gas phase: (▲) C_2 and (♦) DME.

After calcining 2 wt.% Fe/ZSM-5 at 950 °C, it is observed that the methanol conversion is much more stable than its analogue calcined at 550 °C. The products selectivity is also altered as DME is formed throughout the 2 h and only a small percentage of C_2 species were detected.

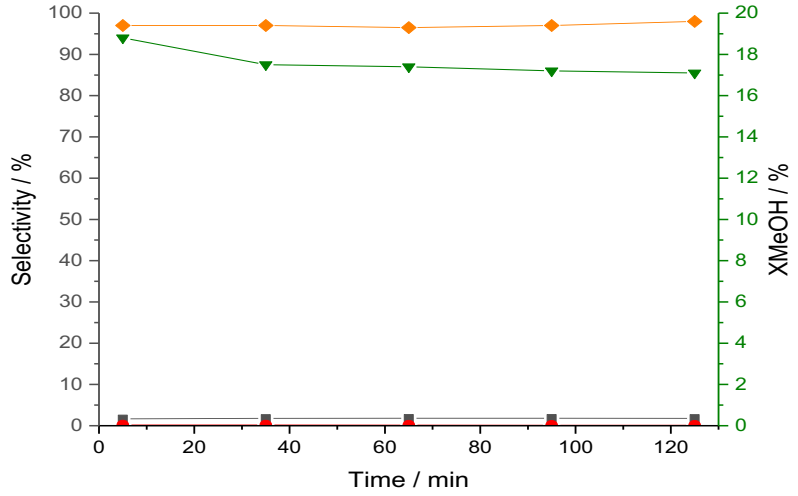

Figure 3.17: Time online data for MeOH control experiment at 300 °C for 2 wt.% Fe/TS1 calcined 550 °C. (▼) MeOH conversion and products selectivity in the gas phase: (●) CO_2; (■) CO and (♦) DME.

As show in figure 3.17, using the Fe - titanium silicate-based system, it was observed that DME had a selectivity of >95%. Interestingly, there were no C2 species formed and only a minor amount of carbon oxides were present.

The MeOH control experiment over steam treated 0.5 wt.% Fe/SIL-1 (875 °C) is shown in figure 3.18.

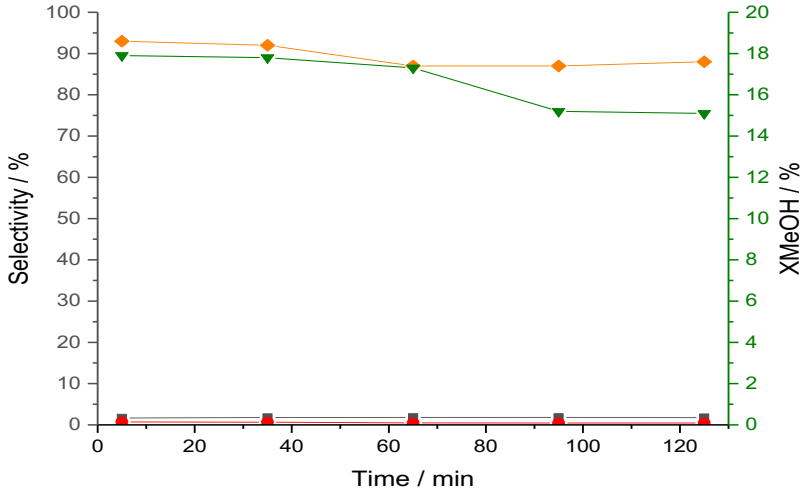

Figure 3.18 Time online data for methanol control experiment at 300 °C for 0.5 wt.% Fe/SIL-1 steamed 875 °C. (▼) MeOH conversion and products selectivity in the gas phase: (●) CO_2; (■) CO and (♦) DME

The product distribution on 0.5wt.% Fe/SIL-1 is similar to what is observed with the 2 wt.% Fe/TS-1 as over 90% DME is formed along with small amount of carbon oxides. There are no C_2 species observed unlike the case of HZSM-5.

Interestingly, methanol conversion was observed in HZSM-5 and all the Fe-containing catalysts and the primary product in these cases was DME. The results over the SIL-1 and TS-1 materials (in this case the zeolite has no Al present) strongly indicate that Brønsted acidity is required to complete the formation of DME as previously reported.[40, 43]

Over HZSM-5, the selectivity to DME was *ca.* 44 % and for ethene *ca.* 16 % at 65 minutes, which is consistent with previous reports.[37] The time online data clearly indicates that the increased selectivity to C_{2+} products leads to low mass balance observed through the subsequent formation of retained organics. The time online data suggests that the catalyst is relatively stable over the 2 h of reaction (see figure 3.14). In contrast, the yield of DME, over the 2 wt.% Fe/ZSM-5 (550 °C) catalyst decreases rapidly over the 2 h reaction period and an increase of ethene was observed. Although, ethene was formed over the 2 wt.% Fe/ZSM-5 (950 °C) catalyst, the STY was relatively low at *ca.* 4 μmol g^{-1} h^{-1} after 125 min time online. Over the 0.5 wt.% Fe/SIL-1 catalyst steamed at 875 °C, the conversion of methanol to DME proceeds readily despite the absence of Al and extra-framework Fe. This is exemplified by the high DME selectivity of 95 % achieved over the Fe/TS-1 catalyst.

These results imply that the presence of acidity associated with Al is not necessarily required to facilitate the methanol condensation reaction to form DME. However, it is observed that the strength of the acid sites can affect the rate of products desorption and their subsequent reduction in mass balance is observed. Furthermore, these results support the low methanol selectivity observed in the methane oxidation reactions where water is not present in the feed (Table 3.1).

The challenge of selective methane oxidation is exemplified here as methanol is significantly more reactive than methane over the acidic MFI catalysts. Indeed, over MFI catalysts with moderate to high acidity such as 2 wt.% Fe/ZSM-5 (550 °C) any DME produced at the low methane conversions achieved, appears to convert rapidly to other products such as ethene, unlike over 2 wt.% Fe/ZSM-5 (950 °C) catalyst shown

in Table 3.8. Parfenov *et al.* also reported that the surface diffusion of MeOH is much more favourable than desorbing from the catalyst surface.[2, 5]

An additional consideration is the relatively high concentration of methanol in the feed stream that may operate in a comparable manner to using methane diluted with water[44, 45]. That is the product which is displaced rapidly from the active sites with water and hence the selectivity to methanol from methane is high, such as DME from methanol in these experiments. Furthermore, ethene and coke are only formed over the catalyst with Al present, via the Brønsted acid sites under these reaction conditions. The implication is that framework Al sites free of Fe are able to convert methanol efficiently. Therefore, tailoring the acidity and Fe loading of the catalyst can significantly improve methanol yields.

3.7 Methane oxidation using O_2 over Fe/ZSM-5

The other aspect of this industrial funded project is to investigate the use of molecular oxygen rather than N_2O for the CH_4 activation over 2 wt. % Fe/ZSM-5 (prepared by CVI) to monitor how active sites are operated in this reaction system. The α-oxygen species are generated via the catalytic decomposition of N_2O over the Fe/ZSM-5. Although it has been reported that this radical like α-oxygen species can only be formed only using N_2O[1, 5, 46, 47], the work in the following section investigates whether it is possible to generate this active Fe-O species after the Fe/ZSM-5 is first reacted with N_2O and regenerated using molecular oxygen. The hypothetical reaction scheme is shown in figure 3.19.

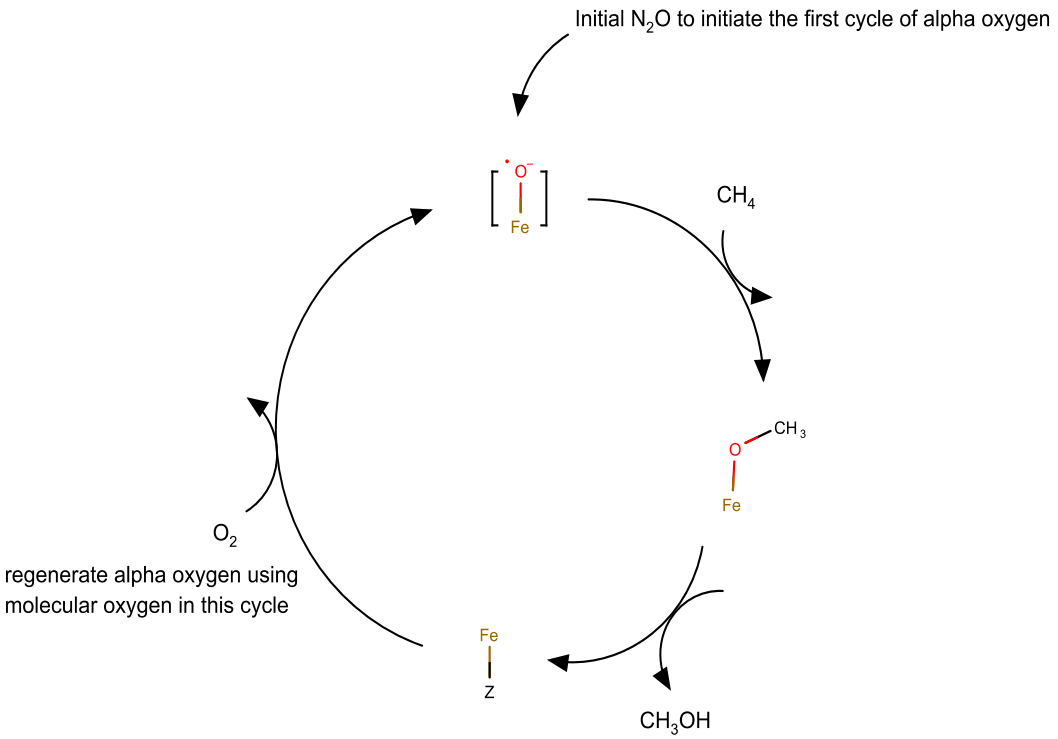

Figure 3.19 The hypothetical reaction scheme involving using molecular oxygen.

3.7.1 Preliminary study on CH_4 + O_2 over 2 wt.% Fe/ZSM-5

The preliminary work was carried out by reacting O_2 and CH_4 simultaneously between 250 to 300 °C to see whether it is possible to produce methanol or other oxygenates using molecular oxygen as the oxidant. The reaction was essentially inactive when the reaction temperature was set at 250 °C. Minor activity occurred at 275 °C and the time on stream and conversion plot are shown in figures 3.20 a and b. The conversion and selectivity at 300°C are reported in figures 3.21 a and b.

a)

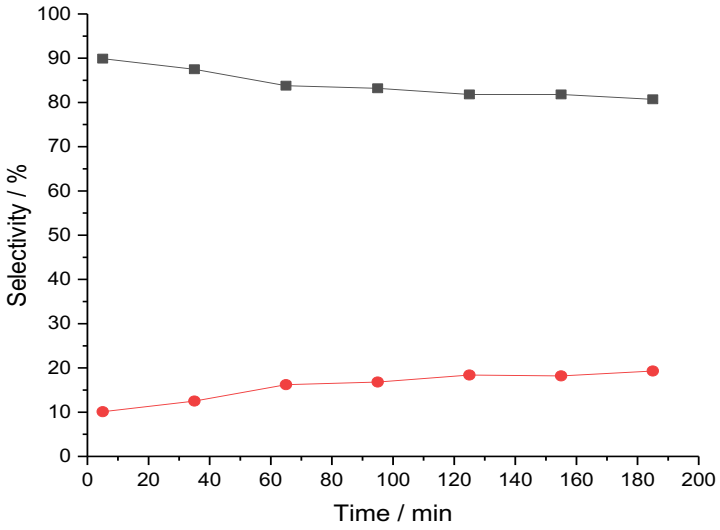

b)

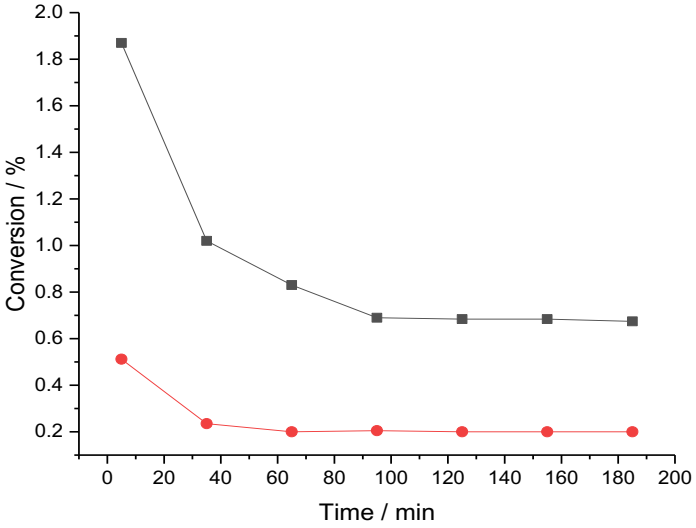

Figures 3.20: Time online data for methane oxidation at 275 °C using O_2 over Fe/ZSM-5; (a) Product selectivity in the gas phase: (●) CO_2 and (■) CO, (b) (●) CH_4 and (■) O_2 conversion.

a)

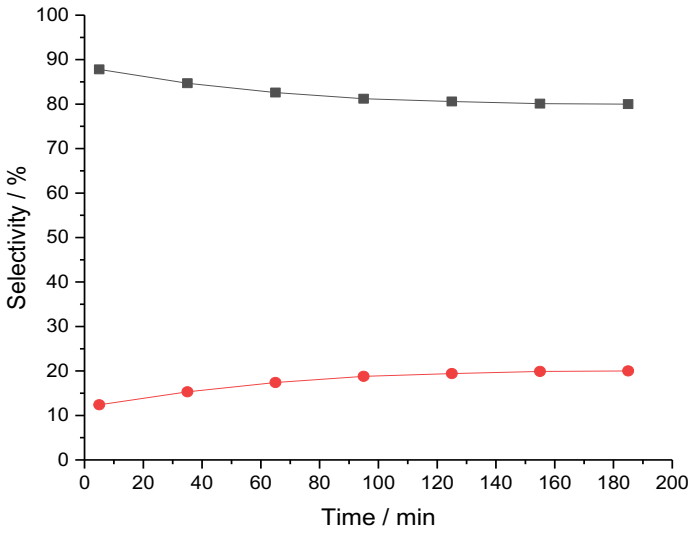

b)

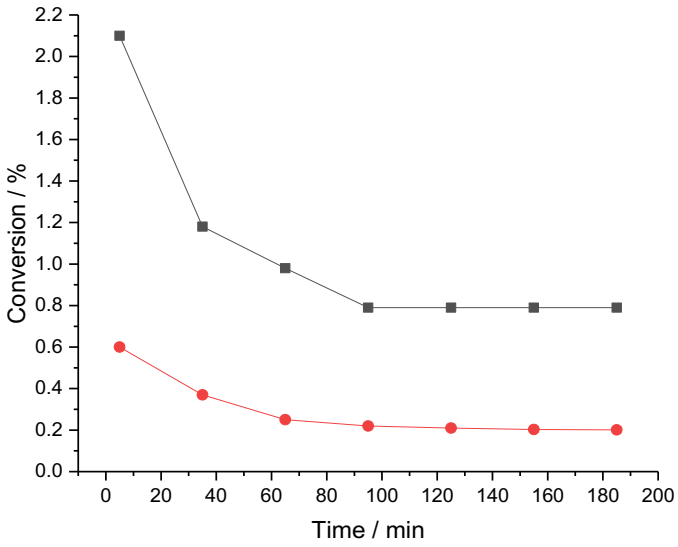

Figures 3.21 Time online data for methane oxidation at 300 °C using O_2 over Fe-ZSM-5; (a) Product selectivity in the gas phase: (●) CO_2 and (■) CO, (b) (●) CH_4 and (■) O_2 conversion.

The time online data for methane oxidation using molecular oxygen over Fe/ZSM-5 prepared using CVI is shown in figure 3.20 a and b. The methane activity became

modestly active at approximately 0.9% conversion at 275 and 300 °C. This preliminary study attempted to oxidise methane using molecular oxygen only produce carbon oxides with below 1% methane conversion. This, supports literature results shown by various groups that oxygen does not behave like N_2O when it is reacted over Fe/ZSM-5 that the Fe-O active species cannot be formed due to the strong stabilisation energy of ZSM-5 over O_2.[3, 48]

3.7.2 Sequential methane oxidation using N_2O and O_2

The α-oxygen can only be generated over N_2O as results shown from reaction carried out by flowing CH_4 and O_2 simultaneously shown in section 3.7.1 and only carbon oxides were produced with no oxygenate detected. The second approach was based on the idea that active Fe-O species were first being generated over Fe/ZSM-5 after reacting with N_2O and CH_4 to form desired methanol in the first cycle. After that, N_2O would be substituted by molecular oxygen in attempt to regenerate the active sites once again to keep the active Fe sites being regenerated and to oxidise methane (figure 3.19).

The 2 h experiment started by reacting CH_4 and N_2O simultaneously for 60 min before switching to O_2 + CH_4 as the second cycle for the remaining 60 min reaction. The time on stream data for the MeOH produced and the CH_4 and N_2O activity plot from this cyclic scheme are presented in figure 3.22 a and b.

a)

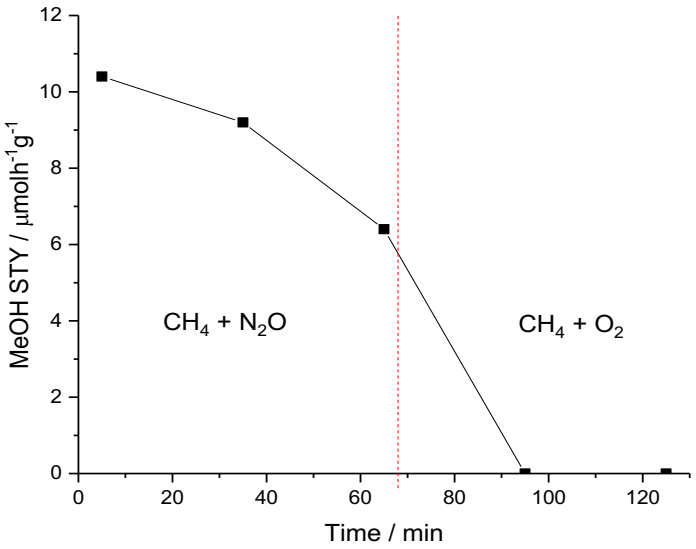

b)

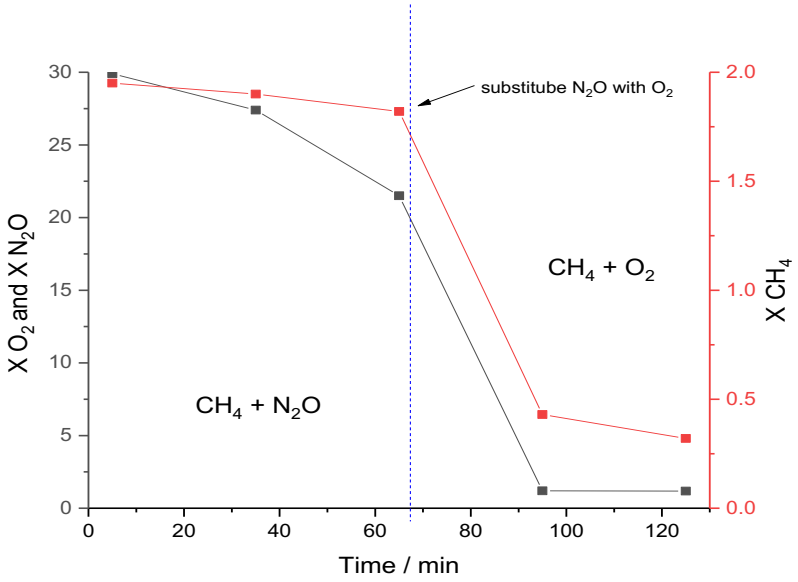

Figure 3.22 Time on stream data for the sequential methane oxidation at 300 °C over 2 wt.% Fe/ZSM-5; (a) Space time yield of MeOH recorded in the gas phase; (b) (●) CH_4 and (■) O_2/N_2O conversion.

It was observed that the conversion of N_2O and CH_4 were 28 % and 1.9 % respectively over the first 60 min. The products composition was CH_3OH, carbon oxides and trace quantities of C_2 were also observed as expected. However, after entering the $CH_4 + O_2$ cycle the activity drops to almost inactive. The conversion decreased to 0.2 % and 0.8 % for O_2 and CH_4 respectively. There are no partial oxygenates being produced when N_2O was substituted with O_2 and only minor carbon oxides recorded. This result suggests that the experiment does not support the hypothesis.

3.7.3 Reintroduce N_2O in sequential reaction.

Following the sequential reaction study presented in section 3.7.2, N_2O was introduced after reacting a mixture of O_2 and CH_4 simultaneously to see whether if MeOH can only be generated using N_2O. MeOH was detected immediately at the first GC measurement after N_2O was introduced. The cycle was continued for 2 more cycles and it suggested that only N_2O can generate active sites available for MeOH production. The sequential experiment incorporation N_2O and O_2 with CH_4 is presented in figure. 3.23 and the MeOH yield is shown in 3.24.

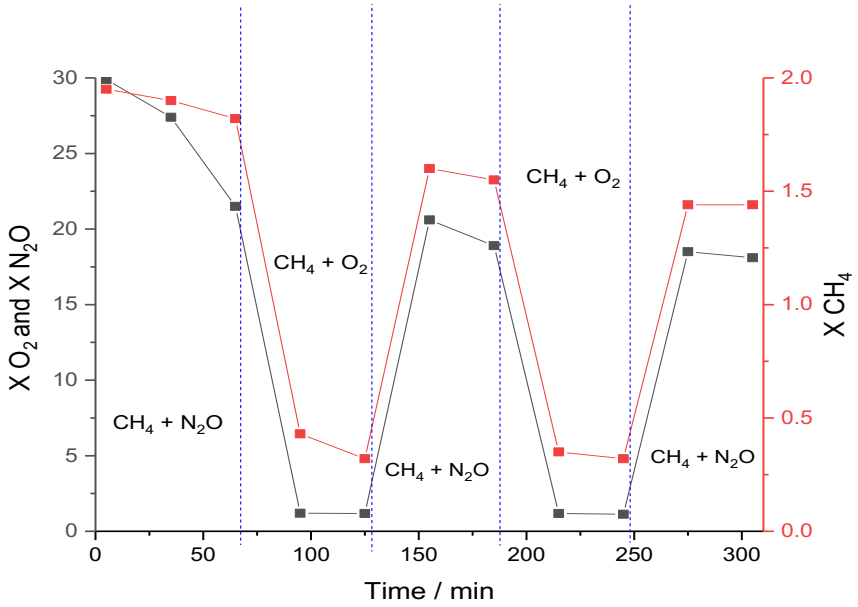

Figure 3.23 Time on stream data for the sequential methane oxidation at 300 °C over 2 wt.% Fe/ZSM-5; (■) CH_4 and (■) O_2/N_2O conversion.

Figure 3.23 shows the conversion of N_2O/O_2 and CH_4 conversion in different blocks as labelled. It is clear that the CH_4 conversion drops to ca. 0.4 % when the reaction mixtures is switched to CH_4 and O_2. The CH_4 activity reaches >1.2 % during N_2O + CH_4 cycle.

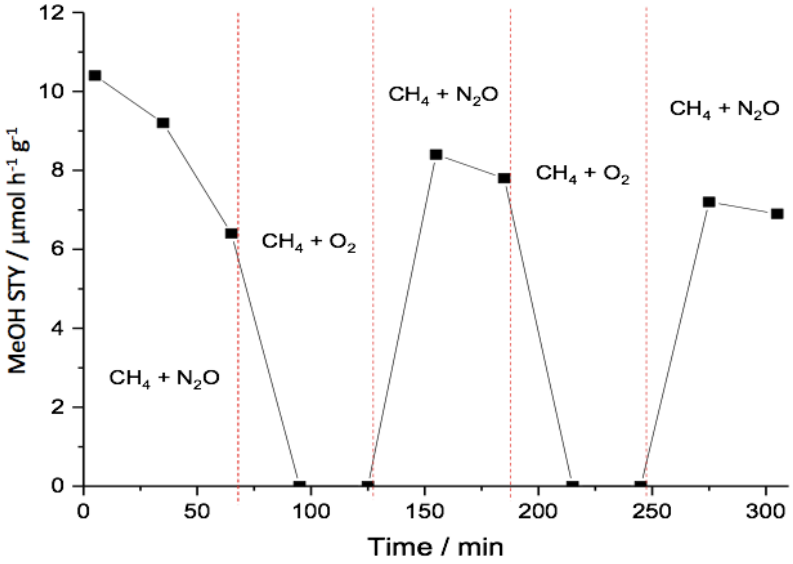

Figure 3.23 Time on stream data for the sequential methane oxidation at 300 °C over 2 wt.% Fe/ZSM-5; Space time yield of MeOH recorded in the gas phase.

Figure 3.23 shows that MeOH is only detected during the N_2O + CH_4 period. The catalyst becomes active again for MeOH generation after exposing to oxygen. It is observed that *ca*. 6 -10 μmol h^{-1} g^{-1} can be generated in each cycle. It indicates that it is important to generate α-oxygen species over Fe/ZSM-5 using N_2O for MeOH production. The O_2/CH_4 exposure in-between each N_2O/CH_4 cycle does not significantly deactivate the catalyst during the 5 h experiment. A table summary for this methane partial oxidation using oxygen over 2 wt. % Fe/ZSM-5 is presented in table 3.9 for comparison.

Table 3.9: Methane oxidation performed at different temperature over Fe-ZSM-5 catalysts prepared by CVI using molecular oxygen.

Reaction temperature / °C	Conversion[a] (%)		Selectivity[a] (%)					STY_{MeOH}[b] ($\mu mol.g^{-1}.h^{-1}$)
	O_2	CH_4	MeOH	CO	CO_2	C_2H_4	Coke	
250	-	-	-	-	-	-	-	-
275	0.21	0.82	-	83.8	16.2	-	-	-
300	0.25	0.9	-	82.6	17.4	-	-	-
300[c]	0.19	0.85	-	82.8	17.2	-	-	-
300*	21.5*	1.8	1.1	24.3	9.5	3.5	62.6	6.4

[a] Values at 1 h; [b] STY_{MeOH}: space time yield of methanol; [c] sequential reaction using O_2 + CH_4 Reaction conditions: 0.44 g catalyst; Pellet Mesh size = 600 µm ; V = 0.9 ml; 2 h; Feed mixture: 20% CH_4 + 2% N_2O with Ar balance; Flow rate = 55 ml min^{-1}; P(total) = 1 atm; GHSV= 3600 h^{-1}. *Reaction carried out using N_2O for comparison

3.8 Conclusions

The first goal of this chapter was to investigate the nature of the Fe species and acid sites involved in the activation of the C-H methane bond during the oxidation of methane in the presence of N_2O.

The continuous oxidation of methane by N_2O was investigated using a series of different MFI-based zeolites and their Fe-analogues catalysts prepared through ion exchange process. The parent zeolites; SIL-1, TS-1 and H-ZSM-5 were tested and the results suggest that the activation of methane occurs only in the case of H-ZSM-5. However, this observation is likely to be caused by the presence of metal impurities and Hammond *et al.* also reported this minor activity observed using H_2O_2 as the oxidant.[8] It is also observed that the Al coordinated to Fe is required to generate MeOH.

The addition of Fe to the parent zeolite enhanced the methane activation when ZSM-5 was used, although the catalyst generated a significant amount of coke that led to poor carbon mass balance as the reaction proceeded throughout the 3 h reaction. The origin of the low mass balance and increased catalyst fouling was investigated through exploration of the catalyst acidity and the location and speciation of Fe formed using various ion exchange approaches. The study on the steam /high temperature treatment to Fe/SIL-1 to create extra-framework Fe sites suggests that having those Fe species alone, only modest C-H bond activation was observed. It is considered that those extra-framework Fe sites becomes more active in the presence of Al.

Methanol control experiments indicated that methanol is unstable over catalysts with high Brønsted acidity such as H-ZSM-5 and those containing Fe such as Fe-SIL-1 and Fe-TS-1. However, the formation of C_{2+} and aromatic species was only observed in the case of the ZSM-5 catalysts. This supports the observed low methanol selectivity and poor mass balances observed in the methane oxidation reaction presented. The results suggest that through manipulation of catalyst acidity and Fe concentration, improvements in methanol selectivity can be achieved where desorption of the primary product is facile. This study also demonstrates that for selective methane oxidation with N_2O, extra-framework Fe species co-ordinated to framework Al are required. However, Brønsted acid sites located on Fe-free Al lead to the transformation of methanol into coke.

Simultaneously reacting CH_4 and oxygen together between 250-300 °C over Fe/ZSM-5 shows that only minor CH_4 conversion was achieved. The experiment produces trace amount of carbon oxide with no methanol detected. The attempt of using a cyclic N_2O and oxygen approach to regenerate the active species for continuous methane oxidation did not yield any partial oxygenates in the subsequent O_2 cycle after N_2O was substituted.

3.9 References

1. G. I. Panov, A. K. Uriarte, M. A. Rodkin and V. I. Sobolev, *Catalysis Today*, 1998, 41, 365-385.
2. E. V. Starokon, M. V. Parfenov, S. S. Arzumanov, L. V. Pirutko, A. G. Stepanov and G. I. Panov, *Journal of Catalysis*, 2013, 300, 47-54.
3. E. V. Starokon, M. V. Parfenov, L. V. Pirutko, S. I. Abornev and G. I. Panov, *Journal of Physical Chemistry C*, 2011, 115, 2155-2161.
4. E. V. Starokon, M. V. Parfenov, S. E. Malykhin and G. I. Panov, *Journal of Physical Chemistry C*, 2011, 115, 12554-12559.
5. M. V. Parfenov, E. V. Starokon, L. V. Pirutko and G. I. Panov, *Journal of Catalysis*, 2014, 318, 14-21.
6. A. Zecchina, M. Rivallan, G. Berlier, C. Lamberti and G. Ricchiardi, *Physical Chemistry Chemical Physics*, 2007, 9, 3483-3499.
7. B. E. R. Snyder, P. Vanelderen, M. L. Bols, S. D. Hallaert, L. H. Bottger, L. Ungur, K. Pierloot, R. A. Schoonheydt, B. F. Sels and E. I. Solomon, *Nature*, 2016, 536, 317-321.
8. C. Hammond, N. Dimitratos, R. L. Jenkins, J. A. Lopez-Sanchez, S. A. Kondrat, M. H. ab Rahim, M. M. Forde, A. Thetford, S. H. Taylor, H. Hagen, E. E. Stangland, J. H. Kang, J. M. Moulijn, D. J. Willock and G. J. Hutchings, *Acs Catalysis*, 2013, 3, 689-699.
9. C. Hammond, M. M. Forde, M. H. Ab Rahim, A. Thetford, Q. He, R. L. Jenkins, N. Dimitratos, J. A. Lopez-Sanchez, N. F. Dummer, D. M. Murphy, A. F. Carley, S. H. Taylor, D. J. Willock, E. E. Stangland, J. Kang, H. Hagen, C. J. Kiely and G. J. Hutchings, *Angewandte Chemie-International Edition*, 2012, 51, 5129-5133.

10. K. A. Dubkov, N. S. Ovanesyan, A. A. Shteinman, E. V. Starokon and G. I. Panov, *Journal of Catalysis*, 2002, 207, 341-352.
11. A. M. DeGroote and G. F. Froment, *Catalysis Today*, 1997, 37, 309-329.
12. G. K. Boreskov, Springer Berlin Heidelberg, Berlin, Heidelberg, 1982, pp. 39-137.
13. K. Narsimhan, K. Iyoki, K. Dinh and Y. Roman-Leshkov, *Acs Central Science*, 2016, 2, 424-429.
14. E. G. Derouane, J. C. Vedrine, R. R. Pinto, P. M. Borges, L. Costa, M. Lemos, F. Lemos and F. R. Ribeiro, *Catalysis Reviews-Science and Engineering*, 2013, 55, 454-515.
15. C. Mirodatos and D. Barthomeuf, *Journal of the Chemical Society-Chemical Communications*, 1981, DOI: 10.1039/c39810000039, 39-40.
16. M. Niwa, S. Sota and N. Katada, *Catalysis Today*, 2012, 185, 17-24.
17. W. F. Hoelderich, *Applied Catalysis a-General*, 2000, 194, 487-496.
18. J. Perez-Ramirez and A. Gallardo-Llamas, *Applied Catalysis a-General*, 2005, 279, 117-123.
19. M. He, J. Zhang, X. L. Sun, B. H. Chen and Y. G. Wang, *Journal of Physical Chemistry C*, 2016, 120, 27422-27429.
20. E. J. M. Hensen, Q. Zhu, R. A. J. Janssen, P. Magusin, P. J. Kooyman and R. A. van Santen, *Journal of Catalysis*, 2005, 233, 123-135.
21. M. Schwidder, W. Grunert, U. Bentrup and A. Bruckner, *Journal of Catalysis*, 2006, 239, 173-186.
22. S. Bordiga, R. Buzzoni, F. Geobaldo, C. Lamberti, E. Giamello, A. Zecchina, G. Leofanti, G. Petrini, G. Tozzola and G. Vlaic, *Journal of Catalysis*, 1996, 158, 486-501.
23. E. J. M. Hensen, Q. Zhu, M. M. R. M. Hendrix, A. R. Overweg, P. J. Kooyman, M. V. Sychev and R. A. van Santen, *Journal of Catalysis*, 2004, 221, 560-574.
24. G. N. Li, E. A. Pidko, I. A. W. Filot, R. A. van Santen, C. Li and E. J. M. Hensen, *Journal of Catalysis*, 2013, 308, 386-397.
25. J. Perez-Ramirez, *Journal of Catalysis*, 2004, 227, 512-522.
26. C. Hammond, N. Dimitratos, J. A. Lopez-Sanchez, R. L. Jenkins, G. Whiting, S. A. Kondratt, M. H. ab Rahim, M. M. Forde, A. Thetford, H. Hagen, E. E.

Stangland, J. M. Moulijn, S. H. Taylor, D. J. Willock and G. J. Hutchings, *Acs Catalysis*, 2013, 3, 1835-1844.

27. O. Prokopova, B. Bernauer, M. Frycova, P. Hrabanek, A. Zikanova and M. Kocirik, *Journal of Physical Chemistry C*, 2013, 117, 1468-1476.
28. T. C. Hoff, R. Thilakaratne, D. W. Gardner, R. C. Brown and J. P. Tessonnier, *Journal of Physical Chemistry C*, 2016, 120, 20103-20113.
29. J. Lu, E. Bartholomeeusen, B. F. Sels and D. Schryvers, *Journal of Microscopy*, 2017, 265, 27-33.
30. M. B. J. Roeffaers, R. Ameloot, M. Baruah, H. Uji-i, M. Bulut, G. De Cremer, U. Muller, P. A. Jacobs, J. Hofkens, B. F. Sels and D. E. De Vos, *Journal of the American Chemical Society*, 2008, 130, 5763-5772.
31. F. Jin and Y. D. Li, *Catalysis Today*, 2009, 145, 101-107.
32. L. F. Isernia, *Materials Research-Ibero-American Journal of Materials*, 2013, 16, 792-802.
33. E. Selli, A. Isernia and L. Forni, *Physical Chemistry Chemical Physics*, 2000, 2, 3301-3305.
34. J. H. C. van Hooff and J. W. Roelofsen, *Studies in Surface Science and Catalysis*, 1991, 58, 241-283.
35. Q. Zhao, W. H. Chen, S. J. Huang, Y. C. Wu, H. K. Lee and S. B. Liu, *Journal of Physical Chemistry B*, 2002, 106, 4462-4469.
36. P. Pramatha and K. D. Prabir, in *Handbook of Zeolite Science and Technology*, CRC Press, 2003, DOI: doi:10.1201/9780203911167.pt1
37. M. Bjorgen, S. Svelle, F. Joensen, J. Nerlov, S. Kolboe, F. Bonino, L. Palumbo, S. Bordiga and U. Olsbye, *Journal of Catalysis*, 2007, 249, 195-207.
38. I. M. Dahl and S. Kolboe, *Journal of Catalysis*, 1994, 149, 458-464.
39. C. Wang, X. F. Yi, J. Xu, G. D. Qi, P. Gao, W. Y. Wang, Y. Y. Chu, Q. Wang, N. D. Feng, X. L. Liu, A. M. Zheng and F. Deng, *Chemistry-a European Journal*, 2015, 21, 12061-12068.
40. P. Tian, Y. X. Wei, M. Ye and Z. M. Liu, *Acs Catalysis*, 2015, 5, 1922-1938.
41. X. Wu, S. Xu, W. Zhang, J. Huang, J. Li, B. Yu, Y. Wei and Z. Liu, *Angewandte Chemie International Edition*, 2017, 56, 9039-9043.
42. D. Lesthaeghe, V. Van Speybroeck, G. B. Marin and M. Waroquier, *Angewandte Chemie-International Edition*, 2006, 45, 1714-1719.

43. J. Z. Li, Y. Qi, L. Xu, G. Y. Liu, S. H. Meng, B. Li, M. Z. Li and Z. M. Liu, *Catalysis Communications*, 2008, 9, 2515-2519.
44. P. Tomkins, A. Mansouri, S. E. Bozbag, F. Krumeich, M. B. Park, E. M. C. Alayon, M. Ranocchiari and J. A. van Bokhoven, *Angewandte Chemie-International Edition*, 2016, 55, 5467-5471.
45. V. L. Sushkevich, D. Palagin, M. Ranocchiari and J. A. van Bokhoven, *Science*, 2017, 356, 523-527.
46. G. I. Panov, K. A. Dubkov and Y. A. Paukshtis, *Catalysis by Unique Metal Ion Structures in Solid Matrices: from Science to Application*, 2001, 13, 149-163.
47. G. I. Panov, K. A. Dubkov and E. V. Starokon, *Catalysis Today*, 2006, 117, 148-155.
48. V. I. Sobolev, O. N. Kovalenko, A. S. Kharitonov, Y. D. Pankrat'ev and G. I. Panov, *Mendeleev Communications*, 1991, 1, 29-30.

4

Effect of water addition on the kinetic study of methane partial oxidation over the 2 wt.% Fe/ZSM-5

The goal of this chapter is to investigate how water influences the reaction system and the selectivity to methanol. The product rank will be determined from the reaction paths taken in both water-assisted and water-free system using N_2O over 2 wt. % Fe/ZSM-5. Control experiments were designed to study the N_2O decomposition process occurred in both system.

4.1 Introduction

Methanol is being produced from methane industrially via an energy-intensive two-steps process. It involves a high-temperature reforming of methane followed by methanol synthesis.[1-4] The direct oxidation of methane to methanol would bring economic benefits for energy sectors and this alternative process offers environmental advantage over the current industrial method.[5] However, direct methane to methanol remains the grand challenge for scientists due to limited methanol selectivity and poor reactivity of methane observed when employing metal oxides or supported metal as catalysts.[6]

There are recent publications that applied the zeolite-based systems as an alternative approach for the partial methane oxidation.[7-10] Tomkins *et al.* reported an isothermal catalytic cycle which uses Cu-mordenite to convert methane into methanol.[11] The catalyst is first being activated using molecular oxygen in the first cycle. Then the activated oxygen-copper-species react with methane. Methanol formed on the catalyst surface was subsequently extracted using steam by a hydrolysis process, which provides further oxidation cycles to be carried out over the regenerated active sites. Roman-Leshkov and co-workers have also shown that copper-exchanged-zeolite can be used together with oxygen and water for the continuous catalytic production of methanol from methane oxidation, using carefully designed reaction conditions.[7] Furthermore, Sushkevich *et al*. have reported the direct, partial methane oxidation to methanol by utilising water as both the solvent and oxygen source using Cu-containing zeolites.[12] The water utilisation in this anaerobic methane oxidation system indicated that water has the potential to be further exploited as an oxidant in hydrocarbon oxidation. Water in the reaction also served as an active site regenerating species through facilitating the desorption of partially oxygenates.[12] Higher conversions in a continuous process can be achieved by approaches using H_2O[13] or/and N_2O[14] as primary oxidants.

Panov and co-workers reported the continuous catalytic gas-phase methane oxidation by active α-oxygen species generated by treating Fe/ZSM-5 with N_2O at 300 °C.[14] The authors reported this one step continuous flow system to produce methanol.[14] The catalyst deactivates over two hours and this was due to the formation of coke which led to significant catalyst fouling. The same group has also shown that water can be introduced into the reaction mixture which proved to be beneficial to both carbon balance and methanol selectivity. A massive improvement on the methanol selectivity was seen increased from 1.9 % to 19 % when 20 % v/v steam was added.[14] The addition of water into the N_2O and methane gas mixture also led to higher CO selectivity.[14, 15] However, it is observed that the N_2O decomposition is decreased over Fe/ZSM-5 when the system is operating in the presence of H_2O. This, results in promoting the hydroxylation of the peroxide bridge within binuclear Fe sites. The apparent activation energy for N_2O decomposition in the H_2O assisted reaction was increased from 120 to 196 $kJ.mol^{-1}$.[16]

CH_4 oxidation using N_2O over Fe/ZSM-5 involves a complex reactions mechanism and undergoes parallel reaction pathways. A better understanding towards the system would help further research for direct methane partial oxidation. The delplot technique is a powerful tool first developed by Bhore *et al*. for determining the reaction products rank, where multiple reaction pathways occur simultaneously.[17] This technique uses a plot of molar yield/conversion versus conversion to identify the primary and non-primary nature of the reaction products. For instance, Wei *et al*. have reported the application of delplot analysis on the selective hydrogenation of acrolein on supported silver catalysts.[18] It has been found that allyl alcohol was a primary product and propanal was identified as both the primary product and a secondary product via isomerisation of allyl alcohol. Rajkhowa *et al*. reported a kinetic study of Cu-catalysed liquid phase glycerol hydrogenolysis using this technique to reveal that acetol was the primary product and propylene glycol was a secondary product.[19]

The investigation on the effect of water addition to the gas mixture on the oxidation of methane using N_2O over Fe/ZSM-5 was carried out in this chapter. The application of the delplot technique was analysed to investigate the impact from the addition of water on the reaction pathways. The catalyst deactivation mechanism was probed through the characterisation of the catalysts pre- and post-catalytic testing. The catalyst before and after testing was compared and the results indicate that H_2O can prevent Fe migration along with reducing the formation of retained organics, although N_2O conversion was found to decrease at a similar rate in both systems. The kinetic studies on both water and water-free system highlight the complex nature of the methane oxidation reactions, network changes over Fe/ZSM-5 catalysts.

4.2 Catalytic reactions over 2 wt.% Fe/ZSM-5 in the absence of water.

The methane oxidation over 2 wt.% Fe/ZSM-5 was carried out using 0.44 g of catalyst for at least 2h to obtain the products distribution and the conversion of N_2O and methane under steady-state condition.

Figure 4.1a, shows the conversion of methane and N_2O and the mass balance over the 2 wt.% Fe/ZSM-5 with increasing time online, in the absence of water. Figure 4.1b, reports the products distribution and the missing carbon.

a)

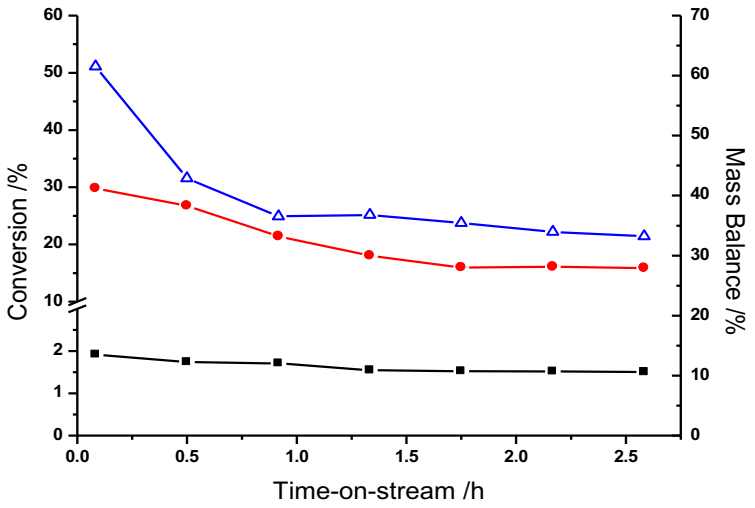

b)

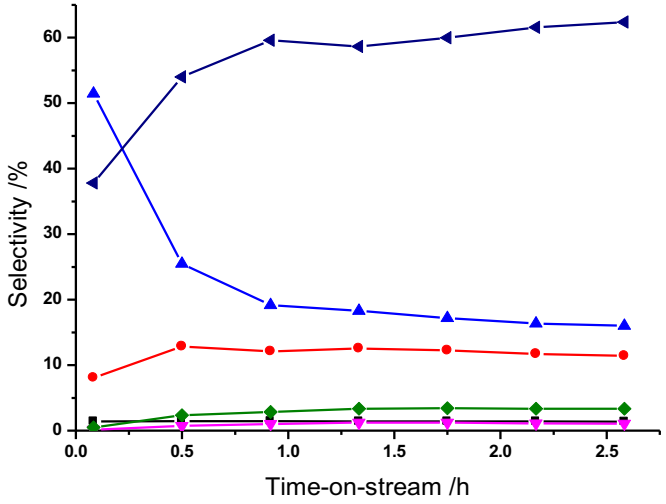

Figures 4.1:Oxidation of methane over 2 wt. % Fe/ZSM-5 (30) using N_2O at 300 °C (0.44 g catalyst) showing (a) carbon mass balance (△) and conversion of CH_4 (■)/N_2O(●) and (b) temporal evolution of products (▲ CO; ■ CH_3OH; ●CO_2; ◆C_2H_6; ▼C_2H_4 and ◀ ''missing carbon'').

Figure 4.1a shows that the CH_4 conversion starts at *ca*. 2 % and stabilised to 1.5 % after the first hour period. The N_2O conversion gradually decreases from 30 % to 19 % and levelled off after 1.5 h.

The products generated from methane oxidised by N_2O are as follows (figure 4.1b): carbon oxides, methanol, C_2H_4, C_2H_6 and retained organic species which are represented by the missing carbon in the figure. It is observed that the CO selectivity

decreases from *ca.* 50 % to 16 %, while selectivity towards C_2 products (ethane and ethene) increases from 0.6 % to 4.4 % over the same reaction period. The selectivity towards methanol and CO_2 (1.4 % and 12 % selectivity respectively) are shown to be constant over the 2.5 h reaction. The low selectivity towards methanol of *ca.* 1 %, is consistent with numerous studies performed over Fe/ZSM-5.[14, 20-22] There are no DME or acetaldehyde as other partial oxygenates present in the reactor effluent. It may suggest that these two oxygenates undergo rapid further reactions to form other species such as coke or CO. This result presented in figure 4.1a is consistent with those observed by Parfenov *et al*.[14] who reported the decreasing rates of methane and N_2O conversion during the initial 100 minutes time-on-stream.

4.3 Catalytic reactions over 2 wt.% Fe/ZSM-5 in the presence of water

Parfenov *et al*.[14] reported that by adding water vapour to the inlet gas stream, it significantly improves the methanol selectivity while also supressing the formation of coke and retained organics. In the aim to improve the methanol selectivity and to suppress catalyst fouling in this study, a consistent approach reported by Parfenov *et al*. is employed that water vapour (20 % v/v) was introduced into the feed stream.

The results obtained after the addition of water to the gas stream over 2 wt. % Fe/ZSM-5 (0.44 g) are shown in figures 4.2a and b.

a)

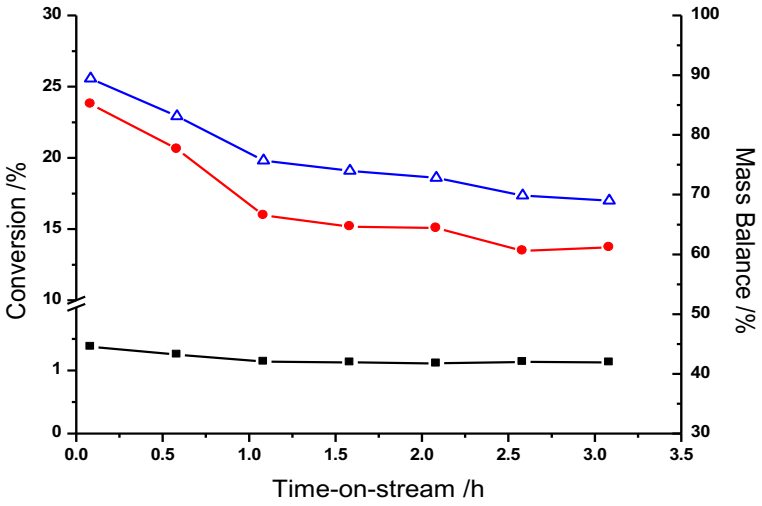

b)

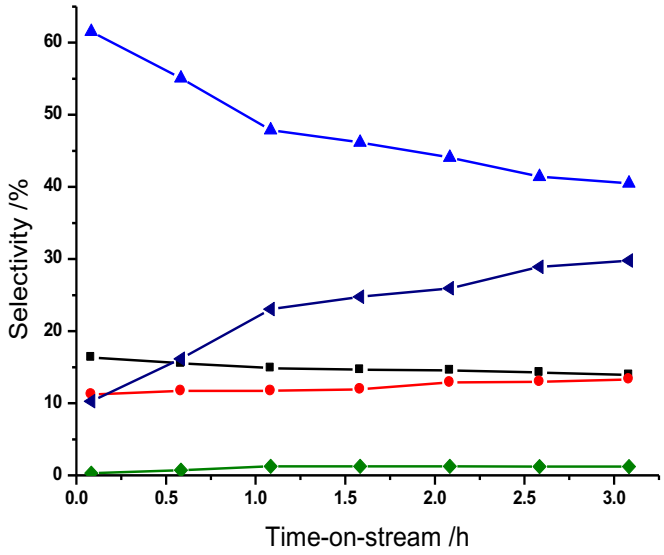

Figures 4.2 The oxidation of methane over 2 wt. % Fe/ZSM-5 (30) using N_2O at 300 °C (0.44g of catalyst) with 20 % v/v H_2O added to the substrate feed, showing (a) carbon mass balance (△) and conversion of CH_4 (■)/N_2O(●) and (b) temporal evolution of products (▲ CO; ■ CH_3OH; ●CO_2; ▼C_2H_4 and ◀ ‘’missing carbon’’).

The addition of water to the system shows first, a significant increase from 1.4 % to 16 % in methanol selectivity in comparison with the water-free system, and the yield at 1.5 h time-on-stream is 0.16 % (without H_2O the yield is 0.02 %). A corresponding increase in mass balance is also observed, as seen in figure 4.2a, resulting in less than

30 % (approximately 70% mass balance in water-free system) of the methane conversion turns into coke. The other benefit observed, is that there is a reduction of C_2 products, specifically C_2H_6, which is supressed in this route.

It has been reported in the literature review chapter that methanol is associated with α-oxygen generated by decomposing N_2O over transition metal centre such as Fe, Cu or Co.[23-26] However, CH_3OH could also react at Brønsted acidic sites provided on the zeolite structure to yield DME and higher hydrocarbons[27, 28]. One potential route to improve both CH_3OH selectivity and carbon mass balance is to induce the dealumination process of the zeolite and thereby decreasing the population of Brønsted acid sites. Dealumination could be achieved through high temperature heat treatment of Fe/ZSM-5. These findings strongly suggest that Brønsted acidity facilitates the conversion of subsequent product of DME from CH_3OH into ethene and eventually forming coke, which has been also discussed in the previous chapter.[27-29] Indeed, the hydrocarbon pool mechanism provides a reaction path for producing C_2H_4 probably via methyl benzenes, which could react further to turn into C_2H_6 , according to the methanol to olefins (MTO) chemistry.[28, 30]

White and co-workers have reported the effect of water on Brønsted acid sites by measuring C-H activation over H-ZSM-5.[31] It is observed that operating under higher water concentrations (> 2-3 molecules of water per Brønsted acid site), the rate of isobutene activation was inhibited. They have concluded that water adsorbed on Brønsted acid sites, inhibiting their effects on the reaction. Therefore, one can guess that in the present study that introducing 20 % water in the reaction mixture of CH_4 and N_2O, is sufficiently high enough to induce the similar observation of Brønsted acidity inhibition and thereby limiting the formation of carbonaceous products precursors of coke formation. The other role attributed to water by another study is the promotion of hydroxylation and the facilitating of methanol desorption.[32]

The CO_2 selectivity was observed to remain fairly stable at *ca.* 12 %, independently of feed composition in both water and water-free system. This implies that CO_2 forms directly from methane at Fe sites, as it is discussed in chapter 3, that low selectivity towards CO_2 (< 1 %) is obtained when methanol was used in the control experiments and passed over various MFI zeolite *i.e.* H-ZSM-5, Fe/ZSM-5, Fe/TS-1 or

Fe/Silicalite.[28] From the result of the control experiments, it is reasonable to postulate that methane can be oxidised to CO_2 via a separate reaction path and not from the deep oxidation of CO.

Parfenov *et al*.[14] reported that the majority of CO is formed through the decomposition of formic acid where it is originated from the disproportionation of formaldehyde. Formaldehyde is present as a short-lived reaction intermediate which may be rapidly being converted and/or produced at a very low quantity that it is beyond the detectable limit of the GC system used in this study.

Figure 4.2a shows that after going through an initial stabilisation period, methane conversion reaches a steady state at 1.1 %. Across the same period, a more pronounced decrease is observed in N_2O conversion. This decrease has been observed also in the system without water. In figure 4.3, the two systems are compared. Both the methane and N_2O conversion were normalised to their initial value (t_0) and plotted as a function of time.

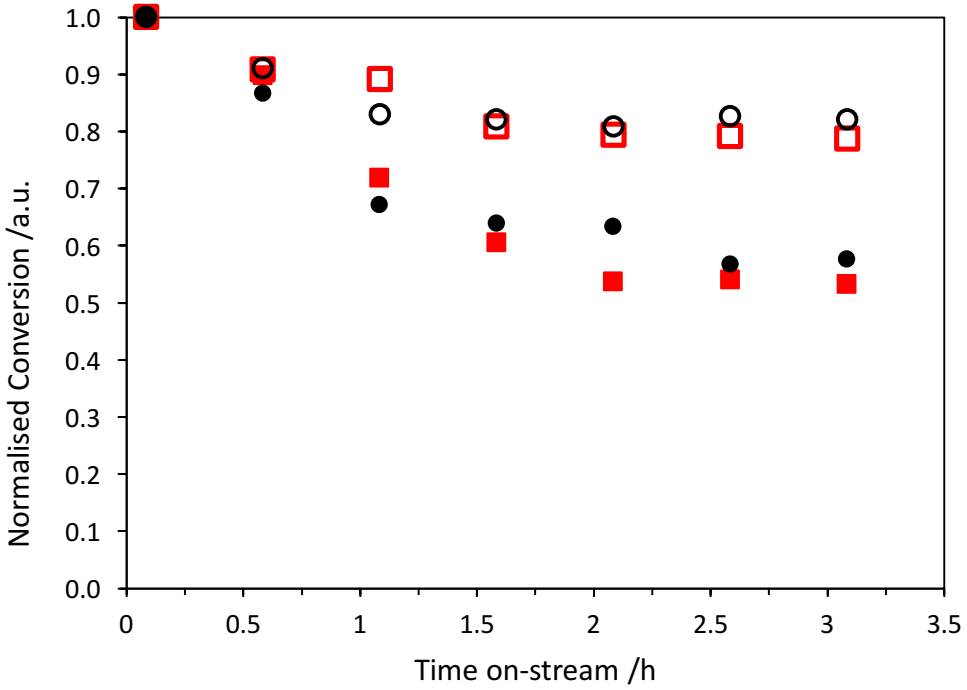

Figure 4.3: Conversion of methane (20 % H_2O ■ and 0 % H_2O ● and N_2O (20 % H_2O □ and 0 % H_2O ○) normalised to their initial values at t_0 over 2 wt.% Fe/ZSM-5 at 300 °C.

A decreasing trend in conversion is observed over the 3 h testing period in both systems. It seems that both, CH_4 and N_2O conversion are insensitive to the presence/ absence of water in the substrate feed. This implies that the deactivation mechanism cannot solely be related to the blocking of active sites through the coke formation as presented in figure 4.1a. This is in contrast to similar studies reported by Panov and co-workers, where they observed a stable N_2O conversion over 2 h time online in the presence of water. However, it is also known that H_2O can act as an inhibitor to N_2O conversion and a more detail study on the deactivation is discussed in later section in section 4.5.

4.4 Investigating the product rank in the reaction system without water

As reported in the introduction of this chapter, the delplot technique, first developed by Bhore *et al*., is a powerful technique used to determine the rank of reaction products, where multiple, simultaneous reaction pathways take place.[17] This technique involves plotting the products selectivity versus conversion and then by plotting (selectivity/conversion) versus conversion and/or (selectivity/conversion)^2 versus conversion. These series of plots allow primary, secondary and higher rank products to be identified independently of the reaction order. It extrapolates the line of best fit to zero conversion, in order to identify primary products where the intercepts are finite in the first plot and are diverge for the second and third plots.

In the aim to perform all these calculation, CH_4 and N_2O were passed over 2 wt.% Fe/ZSM-5 in a series of five experiments using various catalyst masses to obtain selectivity data across different conversions range, whilst the total bed volume was kept constant through addition of SiC fines. The catalyst mass varies between 0.10 g to 1.17 g. The products selectivity and the conversion of CH_4 and N_2O for different catalyst masses are shown in figures 4.4 to 4.8.

Figure 4.4a and b show the conversion, the mass balance and selectivity plots using 0.10 g of catalyst.

a)

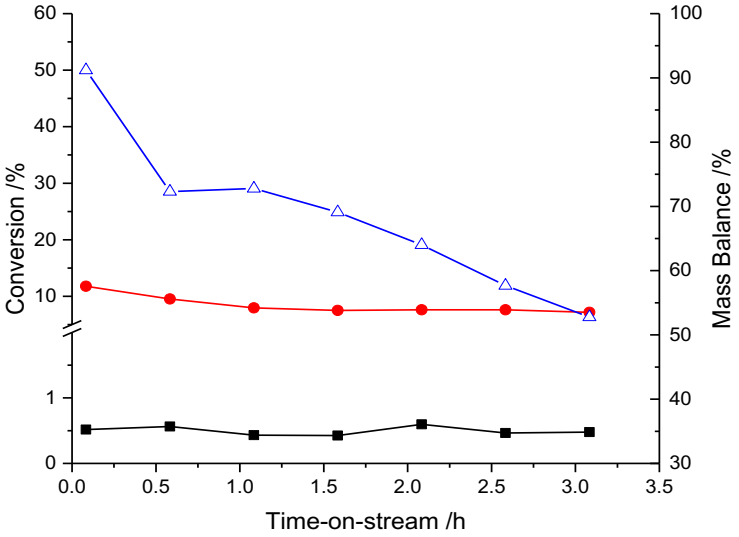

b)

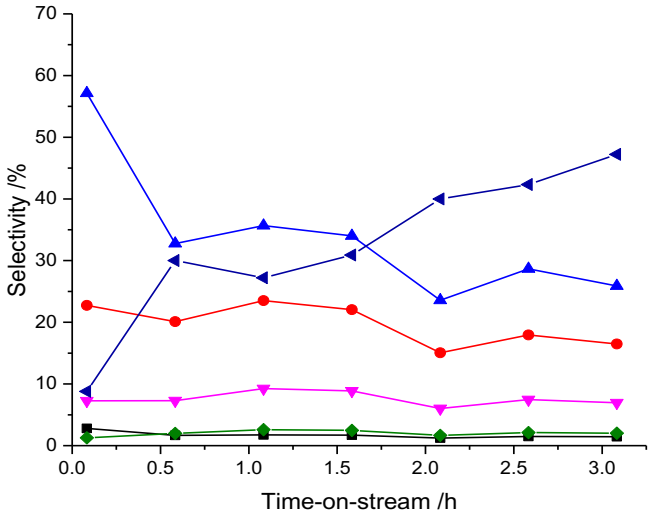

Figures 4.4 The oxidation of methane over 2 wt. % Fe/ZSM-5 (30) using N_2O at 300 °C (0.10g catalyst) showing (a) carbon mass balance (△) and conversion of CH_4 (■)/N_2O(●) and (b) temporal evolution of products (▲ CO; ■ CH_3OH; ●CO_2; ◆C_2H_6; ▼C_2H_4 and ◀ ''missing carbon'')

Figure 4.4a shows that when using a much lower catalyst mass (0.10 g), the CH_4 and N_2O conversion are at approximately 0.5 % and 10 % respectively at a steady-rate. The

mass balance is improved from at the beginning of the reaction compare to the standard experiment presented in previous section (0.44 g catalyst) as the coking process has slowed down. However, the CO selectivity decreases from 60 % to 25 % and consistently after 0.5 h. CO_2 selectivity remains at approximately 20 % throughout the reaction. The low catalyst mass used here seems to give higher C_2H_4 selectivity to *ca.* 8 %. Other minor products such as CH_3OH and C_2H_6 are present at a selectivity of 2 % steadily. By decreasing the amount of catalyst, the conversion of the reactants is slowed down and the conversion of the different products intermediates of the reaction into the final products is also slowed down to better understand the order of reaction.

Figure 4.5a and b show the conversion, the mass balance and selectivity plots using 0.15 g of catalyst.

a)

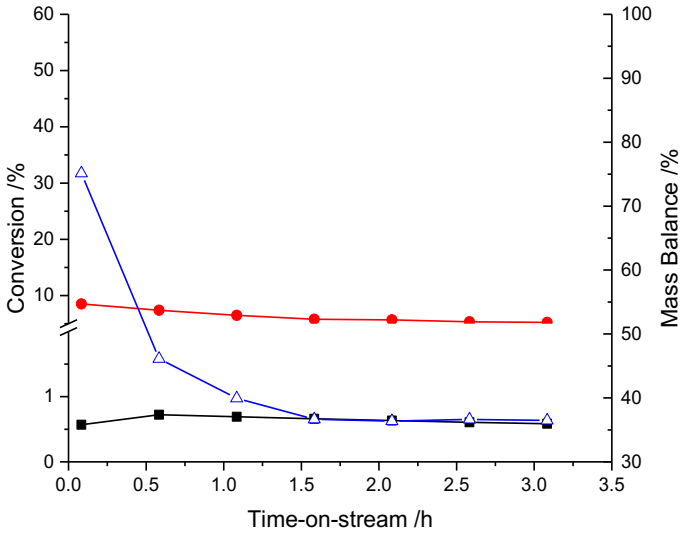

b)

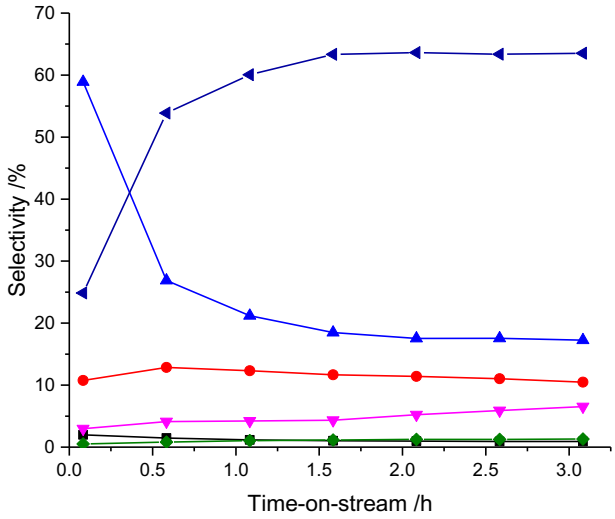

Figures 4.5: The oxidation of methane over 2 wt. % Fe/ZSM-5 (30) using N_2O at 300 °C (0.15g catalyst) showing (a) carbon mass balance (△) and conversion of CH_4 (■)/N_2O(●) and (b) temporal evolution of products (▲ CO; ■ CH_3OH; ●CO_2; ◆C_2H_6; ▼C_2H_4 and ◀ ‘’missing carbon’’).

Figure 4.5a shows that when using only slightly higher mass of 0.15 g catalyst, the improvement seen on the mass balance is not as profound as seen using 0.1 g catalyst and decreases from 80 % to 35 % after 1 h. The CO selectivity decreases sharply from 60 % to 20 % in the first hour and remains constant afterward. CO_2 selectivity remains at approximately 13 % throughout the reaction. Other minor products such as CH_3OH, C_2H_4 and C_2H_6 are all present below a selectivity of 2 % steadily. This is similar to reaction carried out with 0.1 g catalyst where the CH_4 and N_2O conversion are at approximately 0.5 % and 10 % respectively at a steady rate.

Figures 4.6a and b show the conversion, the mass balance and the selectivity plots using 0.32 g of catalyst.

a)

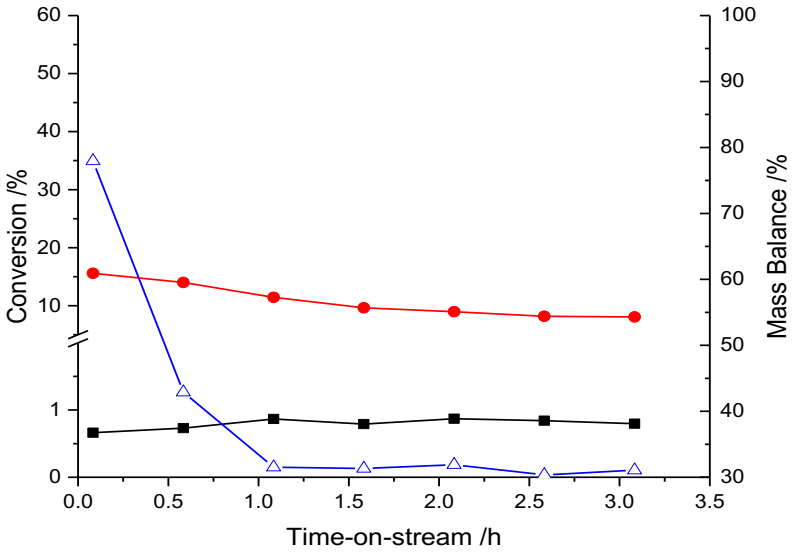

b)

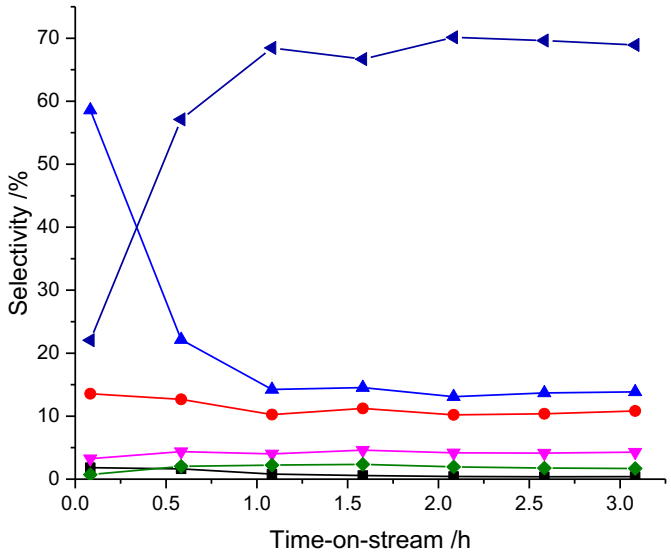

Figures 4: Oxidation of methane over 2 wt.% Fe/ZSM-5 (30) using N_2O at 300 °C (0.32g catalyst) showing (a) carbon mass balance (△) and conversion of CH_4 (■)/N_2O(●) and (b) temporal evolution of products (▲ CO; ■ CH_3OH; ● CO_2; ◆ C_2H_6; ▼ C_2H_4 and ◀ ‘’missing carbon’’).

Figures 4.6a and 4.6b shows that when using 0.32 g catalyst, the selectivity to coke rapidly reaches 60 % in the first 0.5 h unlike the two experiments used with <0.15 g catalyst mass. Therefore, the mass balance decreases to 35% from 80 % after 1 h. The CO selectivity decreases again sharply from 60 % to 20 % in the first hour and remains constant afterward. CO_2 selectivity remains at approximately 13 % throughout the reaction. Other minor products such as CH_3OH, C_2H_6 are present below a selectivity of 5 % steadily.

Figures 4.7a and b show the conversions, the mass balance and the selectivity plots using 0.91 g of catalyst.

a)

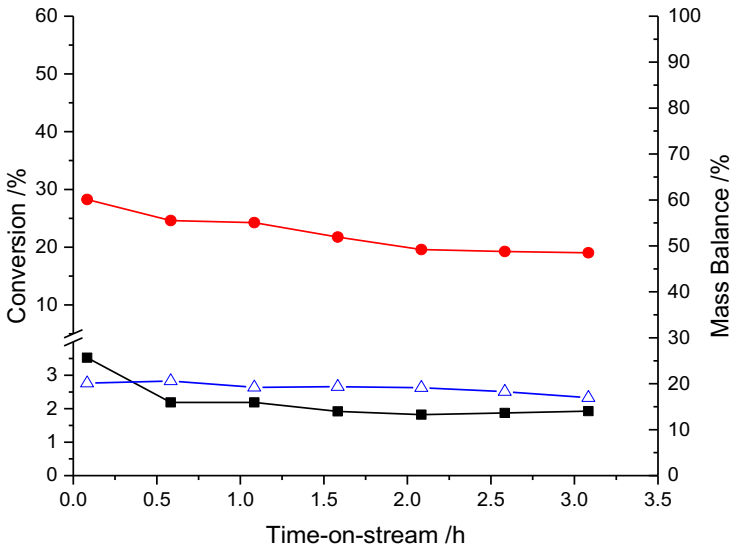

b)

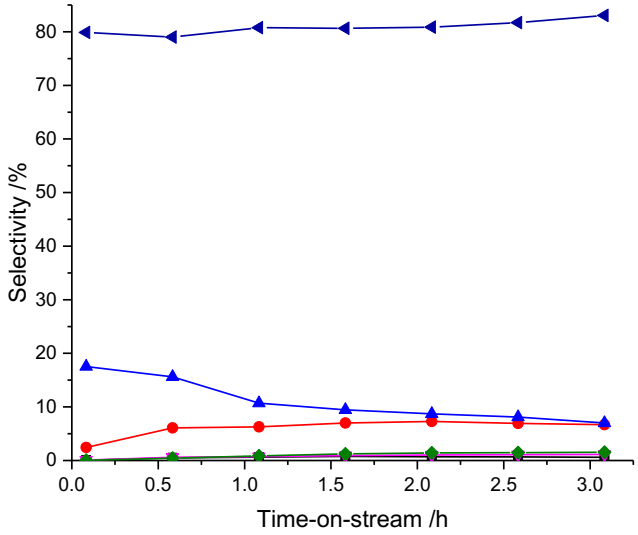

Figures 4.7: The oxidation of methane over 2 % Fe/ZSM-5 (30) using N_2O at 300 °C (0.91g catalyst) showing (a) carbon mass balance (△) and conversion of CH_4 (■)/N_2O(●) and (b) temporal evolution of products (▲ CO; ■ CH_3OH; ●CO_2; ◆C_2H_6; ▼C_2H_4 and ◀ ‘’missing carbon’’)

Figures 4.7a and b show that when using a high catalyst mass (0.91 g), to push for higher conversion range, the selectivity to gas phase products is combined to be less than 20 %. There is over 80 % selectivity to produce coke leading to a poor mass balance of 20 %. The CO_2 production observed under high conversion range, again seemed to undergo a separate reaction path as the selectivity observed is unaffected and remained stable throughout the reaction. The selectivity to CO obtained is much lower in the first 0.5 h (20 %).

Figures 4.8a and b show the conversion, the mass balance and the selectivity plots using 1.17 g of catalyst.

a)

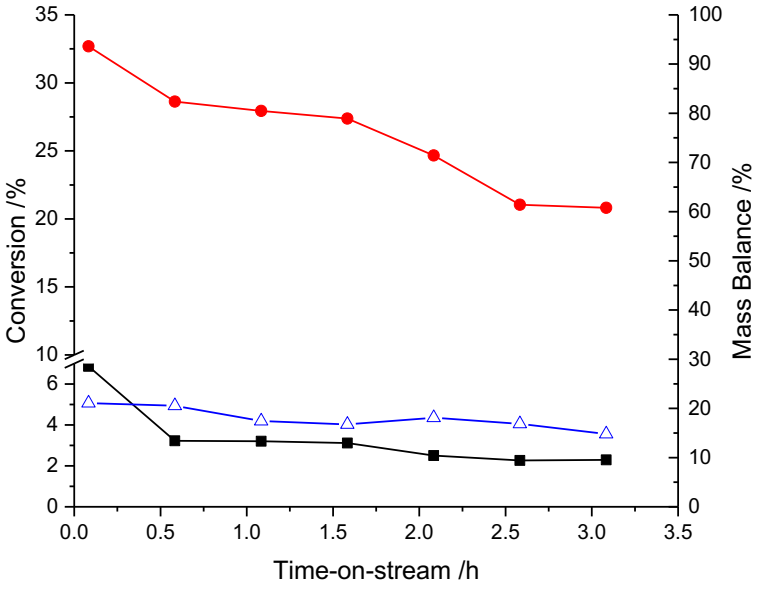

b)

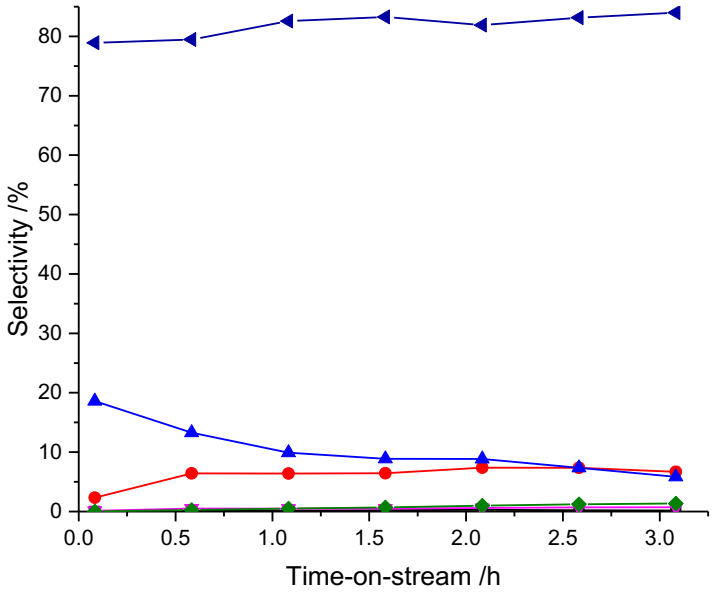

Figures 4.8 The oxidation of methane over 2 % Fe/ZSM-5 (30) using N_2O at 300 °C (1.17g catalyst) showing (a) carbon mass balance (△) and conversion of CH_4 (■)/N_2O(●) and (b) temporal evolution of products (▲ CO; ■ CH_3OH; ●CO_2; ◆C_2H_6; ▼C_2H_4 and ◀ ''missing carbon'').

Under the high conversion range, (1.17g), this is very similar to the experiment that used 0.91 g catalyst. Again, the selectivity to gas phase products is combined to be less than 15 % and there is over 80 % selectivity to coke at the beginning indicating the desorption issues of MeOH is highly suppressed.

The data collected from the above series of plots affords a conversion profile and enables assessment of products rank through the delplot shown in figures 4.9a, b and c which represent the major generated products (*i.e.* carbon dioxide, carbon monoxide and missing carbon) and figure 4.10 the minor products (*i.e.* methanol, ethane and ethene).

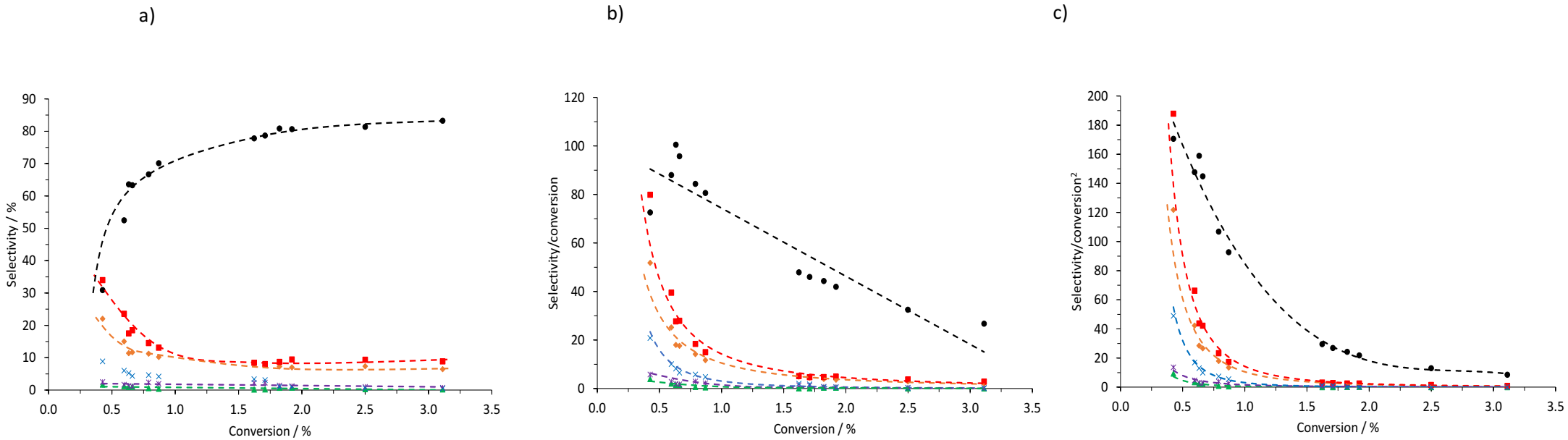

Figures 4.9: First rank (a), second rank (b) and third rank (c) delplots taken from data collected over a series of experiments using different masses of 2 wt. % Fe/ZSM-5 at 300 °C; (▲) CH_3OH, (◆) CO_2, (■) CO, (✱) C_2H_6, (×) C_2H_4 and (●) missing carbon.

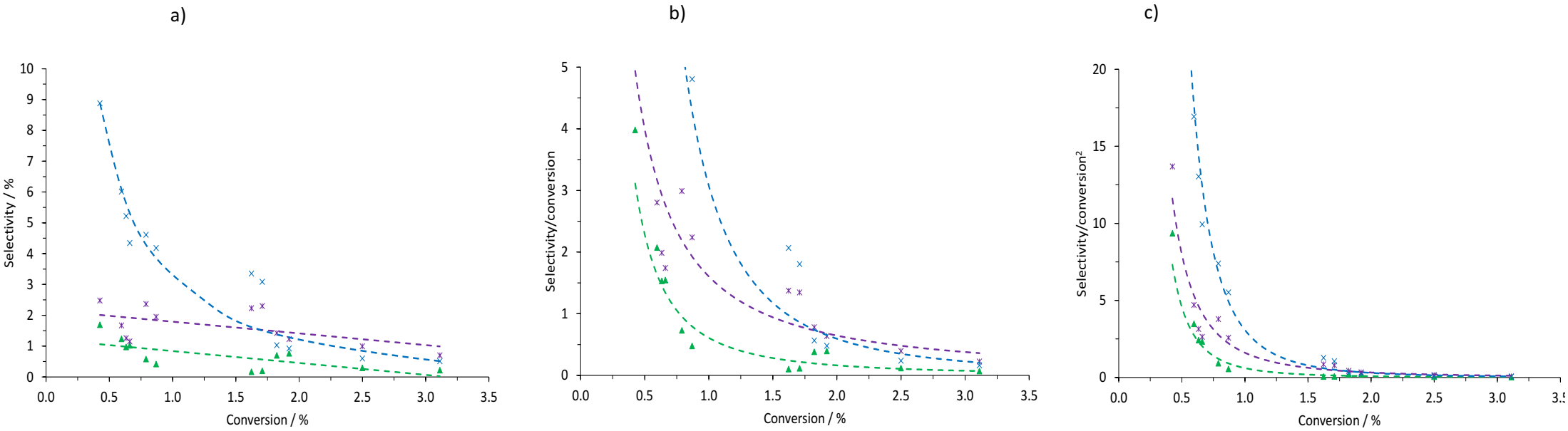

Figures 4.10 First rank (a), second rank (b) and third rank (c) delplots of minor products taken from data collected over a series of experiments using different masses of 2 wt. % Fe/ZSM-5 at 300 °C; (▲) CH_3OH, (✱) C_2H_6 and (×) C_2H_4.

The methane conversion ranges from *ca.* 0.4 to 3.1 % by altering the catalyst mass. Generally, it is observed that the loss of carbon is *ap.* 50 % of the total converted carbon at low conversion conditions. The quantity of the products rank detected in the GC pursues the following order $CO > CO_2 > C_2H_4 > C_2H_6 \geq CH_3OH$. The mass balance decreases significantly as the methane conversion increases, *i.e.* the selectivity to coke or retained organics increases and the overall selectivity towards gas phase products in the reaction outlet decreases.

The delplot analysis suggests that coke formed as a secondary product and the rest of the gas phase products are shown to be primary presented in figure 4.9b. Interestingly, the third-rank delplot analysis presented in figure 4.9c suggests that the missing carbon or coke, indicates that it is not a higher order product due to the line of best fit diverge from the origin. The first rank plots for CH_3OH, CO, CO_2, C_2H_4 and C_2H_6 show that the extrapolation of the line of best fit do not pass through the origin (see figure 4.10) which indicates the primary nature of those products. However, C_2 products generated in the reaction effluent implies the carbon-carbon coupling and thereby C_2 products could also be classified as secondary products. The selectivity of C_2H_6 increases over the initial 100 min online. However, the delplot presents in figure 4.9 is constructed from data points where the steady state of CH_4 conversion is achieved (at times of > 100 min). Therefore, the stabilisation period is not taken into account. Methanol and/or formaldehyde are the primary products from methane oxidation over Fe/ZSM-5 according to a reaction mechanism proposed by Panov and co-workers[14, 22, 33].

Methanol formed on the surface either desorbs into the gas phase or spills over and migrates to other acid sites on Fe/ZSM-5 to eventually form coke via a surface bound ether (DME). C_2H_6 could be formed via a similar mechanism that desorbed from surface bound ether as observed in MTO chemistry.[34] The high level of coke formation observed, also supports the work on Fe/ZSM-5 reported by Panov and co-workers and their following up work on the beneficial effect on enhancing the water CH_3OH displacement. The delplot data present in figures 4.9 obtained from the water free system indicates that coke formation dominates the products distribution as methane conversion increases. The system favours coke formation over combustion products which would indicate that the reaction system would be either oxidant limited or the strength of products adsorption is higher than that of methane.

4.5 Investigating the products rank in the reaction system in the presence of water

To perform the delplot technique on the system in the presence of water, a systematic study using the same approach has been used. A series of experiments have been carried out with different catalyst masses as presented in the previous section. Figure 4.11a and b show the conversion, mass balance and selectivity plots using 0.10 g of catalyst.

a)

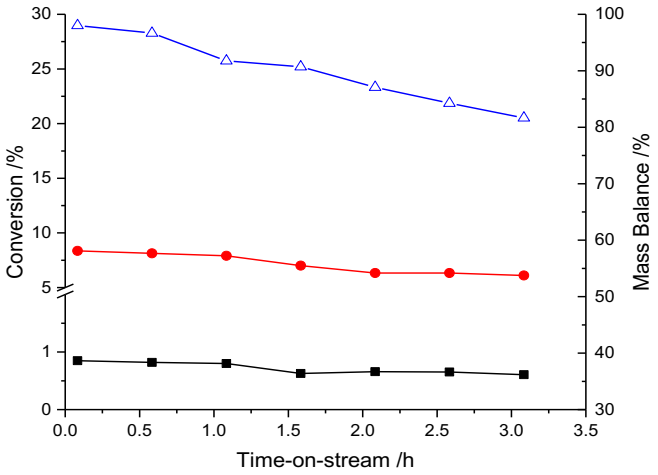

b)

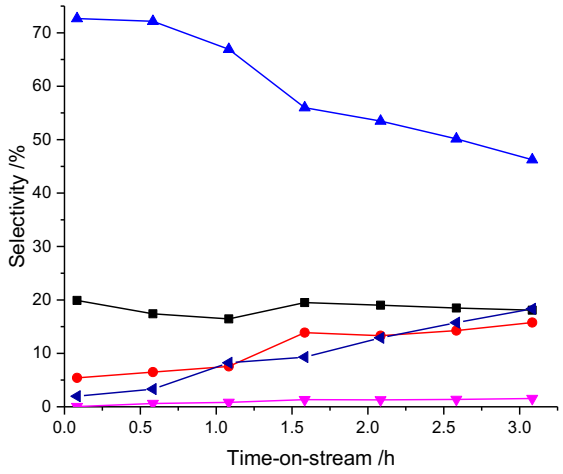

Figures 4.11: Oxidation of methane over 2 wt.% Fe/ZSM-5 (30) using N_2O at 300 °C (0.10g catalyst) showing (a) carbon mass balance (△) and conversion of CH_4 (■)/N_2O(●) and (b) temporal evolution of products (▲ CO; ■ CH_3OH; ●CO_2; ▼C_2H_4 and ◀ ‘’missing carbon’’).

Figure 4.11a shows that the CH_4 and N_2O conversion are averaging 0.5 % and 8 % respectively at a steady rate.

Figure 4.11b shows that when using a much lower catalyst mass (0.10 g), the CO selectivity becomes the dominant product instead of coke and decreases from 70 to 50 % at a similar rate. CH_3OH production is stable at this lower conversion range and is much higher at 20 % selectivity than the water-free system (*i.e.* 1 %). The selectivity of CO_2 increases from 5 to 15 % at a steady rate throughout the reaction. It is observed that C_2H_6 is not produced in the presence of water. The selectivity to coke is increased from 2 % to 20 % at the end of the 3.5 h reaction and this led to a much improved mass balance.

Figures 4.12a and b report the conversion, mass balance and selectivity plots using 0.15 g of catalyst.

a)

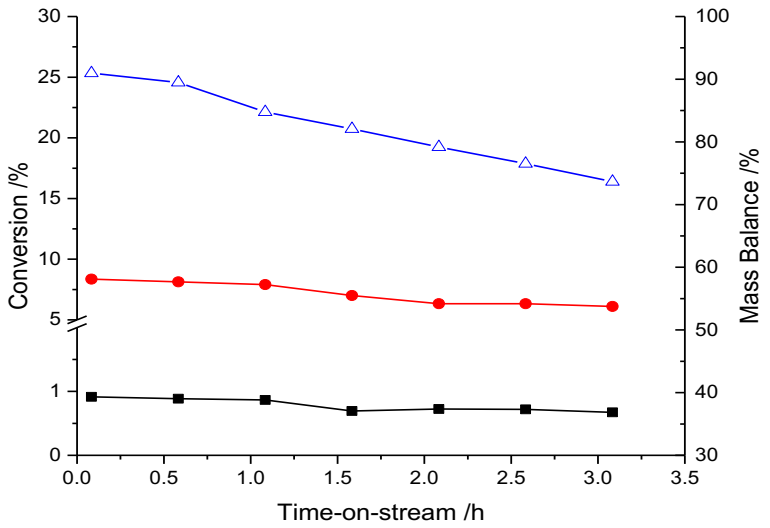

b)

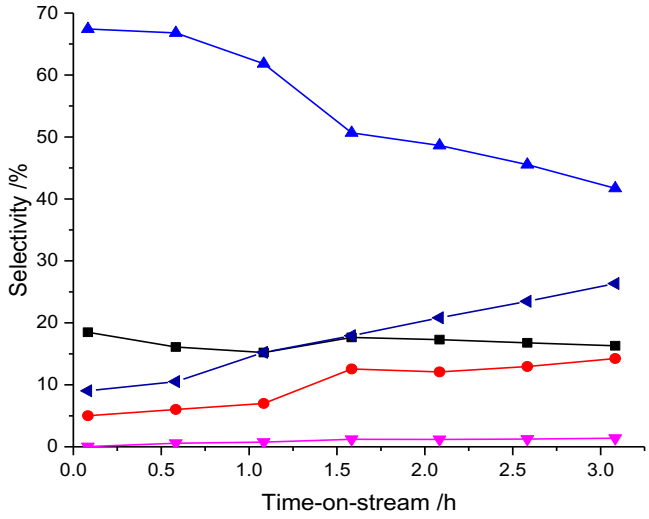

Figures 4.12 Oxidation of methane over 2 wt.% Fe/ZSM-5 (30) using N_2O at 300 °C (0.15g catalyst) showing (a) carbon mass balance (△) and conversion of CH_4 (■)/N_2O(●) and (b) temporal evolution of products (▲ CO; ■ CH_3OH; ●CO_2; ▼C_2H_4 and ◀ ‘’missing carbon’’).

Figure 4.1 a shows that when using similar catalyst mass (0.15 g) in the low conversion range, the product composition is very similar to the 0.1 g analogue. It shows the CH_3OH selectivity is at the highest with low amount of coke in this series of testing using below 0.15 g catalyst while keeping the CH_4 conversion rate at above 0.5 % conversion.

Figure 4.12b also presents a similar selectivity profile as the 0.1 g experiment where a decreasing trend is observed for the CO with the missing carbon slowly increases. This indicates the rate of coke formation is slowed down.

Figures 4.13 a and b show the conversion, the mass balance and selectivity plot susing 0.32 g of catalyst.

a)

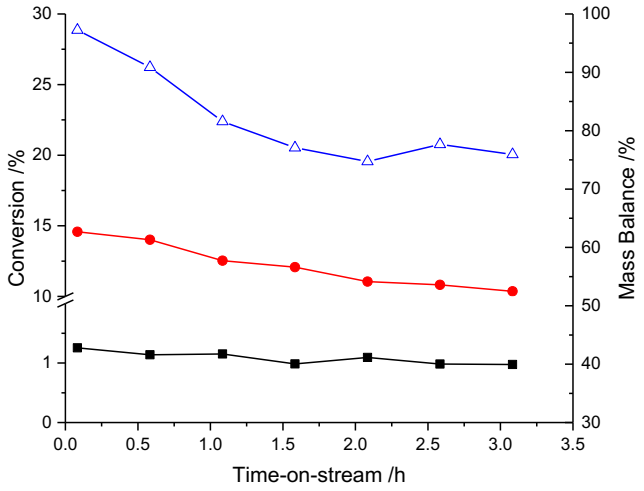

b)

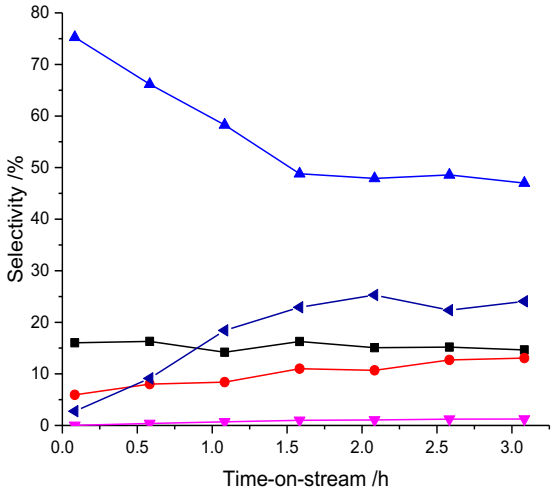

Figures 4.13 Oxidation of methane over 2 wt.% Fe/ZSM-5 (30) using N_2O at 300 °C (0.32g catalyst) showing (a) carbon mass balance (△) and conversion of CH_4 (■)/N_2O(●) and (b) temporal evolution of products (▲ CO; ■ CH_3OH; ●CO_2; ▼C_2H_4 and ◀ ‘’missing carbon’’).

Figure 4.13a shows that CH_4 and N_2O conversion are averaging 1.2 % and 13 % respectively. It is noted that N_2O conversion decreases at a steady rate but CH_4

conversion does not appear to be affected which may be due to the ability of water inhibiting the decomposition of N_2O over the zeolite.

Figure 4.13b shows that when using 0.32 g of catalyst, the CH_3OH selectivity starts to decrease to 15% and an increased selectivity to coke after the first hour is observed compare to the previous experiments where below 1.5 g catalyst is used.

Figures 4.14 a and b show the conversion, mass balance and selectivity plots using 0.91 g of catalyst.

a)

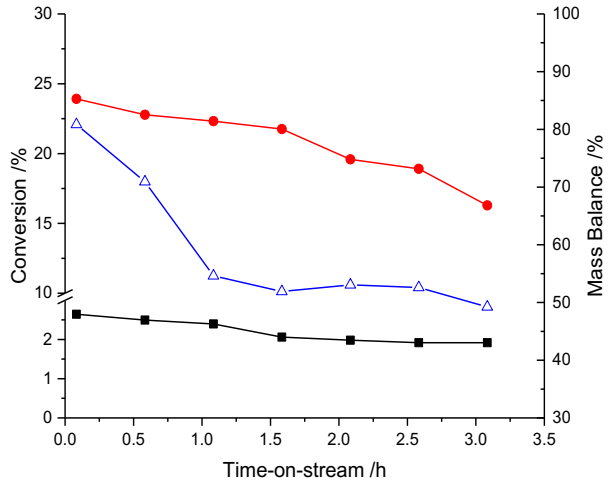

b)

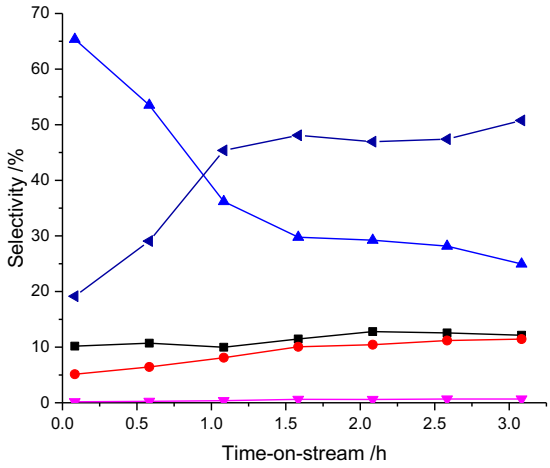

Figures 4.14: Oxidation of methane over 2 % Fe/ZSM-5 (30) using N_2O at 300 °C (0.91g catalyst) showing (a) carbon mass balance (△) and conversion of CH_4 (■)/N_2O(●) and (b) temporal evolution of products (▲ CO; ■ CH_3OH; ●CO_2; ▼C_2H_4 and ◀ ‘’missing carbon’’).

Figure 4.14a shows that CH_4 and N_2O conversion are averaging 2.2 % and 10 % respectively.

Figure 4.14b shows that when using close to 1 g of catalyst mass (0.91g), the CO selectivity decreases rapidly in the first 1.5 h from 60 to 30 % before levelling off. The coke formation appears to increase from 20 to 50 % towards the end of the reaction. It is observed that under much higher conversion range the function of water to displace CH_3OH is less effective hence led to the decreasing trend in mass balance. It is worth mentioning that even at high conversion range. C_2H_6 is not observed which further confirms that water can also prevent the transformation of C_2H_4 to C_2H_6.

Figures 4.15a and b show the conversion, mass balance and selectivity plots using 1.17 g of catalyst.

a)

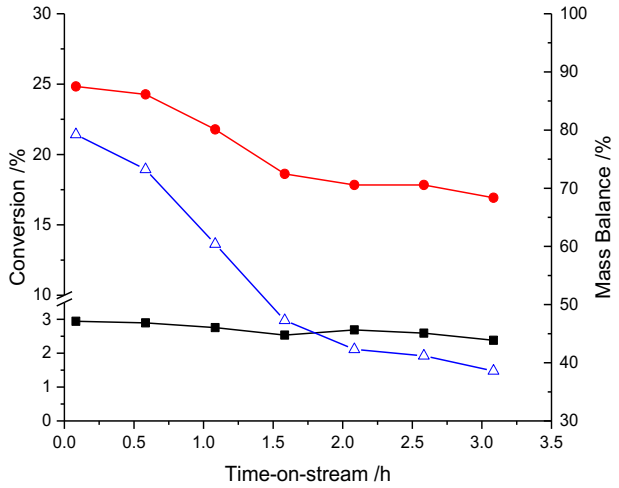

b)

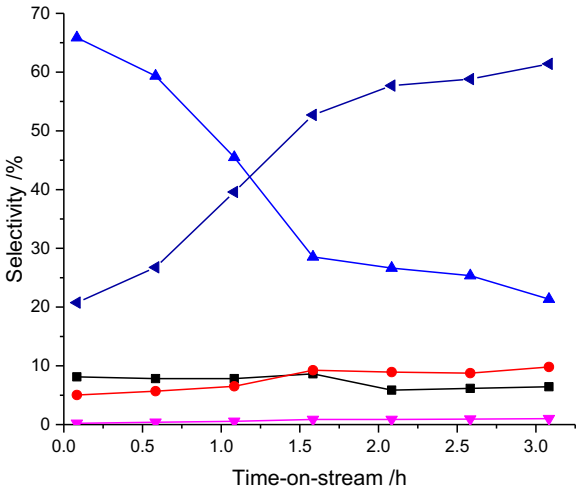

Figures 4.15: Oxidation of methane over 2 wt. % Fe/ZSM-5 (30) using N_2O at 300 °C (1.17g catalyst) showing (a) carbon mass balance (△) and conversion of CH_4 (■)/N_2O(●) and (b) temporal evolution of products (▲ CO; ■ CH_3OH; ●CO_2; ▼C_2H_4 and ◀ ‘’missing carbon’’).

Figures 4.15 and b show that at even higher catalyst mass (1.17 g), a similar observation on the production composition is achieved and the system is close to operating at 3 %

CH_4 conversion. Moreover, the formation of coke appears to increase and effect of water to displace CH_3OH is also less efficient as the system employs higher catalyst mass to push for higher conversion. CH_3OH selectivity decreases to approximately 10 % in this case.

Figures 4.16a-c show the delplot analysis of the reaction for methane and N_2O over 2 wt. % Fe/ZSM-5 where 20 % v/v water is added to the feed-stream (minor products plots are shown in 4.17a-c). Figures 4.16 was constructed from data at times over 100 min where a steady state is observed. The reaction with added water was studied over a conversion range from 0.7 to 2.3 %.

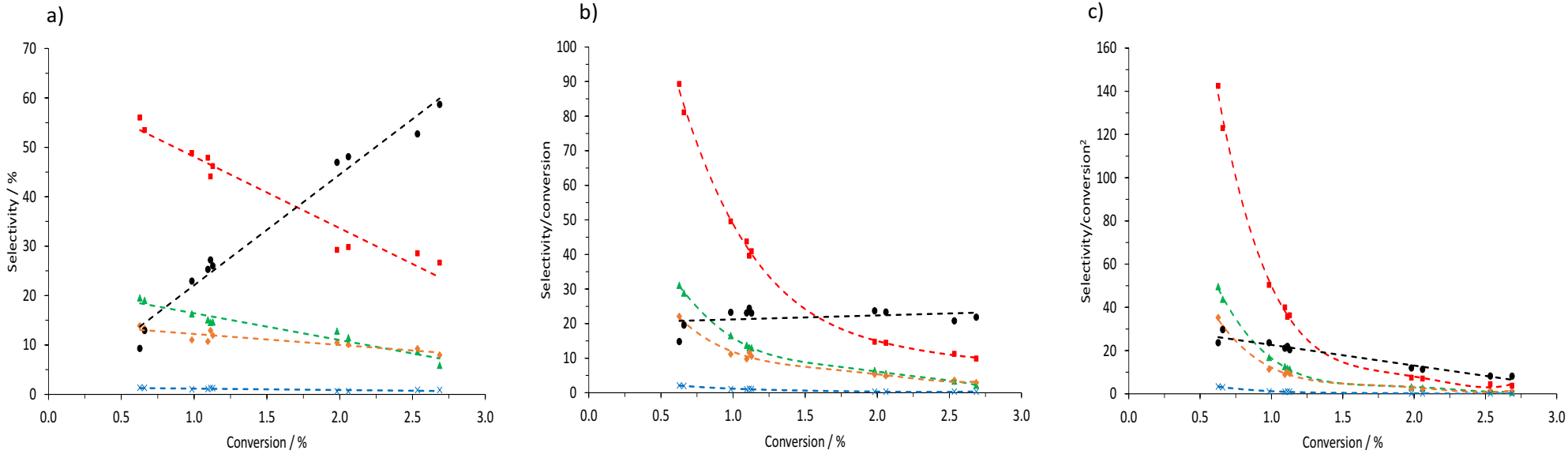

Figures 4.16 First rank (a), second rank (b) and third rank (c) delplots taken from data collected over a series of experiments using varying masses of 2 wt. % Fe/ZSM-5 at 300 °C with water present in the feed-stream; (▲) CH_3OH, (◆) CO_2, (■) CO, (×) C_2H_4 and (●) missing carbon.

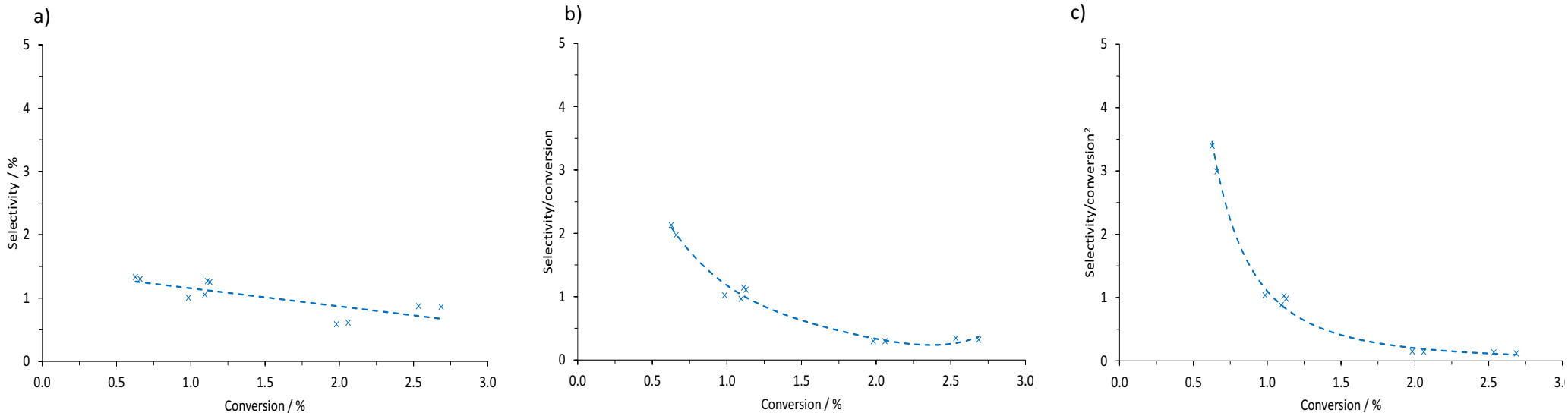

Figures 4.17 First rank (a), second rank (b) and third rank (c) delplots of minor products taken from data collected over a series of experiments using different masses of 2 wt. % Fe/ZSM-5 at 300 °C with water in the feed; (×) C_2H_4.

It is clear, from the delplot data, that the formation of coke is greatly lowered even at higher conversion values when higher catalyst mass was used as seen across the time-online data (figures 4.11 to 4.15). A significant increase for CH_3OH and CO selectivities are observed across the conversion range. This, confirms the importance of water in formation of CO and more importantly, the desired CH_3OH.[14] At low methane conversion region *ca.* below 1 %, the selectivity of combining CH_3OH and coke are less than CO selectivity (*i.e.* 55 %) as shown in figure 4.16a. The formation of coke according the reaction path is most likely due to the strong adsorption of CH_3OH or a surface bound methoxy species. An observation reported by Panov and co-workers that if all the CH_3OH produced under these conditions could be desorbed from the zeolite sites then the CH_3OH : CO ratio would be less than 1:1.[14] Therefore, this implies that the formation of CO cannot solely be originated from the decomposition of HCOOH formed via the disproportionation of HCHO. As the methane conversion increases, this ratio is disrupted significantly. For instance, 30 % CO selectivity is observed at a conversion of 2.5 %, and the selectivity to CH_3OH is 10% whereas coke is 55%. When pushing the system for higher conversion, water is less efficient to facilitate the desorption of CH_3OH hence leads to the build-up of CH_3OH on the zeolite surface to transform further into retained organics.

The second-rank delplot is shown in figure 4.16b for this data set and the intercept is clearly not positioned close to the origin, which suggests that coke is a secondary product. For cases where line of best fit extrapolated back to zero in the second-rank delplot then it would imply that coke is of higher order product. Unlike the previous delplot (for water-free system) shown in figure 4.9c where coke is shown to diverge at low conversion region, this time the results is shown as a linear regression to the y axis intercept shown in figure 4.16c. This plot suggests that the kinetic pathway is altered in the presence of water and the formation of coke here appears to be also a tertiary product. Moreover, it is observed that the CO_2 selectivity is *ca.* 10 % as shown in figure 4.16a and the trend did not change substantially across the conversion region covered in this study. This, implies that the formation of CO_2 is independent to that of CO and CH_3OH. The addition of water seems to also supress the re-adsorption of C_2H_4 since C_2H_6 is not detected in this system.

According to the data collected in the series of experiments, water offers an advantage to push for more favourable CH_3OH product at low conversion conditions (<1 %). As reaction occurs at higher conversion region at above 1 %, the mechanism of water does not work as effective for adsorbing and displacing CH_3OH. Hunger *et al*. reported that methanol has a higher affinity on the ZSM-5 surface compare to water and this could be due to the presence of CH_3 group.[35] As a result of that, CH_3OH adsorbs for a prolonged period of time and undergo further reactions to form coke and hence lowering the carbon balance.

When pushing for higher conversion range, the reaction system employed higher catalyst mass and would lead to higher contact time despite operating with a fixed bed volume. The adsorption of CH_3OH and its interaction with an adjacent Brønsted acid site is captured. It would be possible for the valuable CH_3OH to desorb at the top of the catalyst bed which can then re-adsorb on the catalyst further down the reactor tube to interact with Brønsted sites to form coke. The proposed reaction network is shown in Scheme 1 constructed using the delplot data. It is observed that the formation of CO_2 seems to be largely independent of CH_3OH and CO concentration. The function of water in this system allows facile CH_3OH desorption and the disproportionation of a short-lived intermediate (HCOOH) to CO and H_2O is captured as reported by Panov and co-workers.[14]

The delplot analysis allows one to identify CO and C_2H_4 as primary products, which suggest the cooperativity can exist between the active Fe sites for methanol formation and Brønsted acid sites as reported.[28] The formation of C_2H_6 is thought to occur through hydrogen transfer under the umbrella of the Methanol-to-Hydrocarbons chemistry.[36] However, the expected dienes, trienes or polymethylbenzenes formed post transfer detected were well below the quantifiable limit by the GC. If this follows the MTO reaction route, the reaction would take place in the pores environment of the zeolite. The bulky aromatic species could also be retained in the pores and contribute to the formation of coke.

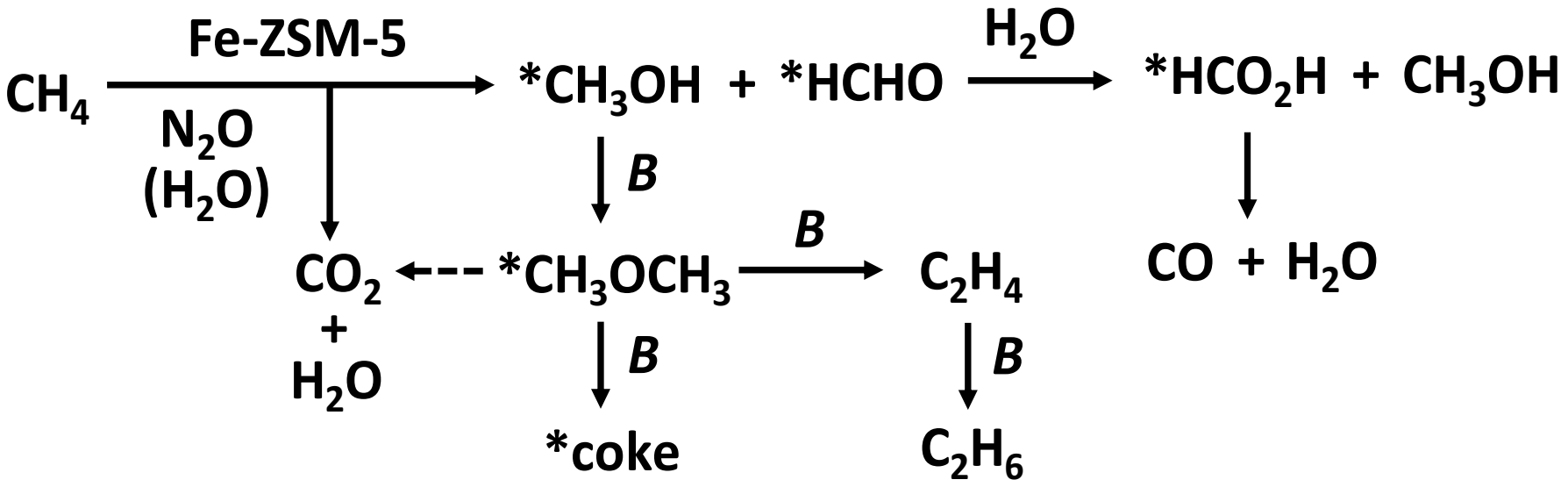

Scheme 1: Proposed reaction network for CH_4 oxidation with N_2O over Fe/ZSM-5 catalysts according to delplot analysis; *B* is Brønsted acid site and * indicates adsorbed or intermediate species not detected in the reactor effluent

4.6 Characterisation of pre- and post-reaction samples

The delplot analysis indicates that the addition of water to the system does not significantly alter the reaction pathways. It provides information on the role of water which enhances methanol selectivity to displace from zeolite before it reacts further. The delplot data analysis shown in figures 4.16b and 4.16c shows that coke can be a secondary or higher rank product. The series of conversion plots (figures 4.11 to 4.15) also suggest that the deactivation rate of the catalyst was not affected by the presence of water. This was unexpected as the accumulation of coke/retained organics in the catalyst is significantly lowered after water is added. The activity of the catalyst would be expected to remain more stable throughout the reaction. A series of characterisation is carried out to investigate the cause of catalyst deactivation from the fresh and used samples of reactions in the presence of water and water-free systems.

4.6.1 TGA studies

TGA was carried out to quantify the amount of coke formed after 3.5 h reaction. The weight loss comparison from using the catalyst Fe/ZSM-5 before reaction, the catalyst after reaction when water is not used (annotated Fe/ZSM-5-0%) in the following sections and figures) and the catalyst after reaction when 20 % v/v water are used (annotated Fe/ZSM-5-20%), is shown in figures 4.18a and b. The sample were heat-treated under flowing air over the temperature range from 30 to 900 °C.

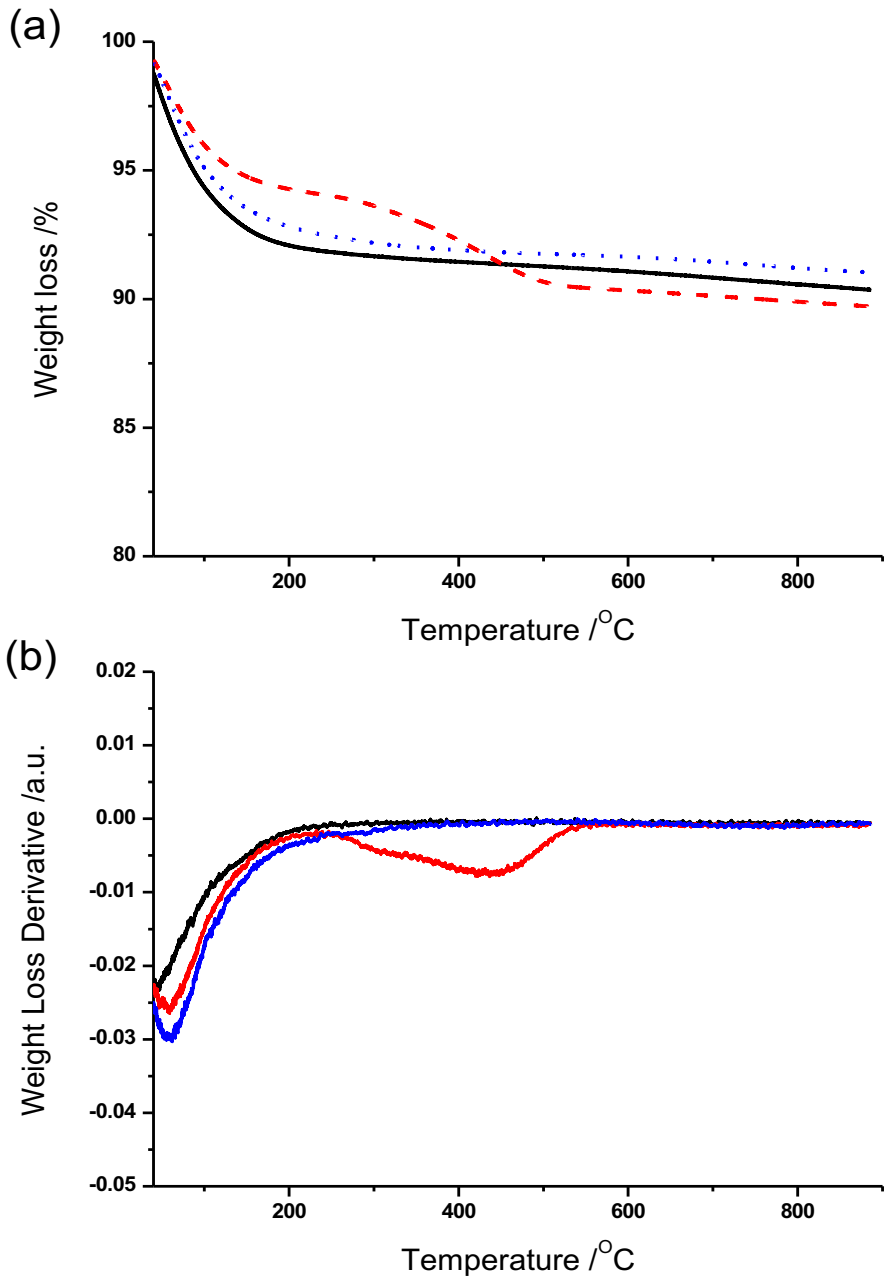

Figures 4.18: TGA profiles of fresh and used catalysts showing weight loss profiles (a) and weight loss derivate profiles (b) for Fe/ZSM-5 (black), Fe/ZSM-5-20% (blue dots) and Fe/ZSM-5-0% (red dashes).

The TGA profiles of the fresh catalyst and sample used with 20% H_2O both shown to have weight losses at region below 200 °C and both looks very similar. The weight loss may be attributed to the loss of physisorbed water. It provides further evidence that the

role of water could suppress the formation of coke as the lack of CO_2 is being formed from coke during the TGA process.

For the water-free system (Fe/ZSM-5-0%), there is a broad weight loss region stretch from 250-550 °C and is assigned to be the coke formed in the reaction and being burnt off as carbon oxides. The broad bi-modal weight loss region shown in figure 4.18b is consistent with the report on the build-up of coke on various sites in ZSM-5 framework by Weckhuysen and co-workers.[37-39] This is also concordant with the data shown in figure 4.1 that poor mass balance and high selectivity to coke is observed from the experiment.

The coke production calculated from mass loss and the expected missing carbon over 200–600 °C from TGA is shown in Table 4.1.

4.6.2 BET surface and pore analysis

Table 4.1: BET surface areas and pore volumes of MFI catalysts pre- and post-reaction.

Entry	Catalyst	Total surface area[a, b] ($m^2.g^{-1}$)	$V_{micropore}$[b] ($cm^3.g^{-1}$)	Coke produced[c] ($\mu molC.g_{cat}^{-1}.h^{-1}$)	Missing carbon[d] ($\mu molC.g_{cat}^{-1}.h^{-1}$)
1	H/ZSM-5	434	0.169	-	-
2	Fe/ZSM-5	359	0.142	-	-
3	Fe/ZSM-5-20%	352	0.134	59	166
4	Fe/ZSM-5-0%	210	0.087	795	587

[a] Surface area determined from nitrogen adsorption measurement using the BET equation at -196 °C. [b] Quantitative analysis is per unit mass of sample – in the case of Entry 4 this includes *ca*. 5 wt. % carbonaceous deposits. [c] Coke production calculated from mass loss over 200 – 600 °C from TGA measeurements as described in experimental section. [d] Expected missing carbon calculated from yield of missing carbon from 3 h time on-stream tests presented in Figs. 4.1 and 4.2.

From the BET (Table 4.1, Entry 4), it is calculated to be 795 μmolC.g_{cat}^{-1}.h^{-1} rate of carbon accumulated on the surface of the catalyst when water is not used in the system. For the system using water, there is 59 μmolC.g_{cat}^{-1}.h^{-1} rate of coke accumulated. Again, here it is apparent from this data that the system with water generate a low amount of coke on the catalyst surface.

The expected coking rate was also calculated in order to compare TGA measurements from the values based on the data presented in figures 4.1 and 4.2. The expected coke produced was calculated as 587 and 166 μmolC.g_{cat}^{-1}.h^{-1} for the Fe/ZSM-5-0% and Fe/ZSM-5-20% respectively. These values, don't match well with the amount of carbon burnt off during the TGA air treatment. The disagreement between the actual and expected coke calculated was also reported by Panov and co-workers in a similar study using TPO.[13] In their report, they measured a rate of 1400 μmolC.g_{cat}^{-1}.h^{-1}, but the expected rate was only at 795 μmolC.g_{cat}^{-1}.h^{-1}. One hypothesis to explain this difference, is that the weight loss between 200-600 °C is not may be due totally to the coke formed from the methane oxidation reaction during the TGA/TPO analysis. May be some other species are desorbing from the surface of the catalysts during the heat treatment.

The large amount of coke deposited in the water-free reaction did not greatly affect the reactivity as shown in figure 4.1b. There is *ca.* 20 % reduction on methane conversion and *ca.* 40 % for N_2O (figure 4.3) over the 3 h reaction in both systems. The methanol and C_2 products selectivity stays at a low level during the course of the reaction. CO selectivity follows a decreasing trend before levelled off which suggest the Fe based active sites did not completely deactivated by coke. This phenomenon is due to the fact that Fe is still available.

Nitrogen adsorption isotherms were applied to the samples in comparison to the parent H-ZSM-5 sample to look at the effect of water on the pore accessibility and the results are shown in figure 4.19. The BET surface area and micro-pore volume of the materials were presented in Table 4.1.

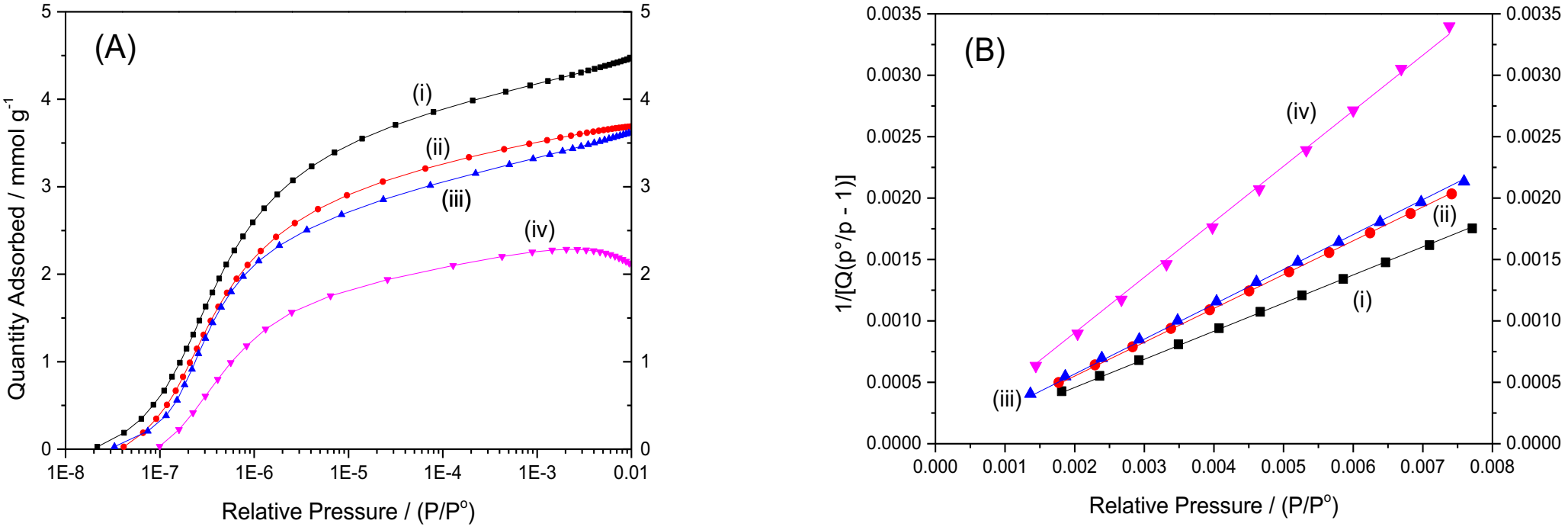

Figure 4.19 N_2 adsorption isotherms (A) and BET surface area plots (B) for: (i) H-ZSM-5, (ii) Fe/ZSM-5, (iii) Fe/ZSM-5-20% and (iv) Fe/ZSM-5-0% following testing at 300 °C for 3 h.

From Table 4.1, it is observed that the surface area of the parent H-ZSM-5 was lowered by *ca.* 75 $m^2.g^{-1}$ after exchanging with 2 wt. % of Fe. The micro-pore volume after Fe exchange was only lowered by *ca*. 15% from 0.169 to 0.142 $cm^3.g^{-1}$. The samples tested in Fe/ZSM-5-20% show that the surface area and the mico-pore volume are comparable to the unused Fe/ZSM-5. This is consistent with the TGA data presented in figure 4.18 where only low quantity of carbon deposit was observed benefited from adding water.

For Fe/ZSM-5-0% (water-free system), it is clear that both surface area and micro-pore volume are lowered according to the nitrogen adsorption measurements. There is approximately 40 % reduction in both BET surface area and micro-pore volume in comparison to the unused Fe/ZSM-5, lowered from 359 to 210 $m^2.g^{-1}$ and 0.142 to 0.087 $cm^3.g^{-1}$ respectively.

The interaction of the adsorbed CH_3OH or HCHO with H_2O to form HCOOH and then CO was proposed by Panov and co-workers.[14] It is excepted that the CH_3OH can still be formed via the $–Fe^{3+}\text{-}O^{\bullet-}$, even though CH_3OH also favours to be retained within the porous system via surface diffusion in the absence of water.[14, 21, 40]

From these data, it is clear that the decrease of the activity, observed in both figures 4.1 and 4.2 is not fully related to coke accumulation. Indeed, it has been observed that in the system of water the carbon rate formation is much lower than in the water-free system. However, when water is used the catalyst deactivates. It has been seen in the previous chapter the importance of the Fe species in the activity of the catalyst. The next section proposes to investigate the eventual transformation of this species before and after reaction.

4.7 The transformation of Fe species observed before and after reaction

UV-Vis spectroscopy was applied to investigate the evolution of Fe species before and after reaction. The UV-Vis spectra overlaying Fe/ZSM-5, Fe/ZSM-5-0% and Fe/ZSM-5-20% is shown in figure 4.20.

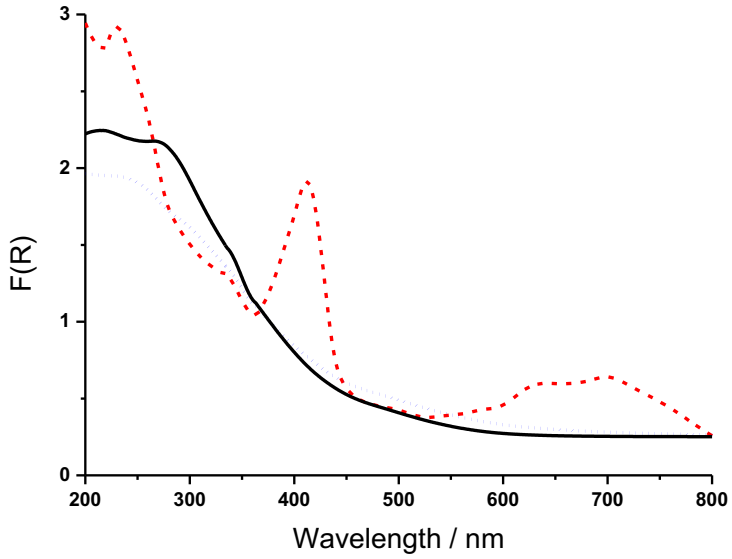

Figure 4.20 UV-vis spectra of Fe/ZSM-5 (black line), Fe/ZSM-5-20% (blue dots) and Fe/ZSM-5-0% (red dashes).

In the figure 4.20, the bands at 210 and 240 nm correspond to the $t_1 \rightarrow t_2$ and $t_1 \rightarrow e$ transitions of the two types of Fe^{3+} that are isomorphously substituted into the tetrahedral sites of the zeolite framework[41]. The bands at 250 nm represent the isolated octahedral Fe^{3+} species in extra-framework Al_2O_3.[42] The bands observed between 300 to 450 nm correspond to the iron oxide clusters and any bulky iron oxide species formed on the zeolite are shown at $\lambda > 450$ nm.[43]

The catalyst before reaction (Fe/ZSM-5) and the catalyst post-reaction when 20 % water is used (Fe/ZSM-5-20%), samples exhibit comparable spectra. In contrast, there are more resolved bands at various region at 210, 240, 410 and 550-800 nm for the water-free system (Fe/ZSM-5-0%). This, indicates that bulky iron oxide and iron clusters were formed on the external surface of the free-water system catalyst sample, meaning that the presence of water supresses the formation of external bulky Fe species.

The use of high temperature calcination conditions[41] or through steam treatment can result in the formation of Fe_xO_y clusters.[44] However, the reaction temperature used in this study (*i.e.* 300 °C) is not sufficient to promote this Fe migration which typically occurs at least at 600 °C and is favoured by high heating rate. Fe_xO_y clusters formation is also favoured by moisture remaining in the zeolite as observed by Kumar *et al*.[41] This formation of external iron oxide clusters in the water-free system sample under the reaction conditions applied in this study cannot be related to the presence of water. The rapid accumulation of coke may be linked to the instability of the Fe^{3+} active sites in the absence of water.

An irreversible Fe agglomeration process that leads to the formation of Fe_3O_4 is common for Fe/ZSM-5 after undergoing reductive treatment. The Fe_3O_4 magnetite phase would then transform into α-Fe_2O_3 particles following subsequent oxidation[45] which may be represented by the broad absorption band observed from 550 to 800 nm. This broad band also indicates the irreversible redistribution of Fe ion species after the CH_4 and N_2O treatment. After forming a large quantity of Fe_xO_y clusters during the reaction, this could also change the redox properties of the isolated Fe^{3+} ions as observed with NO reduction in a previous report.[41] It would be reasonable for weakly bound Fe^{3+} to migrate in the absence of water to yield iron oxide species. However, this kind of migration appears to be unrelated to the activity of the catalyst in this study due to the fact that CH_4 and N_2O conversions remain stable after 100 min time online (figure 4.1a).

This UV/Vis spectra also suggest that the sample from the water-free system has retained a sufficient concentration of FeO_4 tetrahedra and extra-framework Fe species to complete the methane oxidation reaction via the α-oxygen chemistry.

To investigate the origin of the Fe restructuring and catalyst deactivation further, control experiments were carried out on the catalysts after the exposure of 20% CH_4/Ar or 2% N_2O/Ar at 300 °C for 3 h and characterised using UV/Vis spectroscopy. The UV/Vis spectra for the control experiments are shown in figure 4.21.

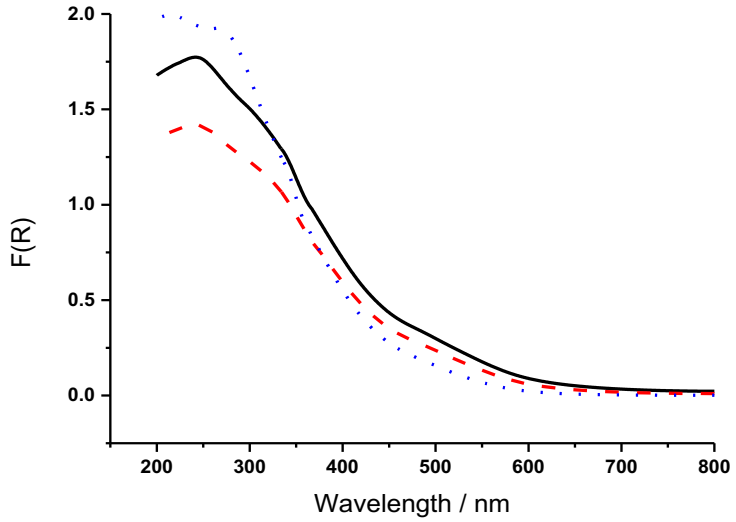

Figures 4.21: UV/Vis spectra of fresh (before reaction) 2 wt.% Fe/ZSM-5 (blue dots) and following control experiments under 20% CH_4/Ar (black line) and 2% N_2O/Ar (red dashes).

The UV/Vis spectrum shown in figure 4.21 for the 2 wt.% Fe/ZSM-5 before reaction, is very similar to the catalysts used in the two control experiments. This indicates that there are very little changes in the Fe speciation after the N_2O or CH_4 treatments. The differences observed from the spectra were the slight shifts to higher wavelengths in both samples that have been exposed to CH_4 or N_2O. This result, may imply that modest restructuring of Fe supported on ZSM-5 can occur after being exposed to CH_4 or N_2O. However, the cause of the significant shifts and more pronounced signals seen in Fe/ZSM-5-0% as shown in figure 18 could be due to a reaction intermediate or product that is only produced during the CH_4 + N_2O reaction.

The stability of N_2O conversion was investigated in the absence of CH_4 to determine if the catalyst deactivation could be due to the poisoning of the active sites by the presence of N_2O in the gas stream. This N_2O control experiment is presented in figure 4.22.

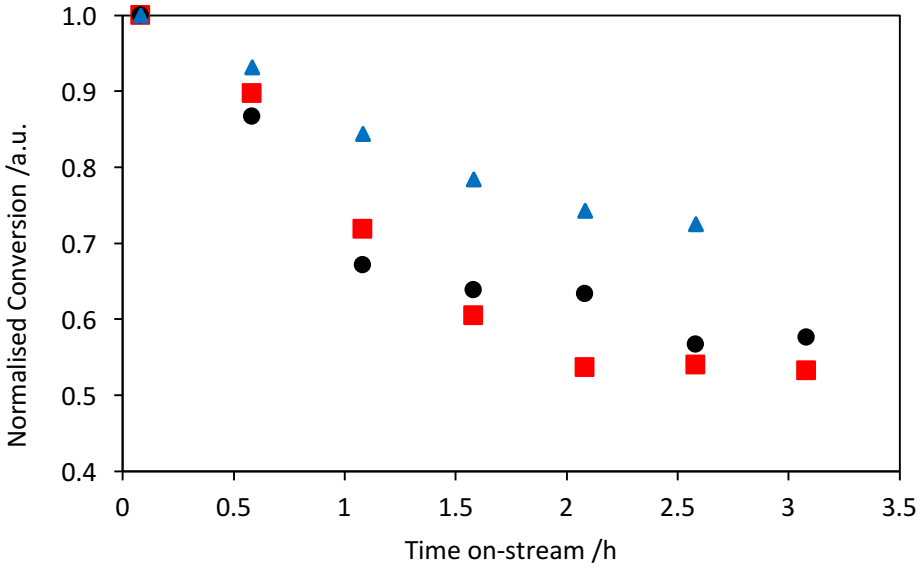

Figure 4.22 Normalised N_2O conversion over 2% Fe/ZSM-5 at 300 ^oC in flows of; CH_4 + 2% N_2O (●), 20% CH_4 + 2% N_2O + 20% H_2O (■) and 2% N_2O (▲) at 300 °C, over 2 wt.% Fe-ZSM-5 normalised to their initial values. All gas compositions balanced with Ar. Total flow rate = 55 ml min^{-1}.

The control experiment was carried out by passing 2 % N_2O in Ar in the presence of CH_4/ H_2O over the Fe/ZSM-5 catalyst. The conversion of N_2O obtained in this case was normalised to the initial value and compared. The N_2O conversion rates obtained from the methane oxidation reactions were also included from figure 4.3 for comparison. The N_2O conversion rate dropped rapidly in the control experiment at a similar rate to the two reaction systems with full reaction feed but appears to be slightly more stable after the first hour. N_2O decomposition is rate-limited in the absence of a reductant at 300 °C via oxygen recombination.[46] The facile dissociation of N_2O is observed over α- Fe sites. The decrease in N_2O conversion could be due to the fact that the -Fe^{2+} sites are fully saturated by N_2O providing that the rate of CH_4 activation is lower than that of N_2O dissociation.

The different techniques used to characterise the catalysts before and after reaction has given a better understanding of the different parameters which may be involved in the deactivation of the catalyst. The role of water to promote the desorption of methanol, which suppresses coke formation, is evident through the TGA characterisations of the fresh and used catalyst. UV-Vis analysis has highlighted that the Fe species were altered

in the water-free system during the reaction. The overall rate of catalyst deactivation was very similar in both water and water free systems which suggests that the coke and restructuration of Fe species were not significantly affecting the catalytic turnover of CH_4. Nitrogen porosimetry provided information on the loss of surface area and reduction in micro-pore volume in the absence of water. The deactivation of the catalyst in the water-free system appears to be caused by a combination of loss of porosity/surface area and Fe restructuration due to coke formation. In addition, a similar rate of deactivation is also observed when water is introduced, which could be explained by the ability of water to inhibit N_2O decomposition.

4.7 Conclusion

A delplot technique was used to investigate the influence of water on the CH_4 oxidation using N_2O over Fe/ZSM-5 catalysts. The yield of methanol produced on the α-oxygen sites ($-Fe^{3+}-O^{\bullet-}$) is low, using the reaction conditions in this study due to the low desorption rate of CH_3OH on Fe/ZSM-5. However, it has been also found that the CH_3OH selectivity can be greatly improved through the addition of water to the feed-stream.

When the reactions are carried out under water-free condition, CH_3OH generated on the surface could diffuse across nearby Brønsted acid sites where it is further converted to coke via the MTO type chemistry.[27, 29] Delplot analysis showed that coke is a secondary reaction product. Coke becomes a secondary or tertiary product when water is added to the feed which indicates that a reduction in the rate of coke formation.

It has been also revealed that CO and C_2H_4 were primary products derived from the surface bound CH_3OH which signifies the slow desorption rate of CH_3OH or methoxy species from the catalyst surface. The CO_2 selectivity remained relatively stable throughout the 3.5 h reaction and is not affected by the productivity of coke or CO when pushing the system to higher conversion. Therefore, this may imply that the total oxidation from this reaction condition operates a separate reaction pathway and is not affected by the addition of water.

The characterisation studies prove that water prevents any Fe clusters or bulky iron oxides from forming on the external surface and also helps retained the surface area and porosity by inhibiting coke formation. The reaction mechanism of selective methane oxidation appears to be highly complex and the reaction pathway is altered in the presence of water and the decomposition of N_2O. The studies on the catalyst deactivation reveals that Fe/ZSM-5 deactivates at a similar rate in both systems despite the significant improvement seen by adding 20% water to the system. This implies coking and the formation of external Fe clusters and Fe oxides species do not have a significant detrimental effect on catalyst performance for the 3.5 h time on line reaction in this study. In the control experiment, it is shown that the rate of N_2O conversion also decreases rapidly when exposing only N_2O to Fe/ZSM-5. It suggests that the deactivation which takes place in that case is independent of catalyst fouling as no

source of carbon is used. The mechanism of deactivation is not clearly understood at this stage of the study, further investigations are needed.

This kinetic study on methane activation using N_2O over Fe/ZSM-5 shows that the reaction is highly complex where a complex reaction network occurs in the confined porous environment. The CH_4 molecules are adsorbed and activated via the active Fe sites and it is observed that multiple competing reaction paths occur. The redesign of the catalyst bed may be required to minimise the plausible reabsorption of CH_3OH from the top position to bottom part of the catalyst bed where it is turned into coke.

4.8 References

1. A. I. Olivos-Suarez, A. Szecsenyi, E. J. M. Hensen, J. Ruiz-Martinez, E. A. Pidko and J. Gascon, *Acs Catalysis*, 2016, **6**, 2965-2981.
2. M. J. da Silva, *Fuel Processing Technology*, 2016, **145**, 42-61.
3. G. A. Olah, *Angewandte Chemie-International Edition*, 2005, **44**, 2636-2639.
4. T. Mokrani and M. Scurrell, *Catalysis Reviews-Science and Engineering*, 2009, **51**, 1-145.
5. C. Hammond, M. M. Forde, M. H. Ab Rahim, A. Thetford, Q. He, R. L. Jenkins, N. Dimitratos, J. A. Lopez-Sanchez, N. F. Dummer, D. M. Murphy, A. F. Carley, S. H. Taylor, D. J. Willock, E. E. Stangland, J. Kang, H. Hagen, C. J. Kiely and G. J. Hutchings, *Angewandte Chemie-International Edition*, 2012, **51**, 5129-5133.
6. J. A. Labinger, *Journal of Molecular Catalysis a-Chemical*, 2004, **220**, 27-35.
7. K. Narsimhan, K. Iyoki, K. Dinh and Y. Roman-Leshkov, *Acs Central Science*, 2016, **2**, 424-429.
8. V. S. Arutyunov, *Journal of Natural Gas Chemistry*, 2004, **13**, 10-22.
9. M. H. Groothaert, P. J. Smeets, B. F. Sels, P. A. Jacobs and R. A. Schoonheydt, *Journal of the American Chemical Society*, 2005, **127**, 1394-1395.
10. P. J. Smeets, M. H. Groothaert and R. A. Schoonheydt, *Catalysis Today*, 2005, **110**, 303-309.
11. P. Tomkins, A. Mansouri, S. E. Bozbag, F. Krumeich, M. B. Park, E. M. C. Alayon, M. Ranocchiari and J. A. van Bokhoven, *Angewandte Chemie-International Edition*, 2016, **55**, 5467-5471.

12. V. L. Sushkevich, D. Palagin, M. Ranocchiari and J. A. van Bokhoven, *Science*, 2017, **356**, 523-527.
13. J. Xu, R. D. Armstrong, G. Shaw, N. F. Dummer, S. J. Freakley, S. H. Taylor and G. J. Hutchings, *Catalysis Today*, 2016, **270**, 93-100.
14. M. V. Parfenov, E. V. Starokon, L. V. Pirutko and G. I. Panov, *Journal of Catalysis*, 2014, **318**, 14-21.
15. M. C. Kung, S. S. Y. Lin and H. H. Kung, *Topics in Catalysis*, 2012, **55**, 108-115.
16. H. A. Xia, K. Q. Sun, Z. C. Feng and C. Li, *Journal of Physical Chemistry C*, 2011, **115**, 542-548.
17. N. A. Bhore, M. T. Klein and K. B. Bischoff, *Industrial & Engineering Chemistry Research*, 1990, **29**, 313-316.
18. H. J. Wei, C. Gomez, J. J. Liu, N. Guo, T. P. Wu, R. Lobo-Lapidus, C. L. Marshall, J. T. Miller and R. J. Meyer, *Journal of Catalysis*, 2013, **298**, 18-26.
19. T. Rajkhowa, G. B. Marin and J. W. Thybaut, *Applied Catalysis B: Environmental*, 2017, **205**, 469-480.
20. G. I. Panov, K. A. Dubkov and E. V. Starokon, *Catalysis Today*, 2006, **117**, 148-155.
21. E. V. Starokon, M. V. Parfenov, S. S. Arzumanov, L. V. Pirutko, A. G. Stepanov and G. I. Panov, *Journal of Catalysis*, 2013, **300**, 47-54.
22. E. V. Starokon, M. V. Parfenov, L. V. Pirutko, S. I. Abornev and G. I. Panov, *Journal of Physical Chemistry C*, 2011, **115**, 2155-2161.
23. K. A. Dubkov, N. S. Ovanesyan, A. A. Shteinman, E. V. Starokon and G. I. Panov, *Journal of Catalysis*, 2002, **207**, 341-352.
24. B. Ipek and R. F. Lobo, *Chemical Communications*, 2016, **52**, 13401-13404.
25. M. F. Fellah and I. Onal, *Journal of Physical Chemistry C*, 2010, **114**, 3042-3051.
26. B. E. R. Snyder, P. Vanelderen, M. L. Bols, S. D. Hallaert, L. H. Bottger, L. Ungur, K. Pierloot, R. A. Schoonheydt, B. F. Sels and E. I. Solomon, *Nature*, 2016, **536**, 317-321.
27. P. Tian, Y. X. Wei, M. Ye and Z. M. Liu, *Acs Catalysis*, 2015, **5**, 1922-1938.
28. K. Chow, N. F. Dummer, J. Carter, C. Williams, G. Shaw, D. J. Willock, S. H. Taylor, S. Yacob, R. J. Meyer, M. Bhasin and G. J. Hutchings, *Catalysis Science & Technology*, 2017.

29. M. Z. Zhang, S. T. Xu, Y. X. Wei, J. Z. Li, J. R. Chen, J. B. Wang, W. N. Zhang, S. S. Gao, X. J. Li, C. X. Wang and Z. M. Liu, *Rsc Advances*, 2016, **6**, 95855-95864.
30. M. Bjorgen, S. Svelle, F. Joensen, J. Nerlov, S. Kolboe, F. Bonino, L. Palumbo, S. Bordiga and U. Olsbye, *Journal of Catalysis*, 2007, **249**, 195-207.
31. C. Y. Wang, G. Garbarino, L. F. Allard, F. Wilson, G. Busca and M. Flytzani-Stephanopoulos, *Acs Catalysis*, 2016, **6**, 210-218.
32. G. N. Li, E. A. Pidko, R. A. van Santen, Z. C. Feng, C. Li and E. J. M. Hensen, *Journal of Catalysis*, 2011, **284**, 194-206.
33. G. I. Panov, K. A. Dubkov and Y. A. Paukshtis, *Catalysis by Unique Metal Ion Structures in Solid Matrices: from Science to Application*, 2001, **13**, 149-163.
34. S. Svelle, F. Joensen, J. Nerlov, U. Olsbye, K. P. Lillerud, S. Kolboe and M. Bjorgen, *Journal of the American Chemical Society*, 2006, **128**, 14770-14771.
35. B. Hunger, S. Matysik, M. Heuchel and W.-D. Einicke, *Langmuir*, 1997, **13**, 6249-6254.
36. S. Ilias and A. Bhan, *ACS Catalysis*, 2013, **3**, 18-31.
37. D. Mores, E. Stavitski, M. H. F. Kox, J. Kornatowski, U. Olsbye and B. M. Weckhuysen, *Chemistry-a European Journal*, 2008, **14**, 11320-11327.
38. D. Mores, J. Kornatowski, U. Olsbye and B. M. Weckhuysen, *Chemistry-a European Journal*, 2011, **17**, 2874-2884.
39. L. R. Aramburo, S. Teketel, S. Svelle, S. R. Bare, B. Arstad, H. W. Zandbergen, U. Olsbye, F. M. F. de Groot and B. M. Weckhuysen, *Journal of Catalysis*, 2013, **307**, 185-193.
40. G. K. Boreskov, Springer Berlin Heidelberg, Berlin, Heidelberg, 1982, pp. 39-137.
41. M. S. Kumar, M. Schwidder, W. Grünert and A. Brückner, 2004, **227**, 384-397.
42. M. Schwidder, W. Grunert, U. Bentrup and A. Bruckner, *Journal of Catalysis*, 2006, **239**, 173-186.
43. J. Perez-Ramirez, M. S. Kumar and A. Bruckner, *Journal of Catalysis*, 2004, **223**, 13-27.
44. H. T. Lee and H. K. Rhee, *Korean Journal of Chemical Engineering*, 2002, **19**, 574-579.
45. A. V. Kucherov, C. N. Montreuil, T. N. Kucherova and M. Shelef, *Catalysis Letters*, 1998, **56**, 173-181.

46. L. Kiwi-Minsker, D. A. Bulushev and A. Renken, *Catalysis Today*, 2005, **110**, 191-198.

5

Conclusions and Future work

5.1 Conclusions

An environmentally friendly and low-cost alternative is always in demand to better utilise methane. This work is industrially sponsored in search for a selective and active route for direct methane partial oxidation to produce methanol. It has been one of the most difficult challenge we face for decades. In the present thesis, N_2O has been used as an oxidant over zeolite-based catalyst to gain a better understanding by probing the active components and the reaction paths occurring in a continuous flow system.

There are some impressive results that employ a cyclic sequential reaction procedure in recent years to improve the methanol selectivity.[1-3] that follows a typically order as: 1) activating the catalyst by setting up the required metal active sites by gas treatment 2) switch the inlet gas mixture to CH_4 to perform methane oxidation where methanol is generated over the surface and 3) perform hydrolysis step to extract those surface bound methanol. However, limited progress has been made on a true, one step methane to methanol conversion. The work presented herein attempted to move away from these step-wised reactions concept.

In the present work, numerous Fe exchanged MFI framework zeolite were successfully synthesised via different ion-exchange processes such as CVI and SSIE methods. It was found that although the synthesised of 2 wt % Fe/TS1, 2 wt % Fe/SIL-1 and 2 wt % Fe/ZSM-5 all possess the same MFI framework, the 2 wt % Fe/ZSM-5 is shown to be

the only active catalyst in the systematic methane activation study. This, is principally due to the presence of Al species which are very important towards methane activation. Indeed, the Al content in the MFI framework not only provide the metal exchange site but more importantly induces Brønsted and Lewis acidity. The study in chapter 3 shows that the acidity profile can be tuned by heat treating the catalyst at different temperature ranging between 550 – 950 °C under oxidising and reducing condition. Pyridine adsorption experiment was adopted, as a widely used technique, to study the relative acidity in the series of catalysts prepared in the investigation and it has been found that the overall acidity decreases as the treatment temperature increases. The decrease in Brønsted acidity, also causes the 2 wt % Fe/ZSM-5 to deactivate, as the catalyst treated at 950 °C has shown almost a ten-fold decrease in methane activity (from 1.8 % to 0.2 %). Moreover, using a diluted hydrogen gas during the calcination instead of an oxidising gas treatment have shown to be able to preserve a high percentage of acidity, therefore the decrease in methane activity has only drop to 1.4 % from 2.0 %. A supplementary ammonia TPD study was carried out to further characterise the relative acidity strength and acid concentration on the same set of catalysts. It is worth mentioning the robustness of the zeolite framework as XRD revealed that the zeolite crystallite structure was retained after heat-treated at temperature close to 1000 °C.

The active Fe/ZSM-5 catalyst is shown to be able to oxidise methane to methanol directly, in chapter 3. However, the selectivity to methanol is limited to below 2 % with *ca.* 2.5 % activity and the majority (*ca.* 70 %) of the converted methane is formed as coke. Methanol control experiment was carried out over the Fe/MFI zeolite with various acidity profiles, in order to monitor how methanol reacts, to simulate scenario where a relatively high concentration of methanol is produced. This also give insight into the type and composition of products formed from methanol. For catalyst with low relatively acidity with Fe/TS-1 and Fe/SIL-1 compare to Fe/ZSM-5, >85 % of methanol is converted to DME and only *ca.* 10 % of coke was observed. In contrast, using Fe/ZSM-5 led to a much lower selectivity to DME at 54 %, coke was observed at a much higher level at 37 % along with 8 % ethene that is not observed in other lower acidity catalysts. This, indicates that the strength of acidity is related to the retention of methanol and further transformation to coke is favourable. The reaction path observed with DME, C_2 and coke indicates that it is possible a MTO (methanol to olefin) type competing reaction path can occur which provide information on the origin of coke.

The methanol generated undergo further transformation in the porous environment to form aromatic intermediates which are easily trapped in the pores and also act as a co-catalyst to produce ethene.[4]

Therefore, the goal of chapter 4 was set out to introduce water which is a known component used to improve the mass balance and selectivity to methanol and to carry out investigation on the reaction paths taken in both water-assisted and water-free system using 2 wt % Fe/ZSM-5. It is found that the addition of 20 v/v % water in the reaction mixture improved the selectivity to methanol from 2 % to 20 % and a significant decrease in coke formation was achieved drop from *ca*. 70 % to 10 %. The delplot technique was applied on both systems by plotting the selectivity profile of products versus a range of conversions obtained by performing experiments using various catalyst masses. The results allow the identification of product rank which suggested the observed following gas phase products, CO, CO_2, CH_3OH, C_2H_4 and C_2H_6 to form as primary products whilst coke is a secondary product. However, C_2 products are likely to be due to an initial condensation of methanol within the pores of the zeolite and hence considered as pseudo-primary products. The control experiments performed in the absence of methane revealed that the rate of N_2O decomposition is similar to reaction mixture with $CH_4 + N_2O$ indicating that the loss of active α-oxygen sites is the likely cause of the decrease in activity observed.

5.2 Recommended Future work

There is continuous research on methane oxidation and many interesting approaches were applied on the direct methane partial oxidation in recent years. Apart from the findings presented in this thesis, there are many other high-quality papers published at the time when this study has taken place. Those published works have investigated some other important parameters which provide very important information on targeting methanol production. The suggestions in this final section would cover the area needed for future works on this project and also other ideas that is inspired from other publications.

1. The study shown in section 3.5 where a range of Fe/ZSM-5 catalysts were prepared that had the same Fe:Al ratio from parent HZSM-5 catalysts with varying SiO_2:Al_2O_3 ratios. However, the work is inconclusive due to the

incomparable conversions of the tested catalyst in the series. Further work should be carried out by adjusting the catalyst mass used in attempt to achieve iso-conversion for making fair comparison.

2. The concentration of α-oxygen of the tested catalyst would be a useful data to investigate how it relates to the activity and methanol yield. This can be accomplished by titrating the N_2O conversion to the number of N_2 produced.
3. A combination of Fe and Cu to form a bimetallic zeolite catalyst have been reported to optimise the yield of methanol and other valuable oxygenates.[5, 6] A study of such synergetic effect would provide valuable information on catalyst designing and optimisation.
4. ^{13}C NMR can be used to characterise the retained organic species formed via the competing mechanism proposed. This would allow the identification of the type of hydrocarbons being trapped in the zeolite pores and surface species formed.[7]
5. There are numerous publications have found correlation that Cu exchanged with zeolite framework consisted of small pore 8 membered ring (i.e. chabazite, mordenite, SAPO) can produce high yield of methanol which may be induced by the zeolite confinement effect.[8-10] Therefore, testing a series of metal exchanged zeolite containing those 8 membered rings should be explored further.
6. The Fe content % of the Fe/ZSM-5 was determined using EDX as shown in chapter 3. The total Fe content/elemental analysis of the catalysts after the Fe ion exchange to the parent HZSM-5 support can be quantified in a more accurate approach by using hydrofluoric acid digestion before subjecting the samples to inductively coupled plasma mass spectroscopy (ICP-MS).[11, 12] The acid digestion step using HF allows the robust zeolite framework to be completely dissolved which will liberate all the Fe ions in the solution.
7. The ammonia TPD experiments presented in chapter 1 for assessing the acidity of a series of Fe/ZSM-5 catalysts can be improved to provide a quantitative analysis on the concentration of acid sites by performing calibrating experiment.

5.3 References

1. E. V. Starokon, M. V. Parfenov, L. V. Pirutko, S. I. Abornev and G. I. Panov, *Journal of Physical Chemistry C*, 2011, **115**, 2155-2161.
2. V. L. Sushkevich, D. Palagin, M. Ranocchiari and J. A. van Bokhoven, *Science*, 2017, **356**, 523-527.
3. P. Tomkins, A. Mansouri, S. E. Bozbag, F. Krumeich, M. B. Park, E. M. C. Alayon, M. Ranocchiari and J. A. van Bokhoven, *Angewandte Chemie-International Edition*, 2016, **55**, 5467-5471.
4. P. Tian, Y. X. Wei, M. Ye and Z. M. Liu, *Acs Catalysis*, 2015, **5**, 1922-1938.
5. C. Hammond, M. M. Forde, M. H. Ab Rahim, A. Thetford, Q. He, R. L. Jenkins, N. Dimitratos, J. A. Lopez-Sanchez, N. F. Dummer, D. M. Murphy, A. F. Carley, S. H. Taylor, D. J. Willock, E. E. Stangland, J. Kang, H. Hagen, C. J. Kiely and G. J. Hutchings, *Angewandte Chemie-International Edition*, 2012, **51**, 5129-5133.
6. C. Hammond, N. Dimitratos, R. L. Jenkins, J. A. Lopez-Sanchez, S. A. Kondrat, M. H. ab Rahim, M. M. Forde, A. Thetford, S. H. Taylor, H. Hagen, E. E. Stangland, J. H. Kang, J. M. Moulijn, D. J. Willock and G. J. Hutchings, *Acs Catalysis*, 2013, **3**, 689-699.
7. X. Wu, S. Xu, W. Zhang, J. Huang, J. Li, B. Yu, Y. Wei and Z. Liu, *Angewandte Chemie International Edition*, 2017, **56**, 9039-9043.
8. K. Narsimhan, K. Iyoki, K. Dinh and Y. Roman-Leshkov, *Acs Central Science*, 2016, **2**, 424-429.
9. M. B. Park, S. H. Ahn, A. Mansouri, M. Ranocchiari and J. A. van Bokhoven, *Chemcatchem*, 2017, **9**, 3705-3713.
10. M. J. Wulfers, S. Teketel, B. Ipek and R. F. Lobo, *Chemical Communications*, 2015, **51**, 4447-4450.
11. M. Niwa, N. Katada and K. Okumura, *Characterization and Design of Zeolite Catalysts: Solid Acidity, Shape Selectivity and Loading Properties*, Springer Berlin Heidelberg, 2010.
12. J. R. Mackey and W. J. Murphy, *Zeolites*, 1985, **5**, 233-239.